MODELLING AND CONTROL OF PIEZOELECTRIC ACTUATORS

A Thesis

Submitted to the Faculty

of

Purdue University

by

Rajesh Ramanujam

In Partial Fulfillment of the

Requirements for the Degree

of

Master of Science in Mechanical Engineering

December 2001

To my parents, who seem to want me to finish this thesis more than I do ...

ACKNOWLEDGMENTS

I would like to thank firstly Dr.Bin Yao, for his patience with my long ordeal with my thesis and his enormous help in reviewing my writing and experiments. Thanks to my committee members for agreeing to spend time reading and evaluating my research work.

This section would not be complete without thanking former and current members of Dr.Yao's research group (Li Xu, Jianquin Gong, Phanindra Garimella, Dontha Ramakrishna) for their input and help during discussions.

Thanks to the people in the ME department (Marty Myrlnaik, Rick Duavall, Jim Hale) for their help with the experimental setup. Finally I wish to thank all those at Purdue who have made my sojourn a very pleasant one.

TABLE OF CONTENTS

Page

Page

LIST OF TABLES

LIST OF FIGURES

ABSTRACT

Ramanujam, Rajesh. M.S.M.E., Purdue University, December, 2001. Modelling and Control of Piezoelectric Actuators. Major Professor: Dr. Bin Yao, School of Mechanical Engineering.

The aim of this work is to study the behavior of a piezoelectric actuator in order to get a better understanding of various important dynamic phenomena associated with the actuator. The results of this work are to help in further research in precisely modelling piezoelectric actuators either for simulation and open-loop feedforward compensation or closed-loop feedback control when these actuators are used in application areas which demand motion accuracy down to nanometers. To this end a commercial piezoelectric positioning system with a sensing resolution less than 1 nanometer is used as a test bed for the experimental work. The responses of the system to different typical input signals (step, sinusoidal, triangular) are first obtained. The responses reveal that the piezoelectric actuator exhibits complicated nonlinear dynamic behaviors such as the nonlinear gains to step inputs, the widely studied hysteresis phenomena, and the slow drifting responses. Individual dynamic and/or nonlinear models are then proposed to capture each of these nonlinearities separately, and carefully controlled experimental tests are performed to obtain the right responses in obtaining the parameters for the proposed individual models. Specifically, the slow drifting responses are approximately modelled by the output of a parallel connection of systems described by first-order linear transfer functions with various time constants. The variations in the static gains to different step input amplitudes are approximated by polynomial functions of the input magnitude. A new model for hysteresis is proposed, which is easy to parameterize and to use in real time implementation. An overall model of the piezoelectric actuator is then presented, which

integrates the individual models proposed for various phenomena. Benefits and limitations of the proposed models are shown with suggestions as to experiments that could be performed to improve the confidence in the proposed models.

1. INTRODUCTION

Due to the drive to manufacture smaller components, achieve higher production rates and tighter product tolerance specifications, the manufacturing sector has turned to improving the process itself as one of the means to achieving this multitude of often contradicting goals. It is very apparent machine tools that are precise and offer a dramatic improvement in throughput along with robustness is one of the solutions to this contradictory set of requirements.

Actuators (be it electromechanical, pneumatic or hydraulic) provide the necessary energy to accomplish most tasks that involve any motion in any machine tool. Hence the need for faster and better machine tools would also imply better actuators or using the existing actuators in a manner to derive better performance from them.

Piezoelectric actuators belong to the type of direct drive actuators that rely on the (inverse) piezoelectric effect to produce a force or motion. The *piezoelectric effect* is a phenomenon in which a charge is produced on the surface of the material exhibiting that phenomenon upon application of an external pressure. The converse effect (production of a force upon application of charge) is the inverse-piezoelectric effect which is exploited in piezoelectric actuators. Due to the solid state nature of this effect, they do not rely on gearing mechanisms or any sliding motion to support the moving parts. This offers them an enormous advantage in attaining high bandwidth (due to the reduced inertia eliminated in the gears) and accuracy (due to the absence of friction, backlash, play and due to the infinitesimal nature of this effect itself).

Some of the disadvantages of using piezoelectric actuators are,

- The crystals can withstand very little tensile stresses. Hence special considerations have to be made during the operation like pre-loading or offset voltages etc.

- The materials are *inherently nonlinear*. Hence to achieve the infinitesimal resolutions that are theoretically possible, feedback control is necessitated.

Piezoelectric actuators are currently used for many Optical (STM's, Adaptive Optics, Optical fibre aligners), Electro-Mechanical (hard disks, vibration control and cancellation, micro-manipulators), Microelectronic (Nano-metrology, micro-lithography, wafer or mask positioning) applications. Their low mass makes them invaluable in applications where a high bandwidth actuator is essential and the range of motion is small. Thus, as the application for micro devices increases in diverse areas, piezo materials are sure to be deployed to a large extent. For a more comprehensive list of the known applications see [1].

Piezoelectric actuators are, typically, used in closed loop mode to control either the deflection or the force generated. But in certain applications, measuring the deflection (or force) is not possible or viable in the systems. In such applications they are used in open loop mode. In either case, the most significant limitations to achieving a good positioning accuracy and high bandwidth are the nonlinearities that piezoelectric materials exhibit. The significant nonlinearities are Hysteresis (with respect to the applied voltage) and Drift (in the output of the system with respect to time). For both open loop and feedback controllers, modelling these phenomena are important issues. In some cases, even controlling the high bandwidth of the actuators is an issue. The following section provides a summary of the principal research directions related to piezoelectric actuators and also the different contributions to these directions.

1.1. Current State of Research on Piezo Actuators

1.1.1. Modelling

One of the earliest, standardized models for piezo-electric material was developed by the IEEE standards committee [2]. This model related the applied electric field to the strain developed in the material by means of two linear tensor equations which

state that the strain and the electric displacements are linear combinations of the mechanical stress (due to the inverse piezoelectric effect and due to any external loads). This linear constitutive relationship between the electric field and the strain, is the basis for using linear models for Piezoelectric actuators by many authors (Croft and Devasia [3]; Duong and Garcia [4, 5]; Buckner et al. [6]; Rubio et al. [7]; O'Hara and Youcef-Toumi [8]; Li et al. [9]; Numasato and Tomizuka [10]; Kim and Nam [11, 12]; Pozzi and King [13]). The disadvantages of using linear models for piezo actuators are well known as, they inherently exhibit nonlinear effects. The use of linear models for designing linear controllers have seemed to be successful so far because of operation primarily at frequencies that are relatively low compared to the closed loop bandwidth. It is when, either operating in open loop mode or with relatively aggressive reference inputs, that the achievable performance of linear formulations degrades.

It should be noted that some authors have used a linear formulation for the dynamics of the system along with a nonlinear block to simulate the effect of hysteresis/creep (Croft and Devasia [14]; Celanovic and Golfarb [15]; Adriaens [16]). These are not strictly linear models for piezo actuators.

The drawbacks of the linear models are discussed in Celanovic and Goldfarb [15] and Adriaens [16]. When the linear models are not accurate enough to be used for high precision applications, the nonlinear phenomena exhibited by piezoelectric materials have been addressed . The best recognized nonlinearity in these materials is the Hysteresis effect. Efforts on modelling hysteresis have taken two principal directions.

Physical Models These models attempt to explain the hysteresis effect from first principles. For example Chen and Montgomery [17], have considered the effect of an external electric field on the dipoles (that are thought to be the fundamental reason behind the existence of the piezoelectric effect) in the material and try to explain the observations about hysteresis in terms of the behavior of dipoles. Another type of physical model derived, again based on the dipole behavior, but taking an energy based approach is provided by Smith et al. [18]

and Zhou and Chattopadhyay [19]. In these they have considered the energy of collections of dipoles (called *dipole domains*) to explain the phenomenon of rate dependent hysteresis.

Physical models of hysteresis share some common drawbacks. For instance, they are difficult to parameterize since they are based on the behavior of dipole domains which cannot be quantified by experimental observation so easily. For the very same reason, it is difficult to verify the validity of these models. They are not, in most cases, amenable for use in real time control or compensation.

Phenomenological Models This classification of models for hysteresis are by far the most popular choice for many people working in this area. These models attempt to explain the overall behavior or the effect of the hysteresis phenomenon by "fitting" known functions to the hysteretic behavior.

Phenomenological models can be broadly classified into two categories based on their method of implementation as Differential Models and Numerical Models. Differential models, as the name suggests, use differential equations to model the behavior of the hysteresis phenomenon. Most of the differential models for hysteresis are derived from research on friction modelling. This probably due to the similarity in the effects of the two phenomena. Examples of this type of models are the Dahl model and the Coleman-Hodgdon model. de Wit et al., in [20], have used the Dahl Model for modelling the dynamic frictional force especially at low velocities. The hysteretic nature between the frictional force and displacement indicates the applicability of the Dahl's model to piezoelectric materials as by Sun and Chang in [21]. The Coleman-Hodgdon's model which is supposed to be a generalization of the Dahl model is used by Adriaens et al. [16, 22] as a part of their overall electromechanical model.

Numerical models are in abundance. Some of the simplest are polynomial models. Croft and Devasia in [23] have used the basic polynomial model to perform open loop inverse compensation. Jung and Kim [24] employ a variation of the polynomial model to compensate for the hysteresis effect. But the polynomial approximation

suffers from some setbacks as it is based on the hysteretic response to a specific type of input. It difficult to use these models to analyze the behavior of the system for a general type of input. Also a number of polynomials need to be used to approximate the several possible hysteresis loops for a give maximum and minimum values of the input.

This has led to the development of models along the lines of neural networks. Neural networks have been used to approximate the behavior of unknown systems using a weighted combination of simple operators. The weights for each of these simpler operators could then be determined based on the hysteresis loops either in an online manner (as in neural networks) or off-line as in parameter estimation experiments. Neural Networks have been used to compensate for hysteresis and nonlinearities by Bakhashwain et al. [25]; Kwan et al. [26]; Song and Li [27].

The method of off-line estimation of the weights for the hysteresis model has been used by Celanovic and Goldfarb [15, 28] and by Galinaitis and Rogers [29]. In [28], the authors have proposed a complete electromechanical model for a piezoelectric stack actuator and the hysteresis model (called Maxwell's model) is a part of this set of equations. The estimation of the weights of the each of the models is done in a non-iterative manner and is determined in one step from a set of test hysteresis loops. Both these models basically approximate hysteresis loops piecewise by a set of line-segments. In simulations performed during the course of this thesis it was discovered that these models seemed to be sensitive to the noise level in the signal as they depend on the derivative of the input signal to determine the output. Due to this, the output of these models were prone to exhibit random jumps near zero velocity regions.

One of the most widely used numerical models for hysteresis is a modification of the Preisach Model. In the originally proposed (scalar) form of this model, by Preisach [30], the output is calculated by integrating a weight function over the domain of the input signal. Determination of the weight function (to parameterize this model) requires one to differentiate the output of the system being modelled twice

with respect to the input signal which will amplify the measurement noise to such an extent that the data obtained is virtually useless. Additional details about the practical implementation, properties and applicability of this model can be obtained in the publications by, Mayergoyz [31] (proposed a vector form of the model), Ge and Jouaneh in [32, 33, 34] (illustrated a numerical implementation of the Preisach model for real-time implementation), Hughes and Wen in [35] and Sreeram and Naganathan in [36].

Piezoelectric actuators also exhibit a drift in the end position of the actuator. This is a nonlinear, time-dependent phenomenon, as will be demonstrated in this thesis with experimental results. Since drift is a much slower phenomenon when compared to the dynamics of the actuator, it can be compensated for easily in closed-loop operation but in open-loop mode, it is a cause for a significant positioning error and hence it is important to model this phenomenon too. Modelling of the drift phenomenon has been performed by Kuhnen and Janocha in [37, 38] and Koops et al. in [39]. Croft, Shedd and Devasia used the inverse of the creep model in addition to the inverse of the Preisach model for compensation of the nonlinearities in open loop operation for an AFM application.

Most of the models for either the hysteresis or the drift phenomenon have considered those effects in isolation. In [32, 33, 34], it has been assumed that the drift phenomenon is absent or that the drift has reached steady state and that the dynamics of the actuator are negligible. This is a good approximation when operating at low enough frequencies, but when the dynamics of the piezoelectric actuator become significant, then the predicted output using these models would not be accurate enough for compensation. Celanovic and Goldfarb ([15, 28]) introduced an overall electromechanical model that accommodates for both the dynamics and the hysteresis effect observed in the actuator. Adriaens, Koning and Banning in [16, 22] used the same model as in [15, 28] but have inverted the model for hysteresis which they claim is to be better applicable to piezoelectric actuators.

In addition to modelling the behavior of piezo actuators many authors have also addressed the issue of model based controller design. Celanovic and Goldfarb [28] and Adriaens et al. [16, 22] have implemented controllers based on their overall electromechanical model which achieve good tracking performance for large amplitude inputs. Performance for more aggressive input trajectories is not shown and hence is unknown. Many authors have used their models in open loop, feed-forward compensation [40, 24, 23] or in feedback loops with the models serving the purpose of feedback linearization.

1.1.2. Control

Linear controllers have been a popular choice in most applications where the applications do not demand a very high bandwidth from the closed loop system. They have been able to achieve a reasonably good level of robust stability and performance, with rather simple control structures like a PID compensator. Some examples of applications of linear controllers can be found in Numasato and Tomizuka [10], Kim and Nam [11, 12], Croft et al. [3], Li et al. [9], Choi et al. [41].

It has been observed through experiments that the relationship between the charge developed on the electrodes of the piezoelectric actuator to the displacement of the actuator is a linear, i.e. non-hysteretic. This has been exploited by some researchers who control the charge on the electrodes instead of the more commonly used voltage control method. This results in linear controllers which can be found in Main et al. [42], Furutani et al. [43, 44]. This method has it own disadvantages that are related to the control loop hardware.

A number of authors have thought it important to include models of hysteresis in their overall system models. This obviously results in nonlinear systems models and in most cases some type of feedback linearization or model compensation have been applied to design controllers for the nonlinear plant models. Examples can be found in Celanovic and Goldfarb [15, 28], Adriaens et al. [16, 22]. The above methods used

hysteresis models where the model had to be parameterized prior to implementation. Another type of nonlinear controllers use adaptive or neural-network methods to estimate the parameters of the nonlinear equations. This method has been adopted by Li et al. [45], Hao et al. [46], Su [47], Kuhnen and Janocha [48, 49]. A hybrid method of modelling and control has been adopted in some publications where the inertial dynamics of the actuator are assumed to be linear which is in series with a nonlinear block representing the hysteretic distortion (Ge and Jouaneh [33], Croft et al. [3, 40].

1.2. Objectives

The principal focus of this thesis is to study the behavior of a piezoelectric actuator and to develop models for it to be used either for open or closed loop control. The emphasis is not on the actual design of the control system itself but rather on models which could be used in controller design. A simple linear controller will be designed in Chapter 4 based on the nominal linear model and it will be shown that the linear controller achieves a better performance than the commercially available controller card specifically "tuned" for the piezoelectric actuator from the same manufacturer.

1.3. Outline

The remainder of the thesis is organized in the following manner:

Chapter 2: Experimental Setup Describes the system that was used for the experiments and the characteristics of the components of the system.

Chapter 3: System Behavior and Nonlinear Effects Presents Experimental results which illustrate the behavior of the system and characterizes the nonlinearities in the system.

Chapter 4: Linear Models and Controller Proposes a nominal linear model for the system and designs a linear compensator based on the nominal model and performance specifications.

Chapter 5: Modelling Drift and Hysteresis Presents a brief summary of the models currently being used to capture the drift and the hysteresis and their drawbacks and proposes new models to approximate these nonlinear behaviors.

Chapter 6: Overall Model Proposes an overall model for the positioning system which integrates the models for the phenomena mentioned in the earlier chapters.

Chapter 7: Conclusion and Directions Summarizes the work done in this thesis and suggests directions for continuation based on the inadequacies of the current work.

2. EXPERIMENTAL SETUP

A common method of classification of the various components in a control loop is by identifying the Plant (i.e. the system being controlled), the Actuator (i.e. the system that supplies the actual control input to the plant), the Sensor (and associated systems for feedback) and the Controller.

In the system to be used for the experiments in this thesis, the various components in the control loop can be classified into the above categories in the following manner:

The Plant is the piezoelectric nano-positioning stage. The output of this stage i.e. the position of the stage that the variable to be controlled.

The Controller is either the dSPACE Digital Signal Processing(DSP) system or the controller card supplied by the manufacturer of the positioning system.

The Actuator is the system that provides the power to drive the plant. In this case that would include the piezoelectric actuator and the power amplifier.

The Sensor is the capacitive sensor, in this case it is physically located and integrated within the nano-positioning stage (i.e. the plant). The electronic components associated with the sensing system are located on the E509.C1 capacitive sensor module which is located in the same chassis holding the Amplifier and the manufacturer's control card.

The schematic (Figure 2.1 on page 11) should give a better idea about the physical location and connectivity of the components in the control loop.

For the purposes of the experimental work involved, it was decided that a commercially available positioning stage be used. This would allow the focus to remain on

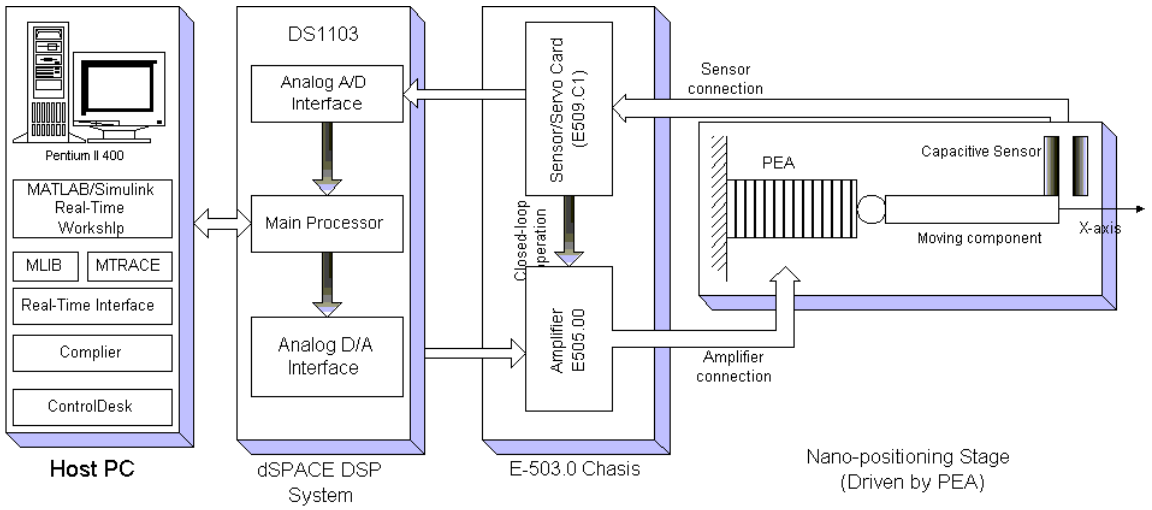

Figure 2.1. Schematic of Experimental System.

the system modelling and controller development aspects instead of on the fabrication of the actuator, sensor and all the associated electronics.

This chapter provides a description of the characteristics of the various components that make up the experimental system and the issues that had to be considered to obtain the optimal combination of the components. This interfacing issue between components is critical because if the components are not selected in an optimal manner the attainable positioning accuracy may be limited by some components in the loop.

2.1. The Plant

As mentioned above, the plant to be controlled is the nano-positioning stage. This includes the piezoelectric actuator and the guiding system for the moving platform (see Figure 2.1 on page 11 and Figure 2.6 on page 17). The integrated unit contains the piezoelectric actuator, the guiding system and the capacitive sensor plates. It was bought from Polytec PI (a subsidiary of Physik Instrumente GmbH) and is

also referred to as P753.11C flexure stage. The manufacturer's specifications for the P752.11C system are available in Table 2.1 on page 12.

Table 2.1. P753.11C : Manufacturer specifications.

PROPERTY	**VALUE**
Active Axis	X
Travel	12 μm
Sensor Type	Capacitive
Resolution (CL/OL)	0.05/0.05 nm
Linearity	0.03 %
Repeatability	$\pm$1 nm
Stiffness	45 N/μm
Max. Push/Pull Force Capacity	100/20 N
Max. Normal Load	3 kg.
Lateral Force Limit	30 N
Tilt (θ_y, θ_z)	2 μ rad.
Electrical Capacitance	1.8 ($\pm$20%)μF
Unloaded Resonant Frequency	5.6 ($\pm$20%) KHz.
Total Weight	150 ($\pm$5%) g

2.1.1. Piezoelectric Actuators

The piezoelectric actuator is the central component in the positioning system. Piezoelectric actuators are available in various configurations like films, beams, stacks (see Figure 2.2 on page 14). In each configuration the fundamental constituent of the actuator is the piezoelectric material used to fabricate the actuator. Hence in each of the above mentioned configurations, the actuator is a thin sheet, a beam or a

stacked configuration of piezoelectric material. When a voltage is applied across the electrodes, a strain is developed in the material. This strain deforms the shape of the actuator i.e. a deflection which is used to produce either a displacement or a force when the displacement is restrained.

The P753.11C uses a stacked configuration of thin piezo-ceramic disks. The electric field is applied in a direction parallel to the axis of each of the disks by means of a voltage applied to the electrode films sandwiched between the disks. The ceramic disks are all electrically connected in a parallel configuration, so that the same voltage is applied across each of the disks. Each disk is poled in such a fashion such that they tend to deform along its axis upon application of an axial electric field. Since the disks are all stacked on end, a net deformation that is equal to the sum of the deflections of each disk is seen at the end of the actuator (see Figure 2.3 on page 15).

2.1.1.1. Piezoelectricity and Piezoelectric Materials : A Brief Background

Any material that exhibits the piezoelectric effect, by definition, develops a mechanical strain on application of an external electric field. The common feature among all piezoelectric materials is the asymmetry in their crystal structure which gives rise to a net dipole moment for each unit cell in the crystal (see Figure 2.4 on page 16). Thus these materials can be thought of as being consisted of by tiny dipoles.e

For the stacked configuration of a piezoelectric actuator, the resultant displacement produced by the actuator is the sum of the deformations of all the disks in the stack. If the axial deformation of each of the ceramic disks is uniform over the surface, then the whole stack tends to deflect only in the axial direction. But due to the very nature of the material (i.e. a poly-crystalline ceramic) it is generally very difficult to guarantee the desired level of uniformity. As a result of which the deflection of the tip of the actuator is composed of two components, a major axial component and a parasitic off-axial component (which is usually small). These off-axial components

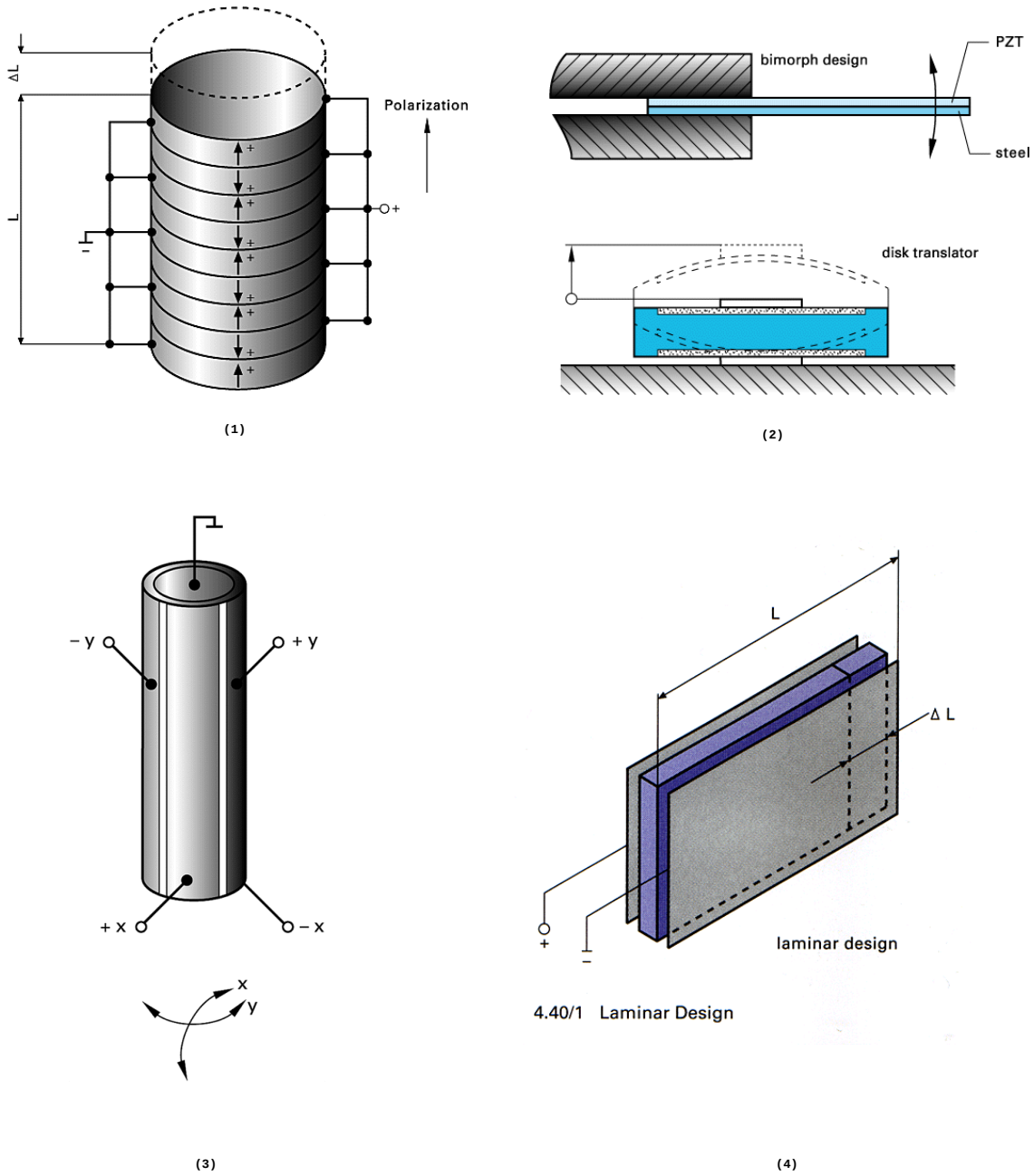

Figure 2.2. Common configurations of Piezoelectric Actuators; (1): Stack Actuator; (2)Bimorph Actuator; (3)Tubular Design; (4)Laminar Design.

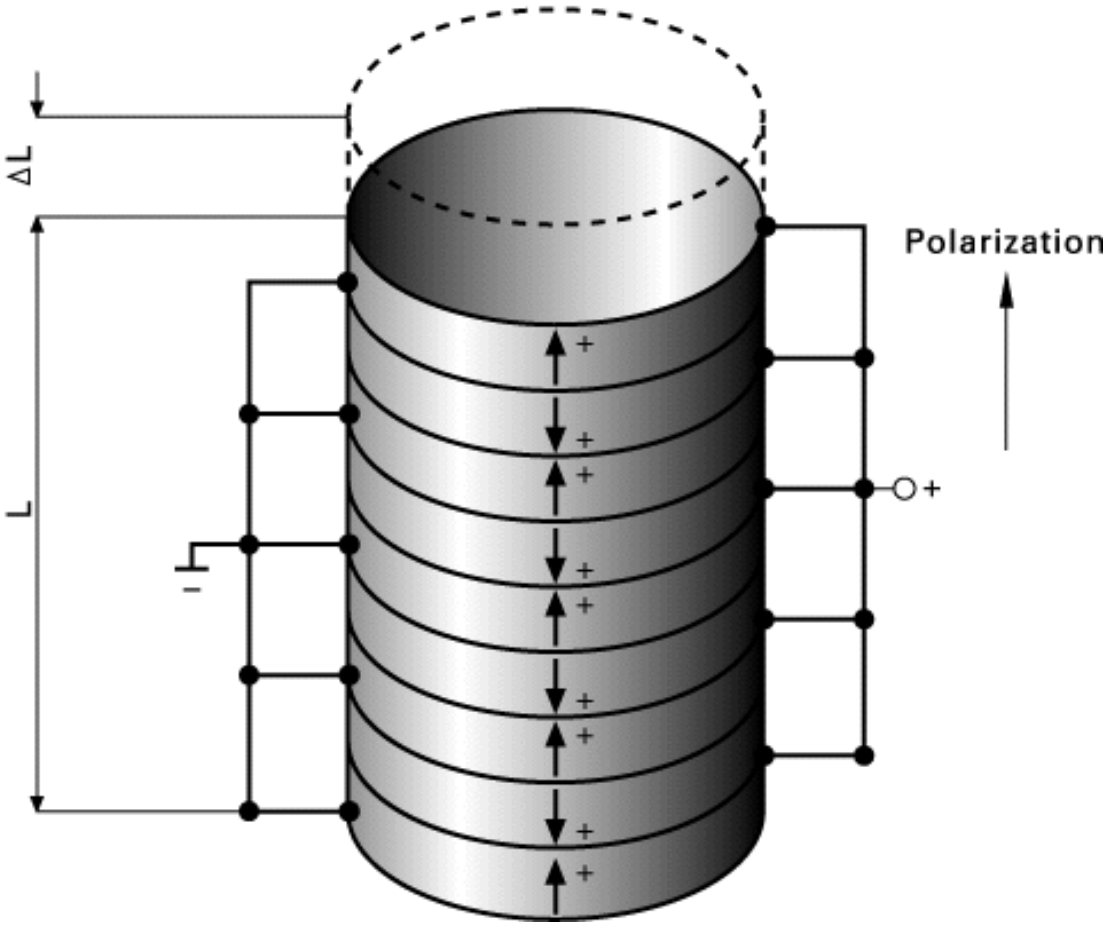

Figure 2.3. Configuration of a stack actuator.

can be eliminated or attenuated by the use of guides very much like the supports on any machine tool table which guide the moving part of the machine tool.

Extensive background reference material on piezoelectricity and piezoelectric materials, actuators etc. can be found in the catalogs of Physik Instrumente (or on their web-site: www.physikinstrumente.com).

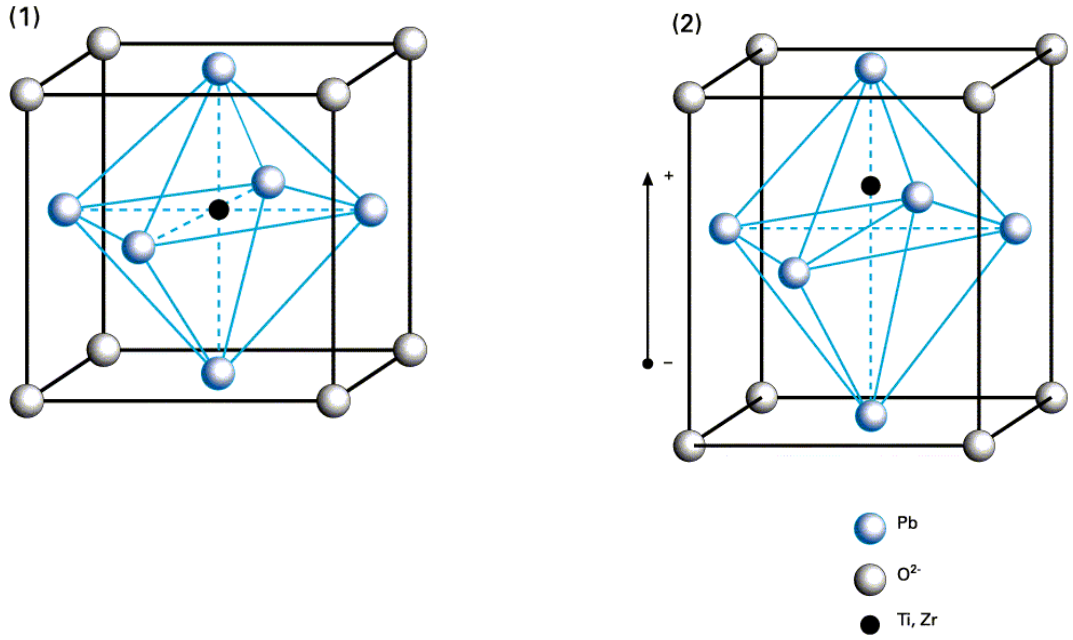

Figure 2.4. (1)Symmetric & (2)Asymmetric crystal structures.

2.1.2. The Guiding System

The guiding system (also called *zero-run-out guides*) in the nanopositioner (see Figure 2.6 on page 17) is used eliminated all transverse displacements as opposed to other commonly used guiding systems which still transmit a certain extent of the off-axial motion. The run-outs occur, as mentioned above, due to asymmetry introduced during the fabrication/assembly of the piezoelectric actuator.

Although the guides in the P753.11C system are employed only to eliminate all parasitic displacements, in general guiding systems could also be used to amplify the displacement of the tip of the piezoelectric actuator. The guides in principle are similar to joints that are flexible in the transverse directions so that they do not transmit forces/displacements in the transverse direction (see Figure 2.6 on page 17).

The external load that is to be driven by the actuator is fixed (by means of screws) onto the moving platform seen in Figure 2.6 . Hence the maximum loads that can

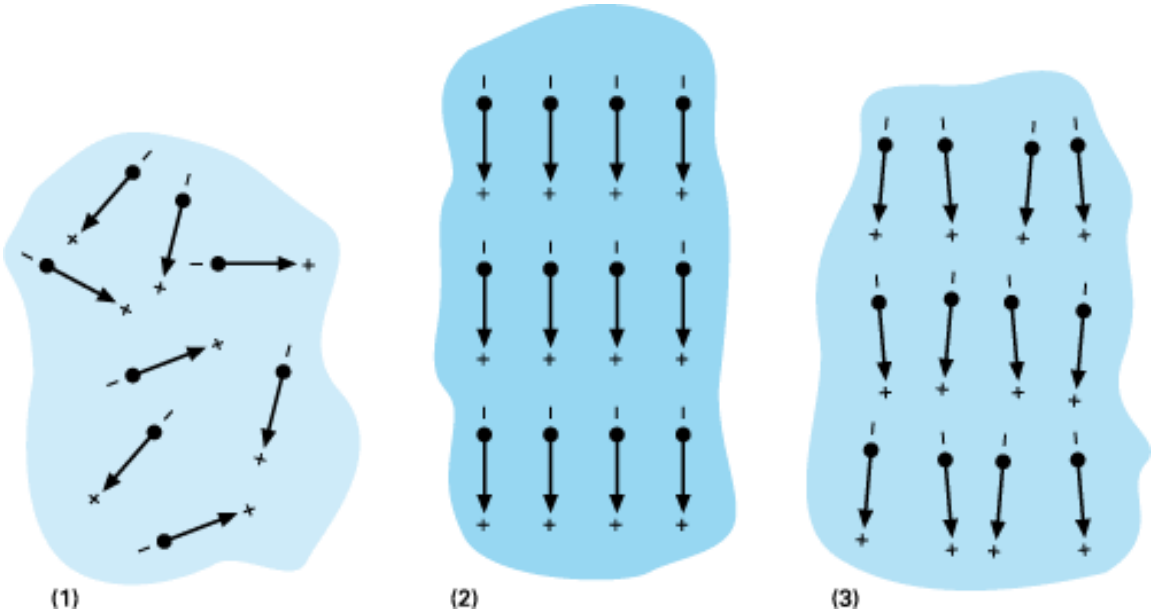

Figure 2.5. Dipole domain orientations; (1)Raw piezo ceramic; (2) During poling; (3)After poling.

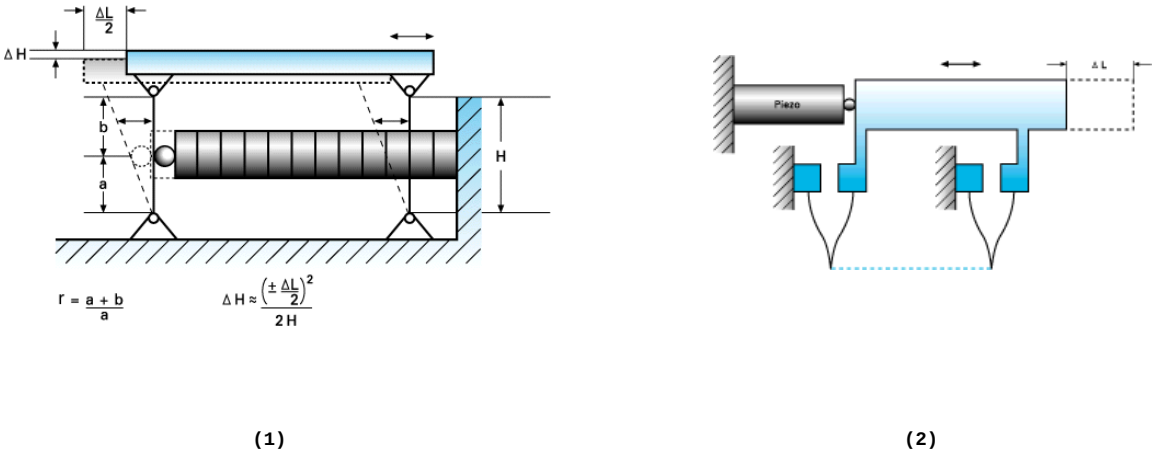

Figure 2.6. (1) Runout in typical positioners (transverse displacement ΔH) ;(2) Zero runout flexure guides.

be placed and the maximum forces that can be generated are greatly influenced by the construction of the guides/flexures used. The flexures are designed so that their dynamics are significant only at much higher frequencies when compared to those of the actuator. For this purpose, the zero-runout flexures used in the P753.11C are solid state flexures machined (by EDM) from a single piece with mass reduction and stiffness enhancement as the primary goals.

Two important assumptions made regarding the zero run-out flexures are:

- The guides serve to eliminate any transverse displacements. Hence they are flexible in the transverse direction.
- They are constructed in a manner that they are quite stiff in in the direction in which motion is to be transmitted, and their mass is minimal. Therefore their fundamental natural frequency is very high. Hence all the dynamics observed are that of the actuator as the natural frequencies of the flexure are not excited.
- There is no play in any of the joints. This is a valid assumption as the flexure hinges are machined out of a single piece of metal.

2.2. The Sensing System

Since the variable that is to be controlled is the position of the platform (or any load attached to it), a position sensor is integrated into the nano-positioning stage. The methods available to sense displacement or absolute position are resistive (strain gauges), capacitive or inductive (LVDT's). Among these alternatives, capacitive sensors offer the best resolution and highest dynamic bandwidth. Hence the P753.11 stage was obtained with the capacitive sensor.

The sensor in the flexure stage is integrated such that the actual displacement of the moving platform is measured. Together with the actuator and the guides the whole stage formed a compact monolithic structure (35 x 30 x 15 mm) in dimension (see Figure 2.7 on page 19).

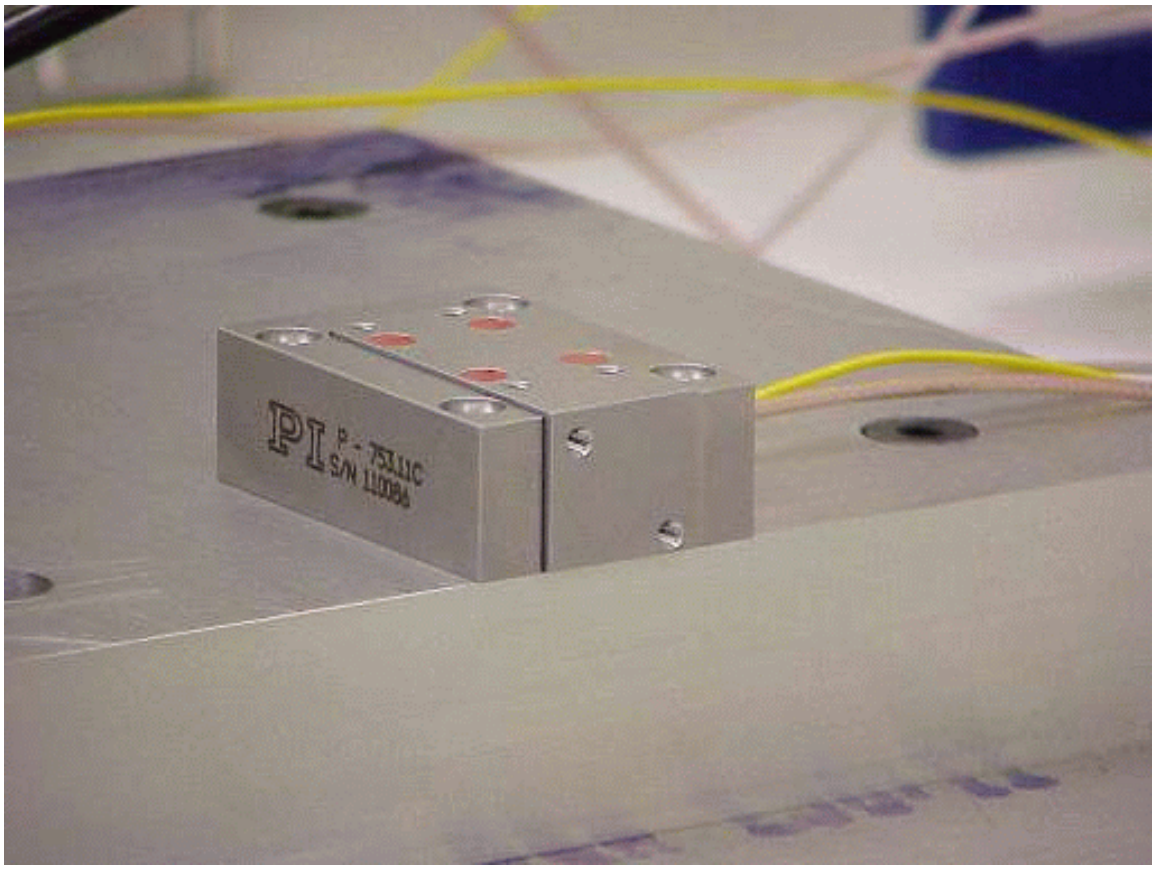

Figure 2.7. Photograph of actual nano-positioner used for experiments.

The sensing system is made up of the sensor and all the electronics used to process the output of the capacitive sensor. The capacitive sensor in the measurement system is a part of a capacitive bridge or a tuned resonant circuit. Thus any changes in the capacitance of the sensing plates is reflected as a change in the output voltage of the bridge or the resonant frequency of the circuit. The ratio of the capacitances in the bridge has to be chosen to achieve a good sensitivity.

The output of the bridge is typically a very low amplitude voltage signal (due to the very small displacements). The signal to noise ratio of this signal is very poor and therefore it has to be amplified and filtered to attenuate the noise. Also, the sensor

is inherently nonlinear, with an inverse dependence of the output voltage on the displacement of the actuator. The Integrated-Linearization-System (see Figure 2.8 on page 21), on the E509.C1 module is used to compensate for the nonlinear sensor characteristics.

The sensor and the closed loop system were calibrated by Polytec PI and the chart supplied is shown in Figure 2.9 on page 26. The first calibration chart is a plot of the control input to the amplifier against the actual displacement of the moving platform in a closed loop configuration (with PI's servo controller). The control input was increased slowly in small steps while allowing the actuator to allow to reach steady state at each step. The displacement of the stage is measured with an interferometer. Since the control input is varied in a quasi-static manner the error between the reference control input and the output i.e. the sensor output is zero (or close to zero limited by the noise resolution). Hence the sensor output is (almost) identical to the control input. The calibration chart indicates that the relationship between the actual position and the control input is highly linear (within 0.02% or 4 nm, which is within the noise limited measurement resolution of the sensor). Hence it can be inferred that the relationship between the actual position and the sensor output is also highly linear.

This can also be verified by conducting a simple test with a quasi-static input to the system and plotting the control input against the sensor output (in closed loop mode) as shown in Figure 2.10 on page 27. This plot is on a scale too large to observe any small nonlinear trends in the output of the sensor. For this purpose, the coefficients of a line that best fits the input-output characteristics of the sensor is determined from this input-output data. This was used to predict the output of the sensor based on the applied control input to the positioning system and the difference between the actual sensor output and the predicted sensor output is plotted in Figure 2.11 on page 28. As is apparent from this figure, the sensor characteristics are highly linear (limited by the noise resolution). The spikes seen in the plots are due to the noise in the sensor signal.

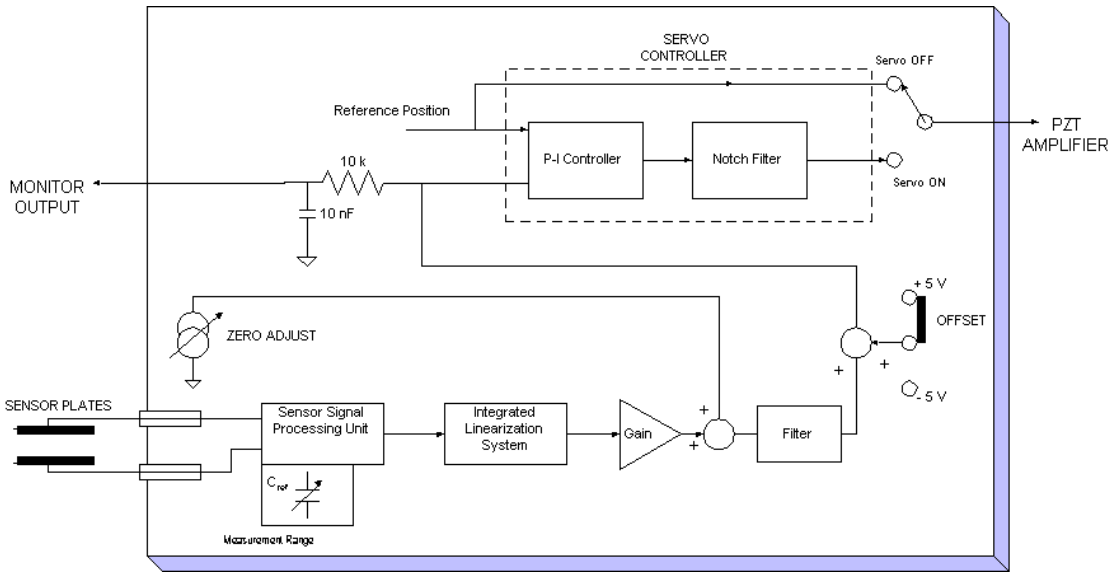

Figure 2.8. Schematic representation of Servo/Sensor electronics.

The sensor electronics includes a filter to attenuate the noise in the circuit. The servo bandwidth filter sets a limitation on the bandwidth of the closed loop servo system when using the controller card supplied by the manufacturer. For the experimental system, this bandwidth was initially set at 3 kHz. It has been increased further to approximately 10 kHz. This also allows a fair comparison between the performance of any controllers designed and the manufacturer's controller, as this servo bandwidth limitation does not have any effect on the sensor signal measured at the monitor output.

2.3. The Amplifier

The amplifier is a necessary component as the dSPACE controller card cannot put out enough electrical power to drive the actuator. Also to drive the positioning system to its full range of motion, the input voltage to the actuator should be +120 V whereas the maximum output voltage of the dSPACE card is +10 V. An important

factor to be considered before selecting amplifiers is their bandwidth. Ideally the amplifier should have an almost flat magnitude plot in its frequency response. But like all real systems, the amplifier has a finite bandwidth.

The chart shown in Figure 2.12 on page 29 is the frequency response of the E-505.00 amplifier for a 10 V (peak-peak) input signal. The multiple curves correspond to the variation of bandwidth with different piezoelectric actuators, indicated by their capacitance values in their relaxed state. The curve corresponding to the P753.11C actuator is the one for the 1.8 μf capacitance (fourth curve from the right). The units on the y-axis is the output amplitude (for the 10 V peak-peak input).

The reason that this is not given as a standard frequency response is that the frequency response varies with the capacitive load (from the piezoelectric amplifiers). The capacitance of the actuators varies with the amplitude of deflections. Hence this chart can be used to determine the frequency response for a 10 V (range) input sinusoid. But for lower amplitudes of the input (corresponding to smaller deflection of the actuator) the drop-off in the amplitude occurs at higher frequencies. Thus the curves in the figure can be used as a lower bound on the bandwidth of the amplifier.

The control input (from the DSP card) passes through a *slew-rate limiting circuit* before it is actually amplified and sent to the piezoelectric actuator. This is used to limit the current being drawn by the positioning stage from the amplifier. The limit can be varied between 15 V/ms to 1500 V/ms. This has currently been set to 1500 V/ms and hence it is important to ensure that the control input being sent from the DSP card does not posses a slew rate higher than this value, in order to neglect dynamics arising from this limiter.

The amplifier used with the nano-positioner is the E505.00 amplifier. The specifications for the amplifier are given in Table 2.2 on page 23. The output voltage of the amplifier can be controlled by two means,

External Input This is useful when the amplifier and the positioning system are to be a part of a control loop. The controller performs the computation of the required control input and sends an appropriate signal to this input terminal.

DC Offset Potentiometer This is used to provide a constant offset in the output voltage signal. A 10 turn potentiometer is used to implement this component. The output voltage can be varied from 0-100 V using this potentiometer.

Table 2.2. Specifications of E505.00 Amplifier.

CHARACTERISTIC	VALUES
Maximum Output Power	200 W
Average Output Power	30 W
Peak Output Current	2 A (¡ 5ms)
Average Output Current	300 mA
Voltage Gain (quasi-static applications)	10 ± 0.1
Control Input voltage range	-2 V – 12 V
Output Voltage Range	-20 V – 120 V
DC Offset Setting	0 V – 100 V(with 10 turn potentiometer)
Output Voltage Socket Type	LEMO ERA.00.250.CTL

2.3.1. The Controller/DSP System

The essential part of the closed loop system is the controller. The controller is implemented on a dSPACE's© DS1103 Digital Signal Processing card. This DSP controller card plugs-into the slots on the motherboard of a PC. It has the hardware circuits for A/D (for reading the sensor output) and D/A (to send the control input to the amplifier) built into it. Since this card also possesses a microprocessor, it can be used for real-time control applications. The control algorithms are built as SIMULINK blocks on the host PC (the motherboard onto which the DSP card is plugged in) which are then translated into C code which is compiled and downloaded onto the processor on the DSP card.

The signal from the monitor output of the sensor electronics is sampled using a 16 bit A/D converter. The maximum sampling rate possible on these converters is 125 kHz (corresponding to an A/D conversion time of 4 $\mu secs$). The conversion time for the D/A converter is around $6\mu secs$. Hence if real time control is to be implemented then the maximum sampling rate for the control algorithm should be much less than 100 kHz. To ensure proper working of the A/D and the D/A converters and to allow enough computation time for the control algorithm, the maximum sampling rate that is usually used is 50 kHz.

2.4. Interfacing & Component Selection Issues

The crucial factor that influences t he achievable bandwidth and positioning resolution is the interfacing between the various components in the loop. As the capacitive sensors offer almost an infinite position measurement resolution, it is natural to want to optimize the other components in the loop so that the positioning accuracy can be achieved.

For the P753.11 system under consideration, the position measurement resolution of the capacitive sensor is limited by the noise introduced into the measurement circuit. The noise level was experimentally determined to be in the range of $\approx \pm 2.5\, mV$ (Figure 2.13 . This corresponds to a position measurement resolution of about 6 nm.

Hence it has to be ensured that the other components i.e. the controller, amplifier and the positioning stage do not limit the achievable positioning accuracy. In this regard the important factors are the quantization by the A/D and the D/A converters. The A/D converters possess a word length of 16 bits. The range of the converters is ± 10 V. Hence the minimum change in the voltage that can be detected by the computer corresponds to a change in the least significant bit. This is about 0.3 mV. Thus the quantization by the A/D converters is not a problem as the noise resolution is much greater (by an order of magnitude). The D/A converters on the dSPACE controller have a word length of 14 bits with an output voltage range of ± 10 V. Thus

the minimum change in the voltage that can be effected at the output of the D/A converter is 1.22 mV. This is again lower than the noise resolution. Hence in terms of achievable positioning resolution, we see that the limiting factor is the noise in the system which effectively limits the positioning accuracy to about 5 nm.

The achievable bandwidth of the closed loop system is limited by the bandwidth of each of the components in the loop. From linear analysis the closed loop bandwidth lies roughly within the range $\omega_{gc} - 2\,\omega_{gc}$ where ω_{gc} is the gain crossover frequency of the system. The natural frequency of the positioning stage is around 5.6 kHz (from both specification and experimental verification). Hence the controller should be able to sample at least at 60 kHz, to neglect sampling effects and implement continuous time control algorithms on the DSP controller. Since the maximum sampling rate that could be used for real time control algorithms while allowing for sampling and conversion was around 50 kHz as discussed before.

To circumvent this apparent conflict two solution were investigated. The first one is to design control algorithms in the discrete domain and the second one is to lower the natural frequency of the actuator so that lower sampling rates can be used while still adopting the continuous-time design principles. The second method is a more straight-forward approach as it merely involved adding a mass onto the moving platform of the flexure stage. As described in the following chapters even this would not be necessary in cases when the actuator is operated at very low frequencies as the natural frequencies of the positioning system are not excited by the low input signal frequencies.

The above is a description of the existing physical system and also the factors that one has to account for before even purchasing a commercial system for experimental work. The next chapter is aimed at studying the behavior of the system to different typical reference input signals and the inferences that could be drawn from the observed behavior of the system.

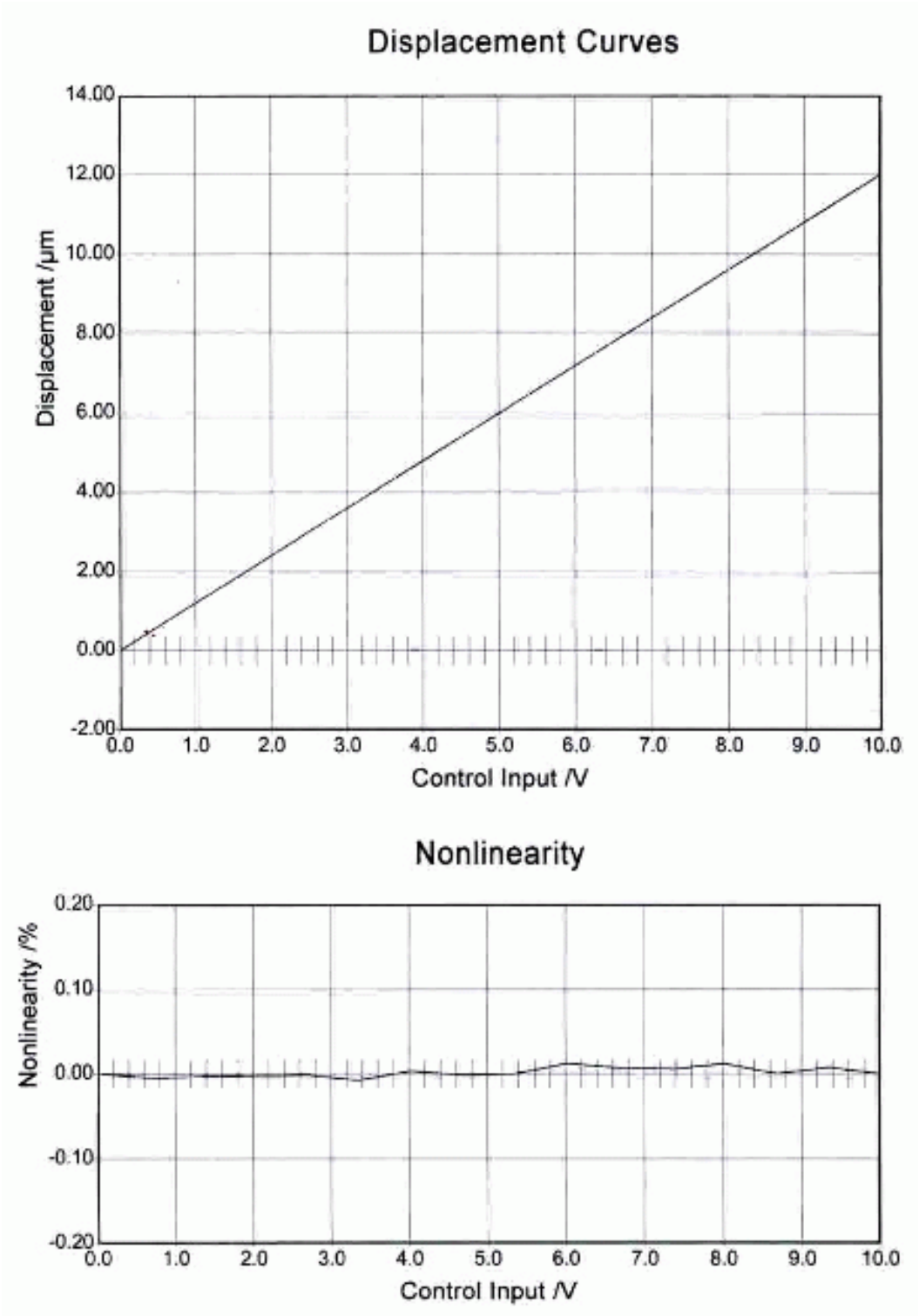

Figure 2.9. Calibration chart (supplied by the manufacturer) for the positioning system.

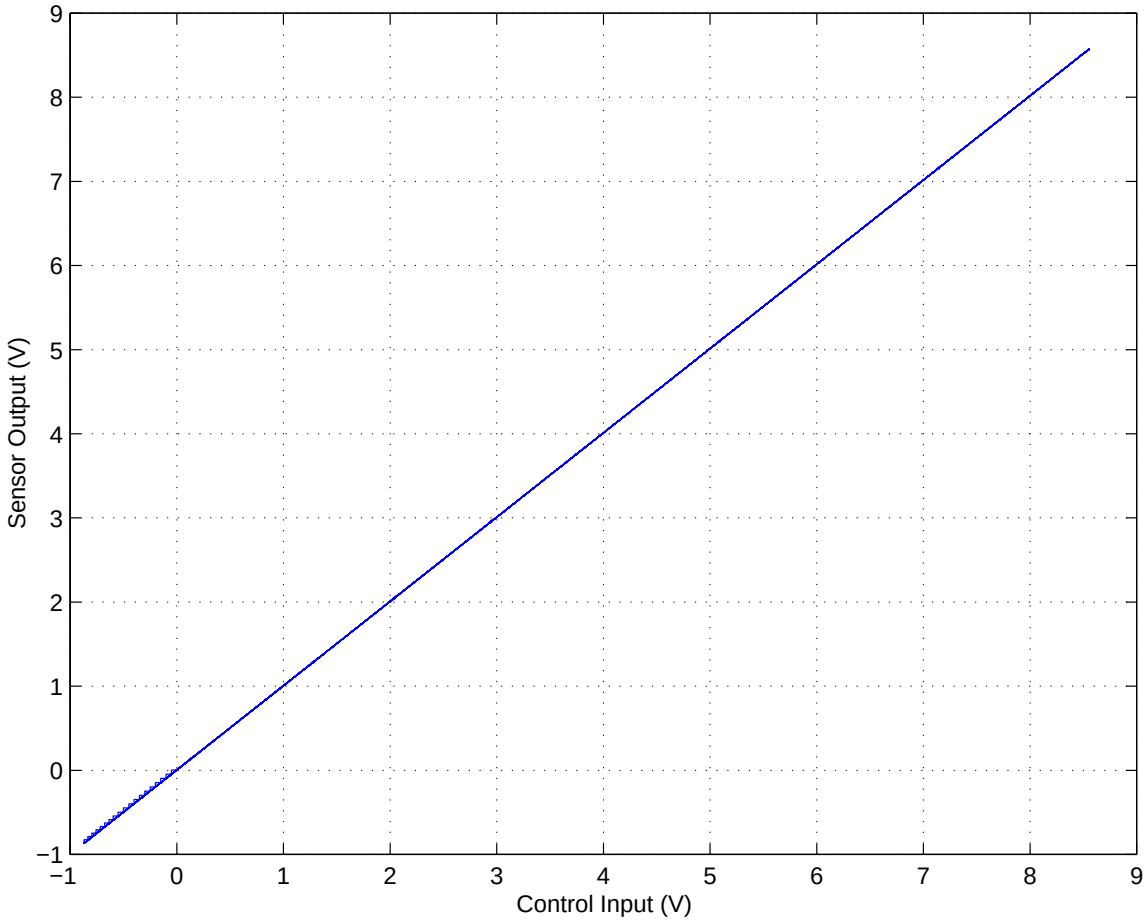

Figure 2.10. Control Input vs. Sensor Output to illustrate linearity of sensor output.

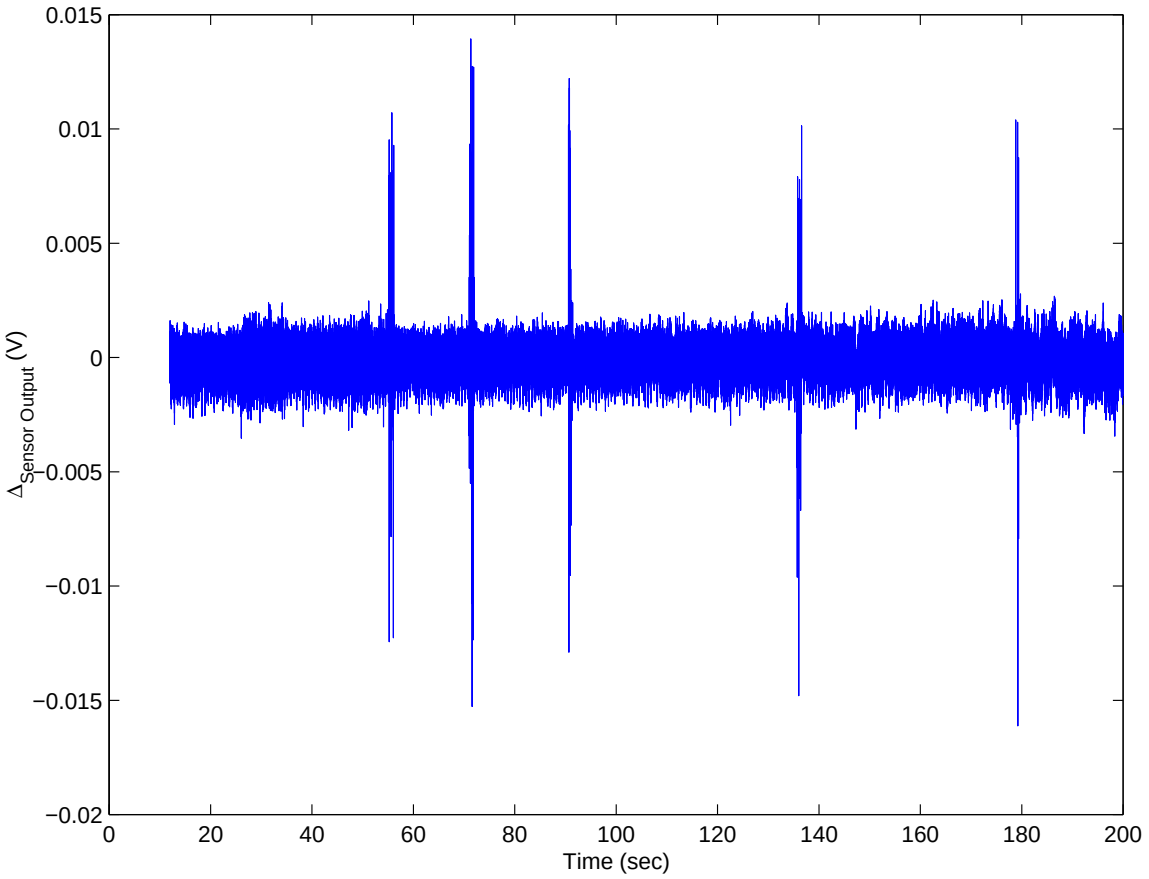

Figure 2.11. Difference in the actual sensor output versus the predicted sensor output (based on a least squares fit from the data in the sensor calibration chart.

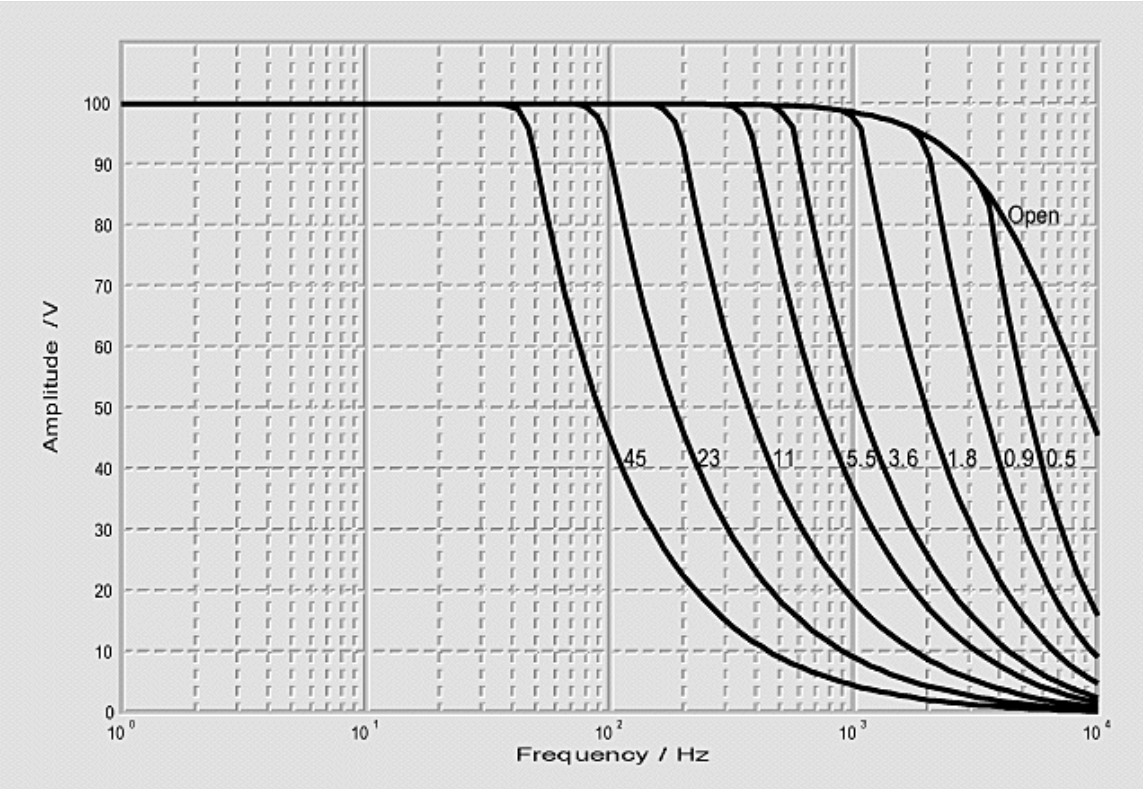

Figure 2.12. Dynamic response of E505.00 amplifier; Values of capacitances on graph are in μf.

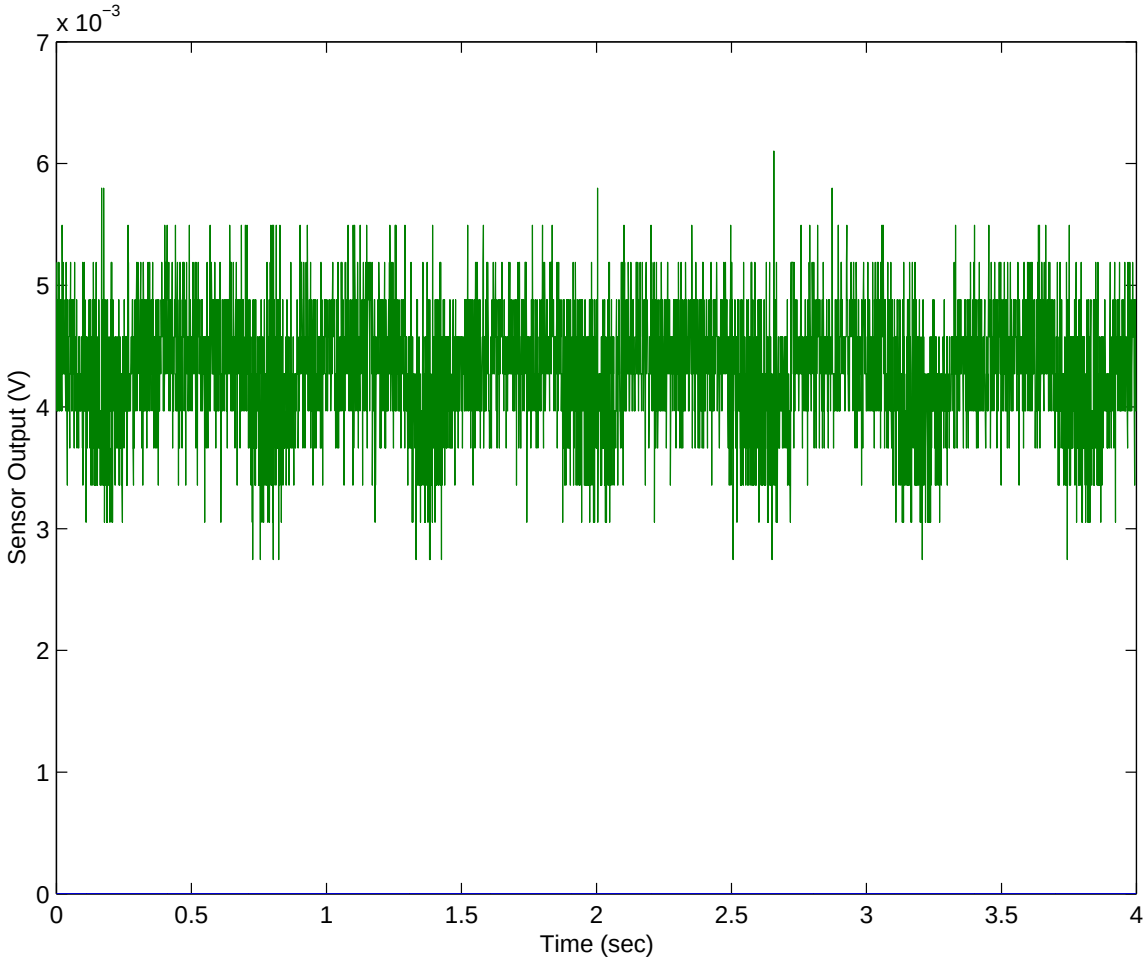

Figure 2.13. Noise level in the sensor monitor output signal.

3. SYSTEM CHARACTERISTICS & SIGNIFICANT PHENOMENA

Mathematical modelling of a system involves developing constitutive equations describing the input-output characteristics of the system. It is very crucial, especially in the context of model based controllers, to have a very good representation of the dynamics of the system to achieve the best performance from the system despite changes in the operating conditions and even in system parameters. In case of such variations, if a very poor plant model is used for the controller design, even though robustly designed controllers will be able to stabilize the plant, the performance will be far from optimal.

Most real-life systems even though are designed based on simple principles and phenomena, give rise to very complex models when one that describes all the relevant phenomena are included. For example, even a hypothetical case as in a mass sliding on a surface could be very difficult to analyze if the friction force on the block is to be modelled in all domains of operation. At low velocities, dynamic friction and stiction are dominant and to date, no complete model exists for these phenomena.

Hence simplification of models has to be performed on almost all complete system models. This is done usually by restricting the operating conditions or making assumptions about the system. This is essential even more so for model based controllers, as complicated design models make the stability analysis and control design extremely difficult. Some examples of such simplifications: Neglecting higher order dynamics, in distributed systems, when they occur at much higher frequencies which result in lower order models. In the case of the sliding block, if an assumption that the velocities are relatively large is made, then the friction model that could be used is a simple coulomb friction model. Making these simplifications and assumptions requires that one knows what the significant factors that affect the behavior of the

system are. For the sliding mass example, one ought to determine what ranges of velocities allow the appropriate approximations in the friction model to be made.

Therefore, for the piezoelectric positioning system, one has to understand the physical phenomena and the behavior of the overall system before developing mathematical models for the system. This chapter is focussed at trying to get a better understanding of the P753.11C positioning system's behavior. Experimental results are shown to illustrate the behavior of the system. Trends in the behavior observed are also brought forth by means of experiments. This is to help during the modelling to decide which of the observed phenomena are significant and should be captured by the model.

3.1. Step Inputs

These are some one of the simplest tests that could be performed. The information that could be obtained from the step response is about the order dominance, delays in the response, the static gain of the system and also about the presence of any nonlinearities in the system. The step response of the piezoelectric nano-positioning system over 1 hour is shown in Figure 3.1 on page 33.

From Figure 3.1 it is apparent that the system seems to posses a multiple-time-scale behavior. The response consists of a very quick component and then a very slow component which seems to reach steady state over approximately 2000 secs. A zoomed in plot of Figure 3.1 on page 33 is shown in Figure 3.2 on page 34.

In Figure 3.2 the fast dynamics are not seen clearly due to the low sampling rates used (to facilitate collection of data over long periods of time). Figure 3.3 on page 35 shows the fast dynamics to be clearly oscillatory.

Also the zoomed-in view on the amplitude axis of Figure 3.1 allows to observe the drifting behavior much clearly (Figure 3.4 on page 36). This plot indicates that the response still has not quite reached steady state (even after 1 hour). For all practical purposes, the response over this time scale is of no use when dealing with

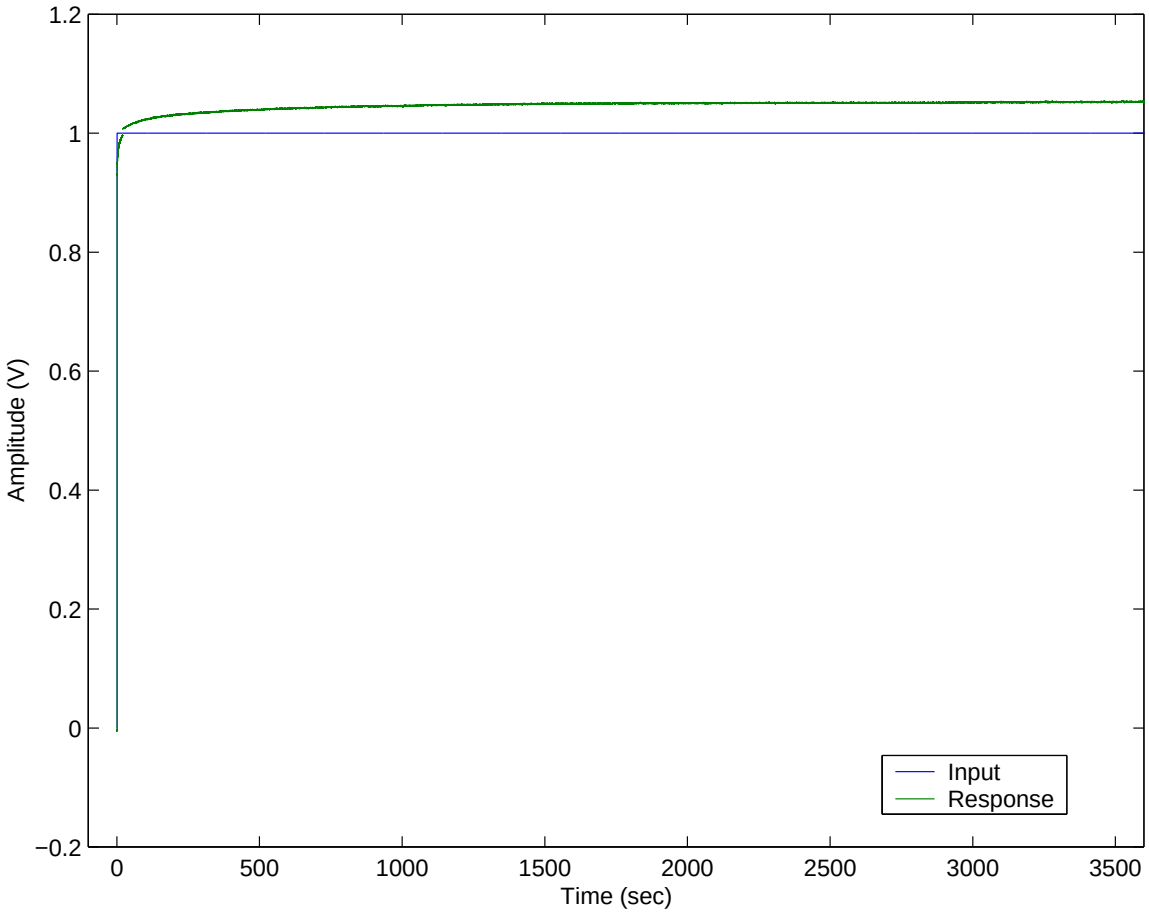

Figure 3.1. Step response of the positioning system (over 1 hour).

piezo-actuators (as they are used mainly for their fast dynamic response). Hence the dynamics of this time scale (1 hour or greater) can be treated as a drift in the response of the system.

The plots in Figure 3.4 and Figure 3.3 illustrate the time scales of the behavior exhibited by the piezoelectric positioning system. Figure 3.3 indicates that the fast dynamics of the system might be dominated by second order dynamics (with a large natural frequency). Figure 3.4 indicates that the large time scale behavior is dominated by over-damped terms.

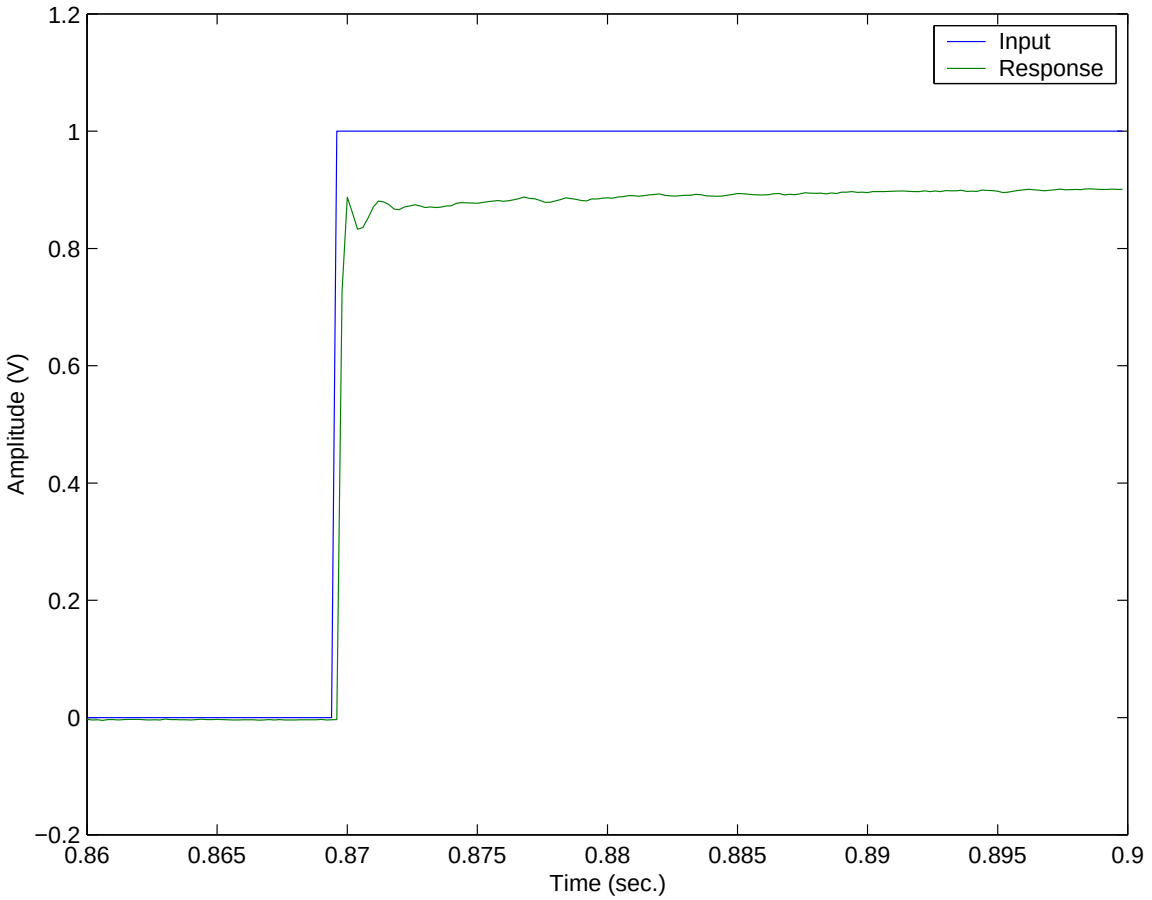

Figure 3.2. Zoomed view of overall step response showing the fast component of response (response appears non-smooth due to the low sampling rates used).

Figure 3.1 on page 33 is the response to a single step input. When the same test was performed with step inputs of different heights, some interesting effects were observed. Figure 3.5 on page 37 shows the large time scale ($\approx$ 20 secs.) behavior for different heights of the reference input.

From the plots of the responses to inputs of different step heights, it is obvious that the static gain of the response over a period of about 600 seconds is not a constant. As previously noted, the response consists of two components. To identify the source of this nonlinear behavior, it is necessary to examine the two components

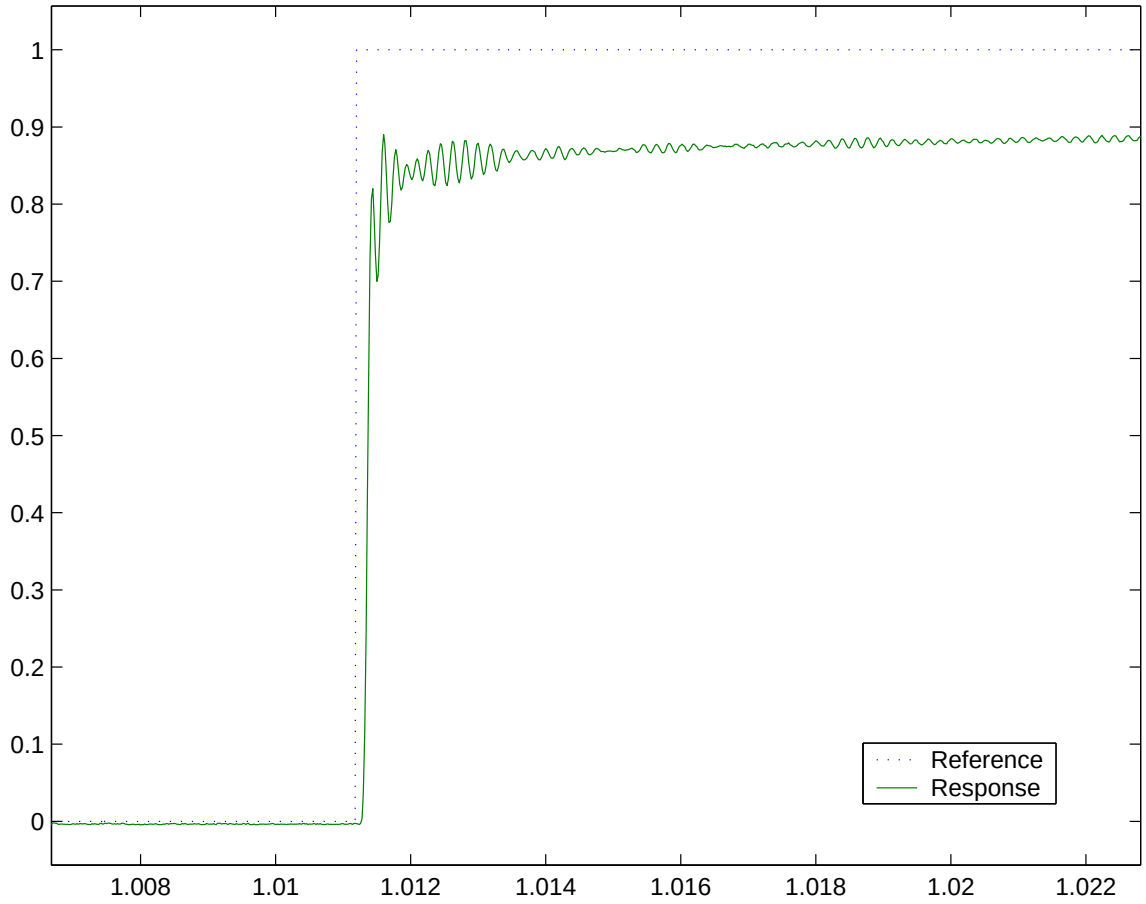

Figure 3.3. Zoomed view of overall step response the oscillatory nature of the fast response (sampling rate:50 kHz).

of the responses by themselves. At first the fast component is examined to see if after a specified interval of time (after the step occurs in the input), the response has a constant gain. Then the static gain of the slow component is examined in the same way, but starting from the instant of time when it is assumed that the fast components have died out. Figure 3.6 on page 38, Figure 3.7 on page 39 and Figure 3.8 on page 40, Figure 3.9 on page 41 illustrate how these gains vary with experimental conditions. In the computation of the static gain for the fast component, the time interval (5 msec.) is chosen based on the time taken for the oscillations to die out in Figure 3.3 on

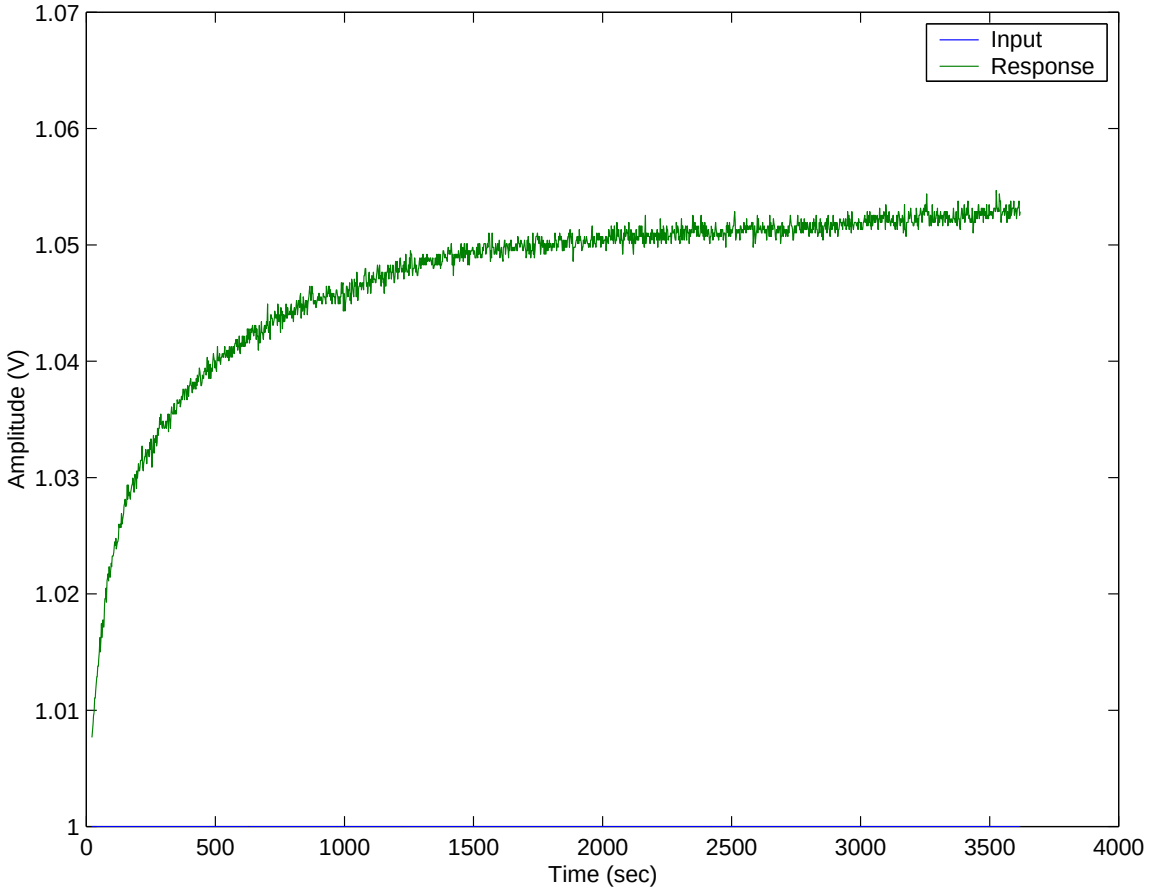

Figure 3.4. Zoomed view (on the y axis) of overall step response showing the drift in the response.

page 35 and the fact that after the oscillations die out, the response seems to be dominated by the slow components in the response.

To check the variation of the static gain with respect to the height of the step input, the static gains were calculated for both the fast response and the drift in the output (over a fixed period of about 600 seconds). This period was chosen as after about 600 seconds, the drift in the output with respect to the height of the step input is very small.

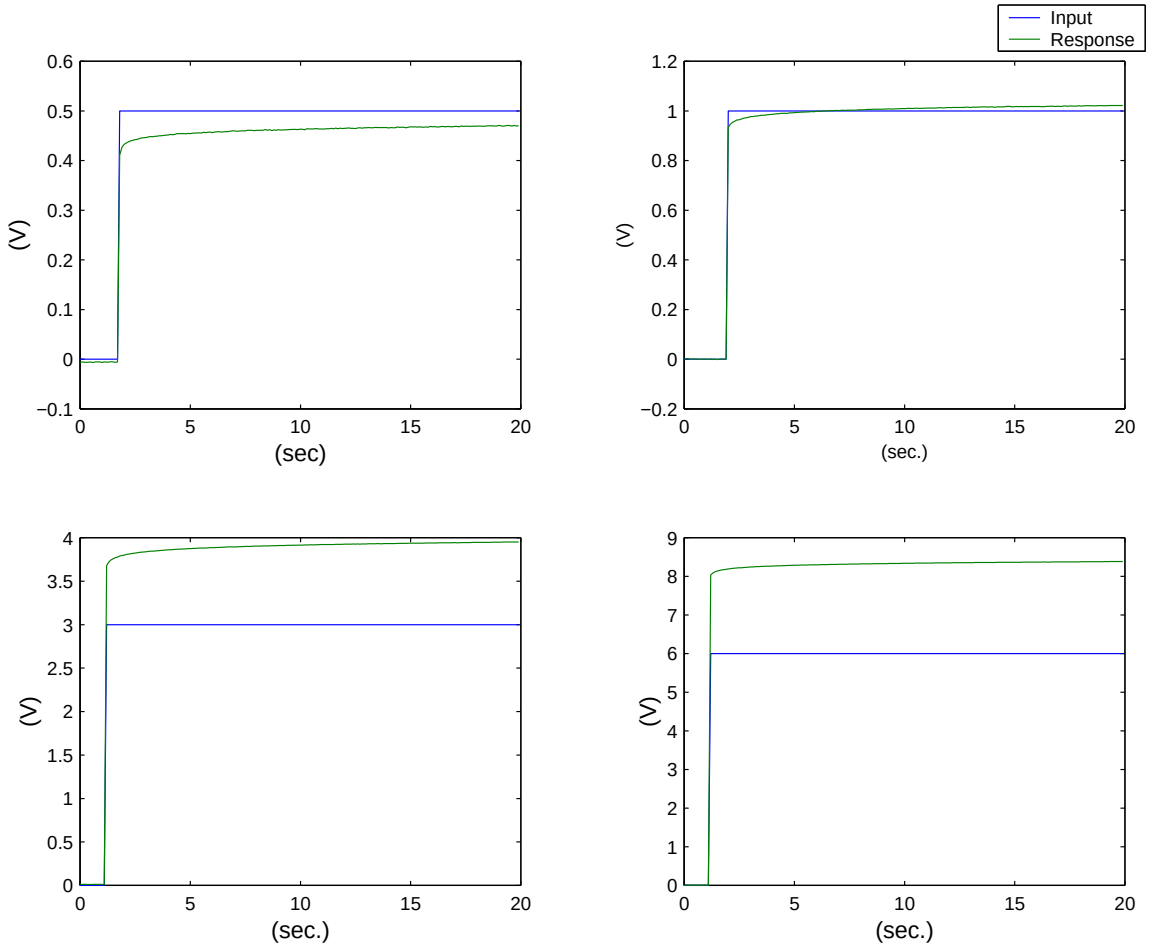

Figure 3.5. Step responses of positioning system to different step heights (y axis is in volts); Note the drift and the non-linear behavior of the response.

The trends observed in the static gain are shown in Figure 3.10 on page 42. It is of interest to note that both the gains show an almost linear variation and a proportional increase with respect to the input step height.

The response observed is also in agreement with the published experimental results with several authors (Croft et al. [40]; Kuhnen and Janocha [37, 38] etc.).

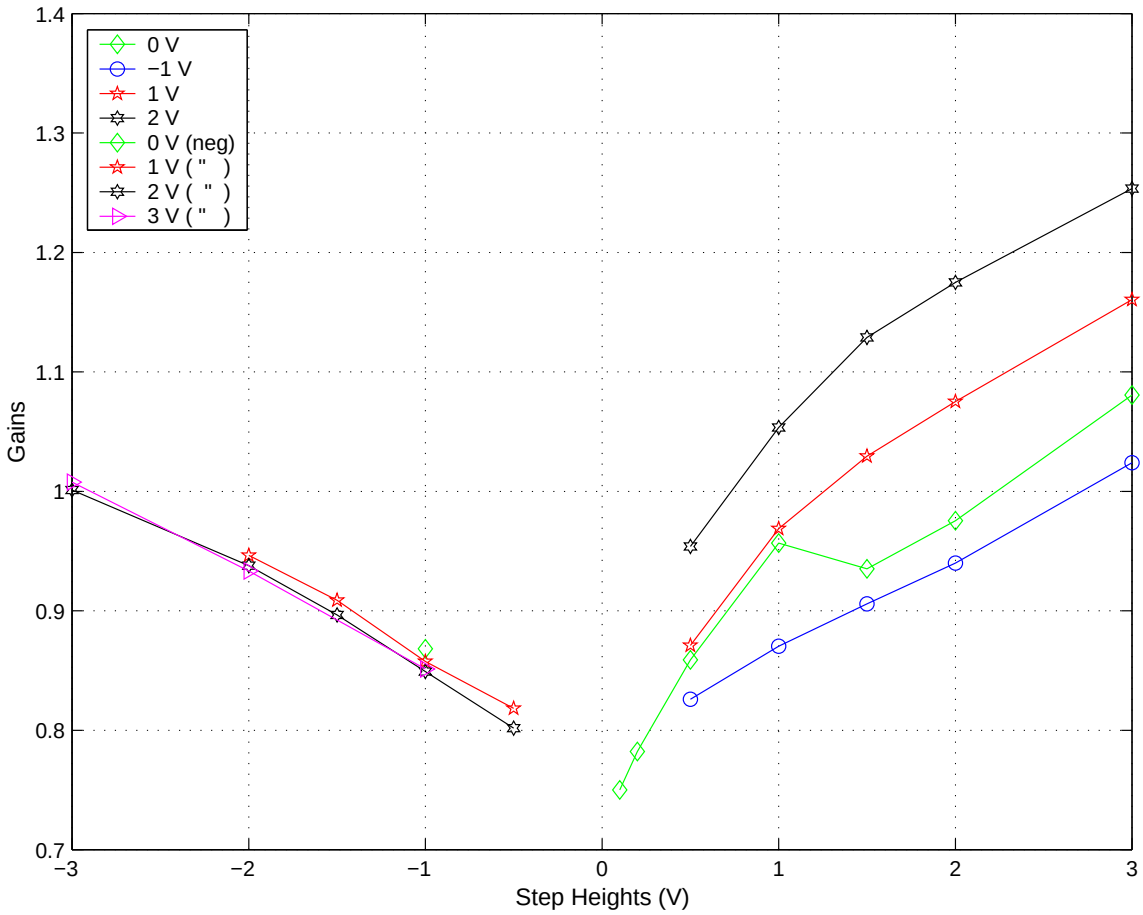

Figure 3.6. Variation of gain versus step heights for different starting values and step directions.

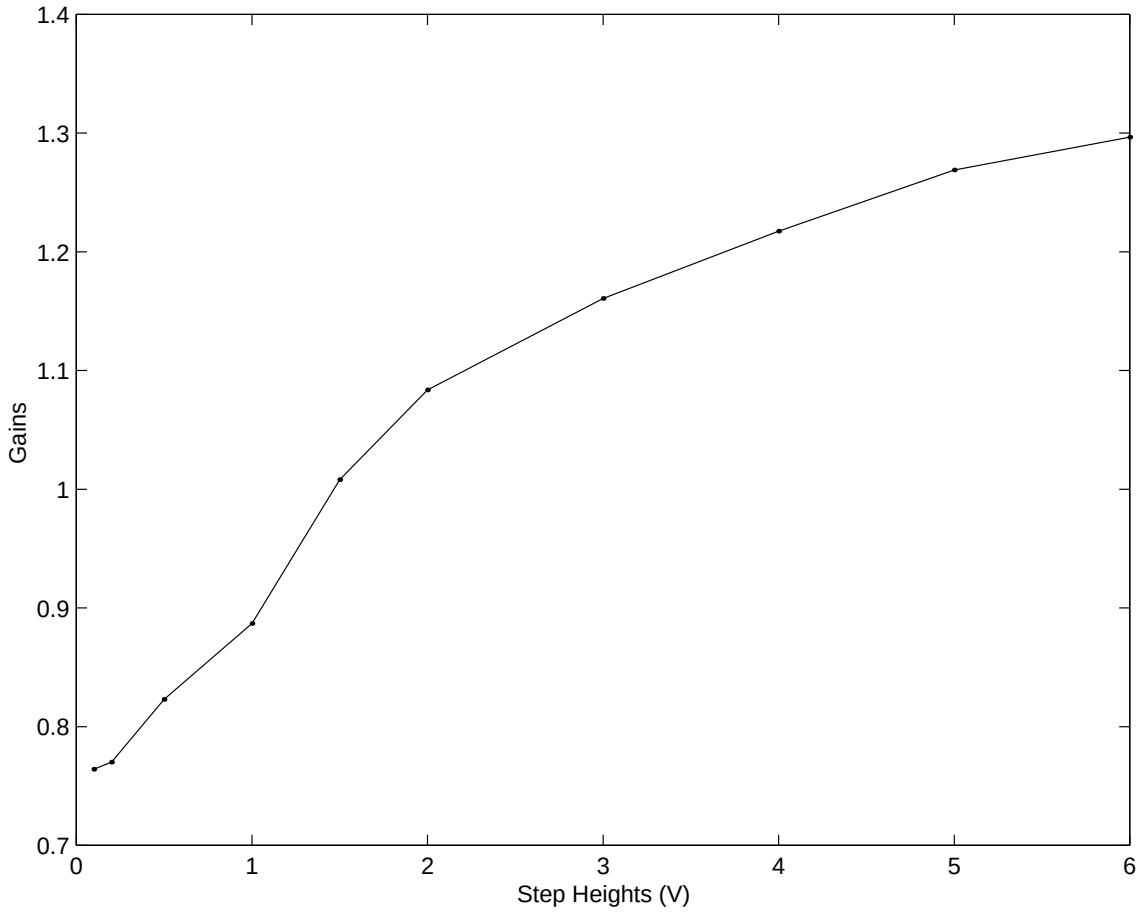

Figure 3.7. Gains of fast response versus step input heights, for step input starting at 0 V.

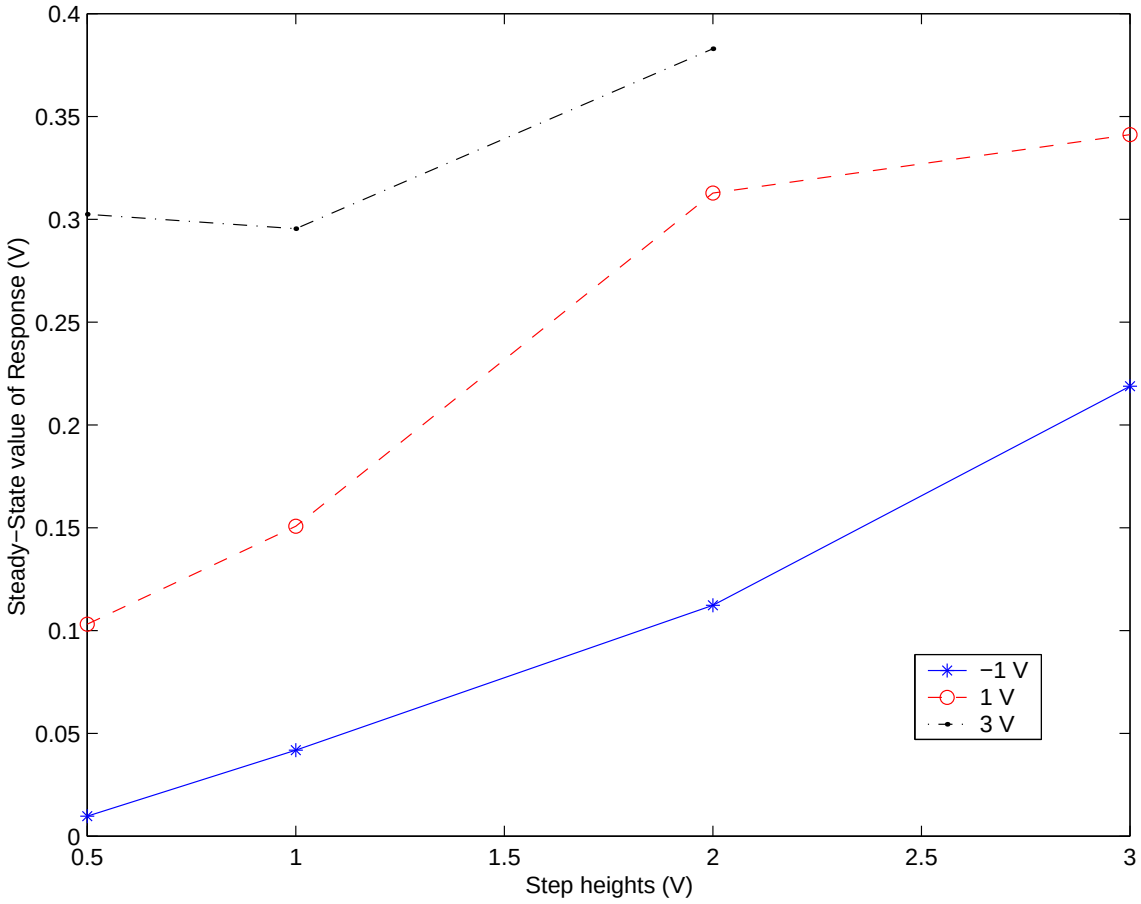

Figure 3.8. Variation of gain of drift with respect to step heights for different step starting values.

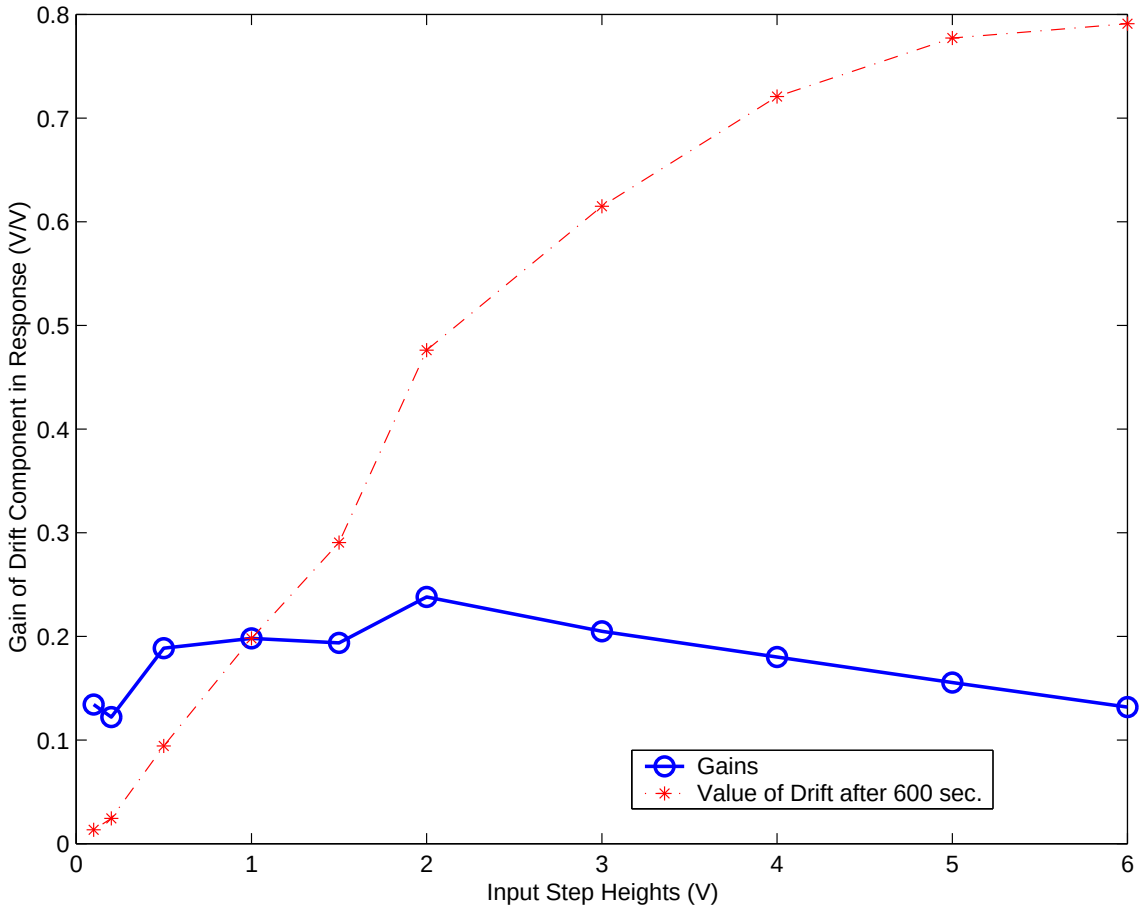

Figure 3.9. Gain of drift component versus step heights for 0 V starting values.

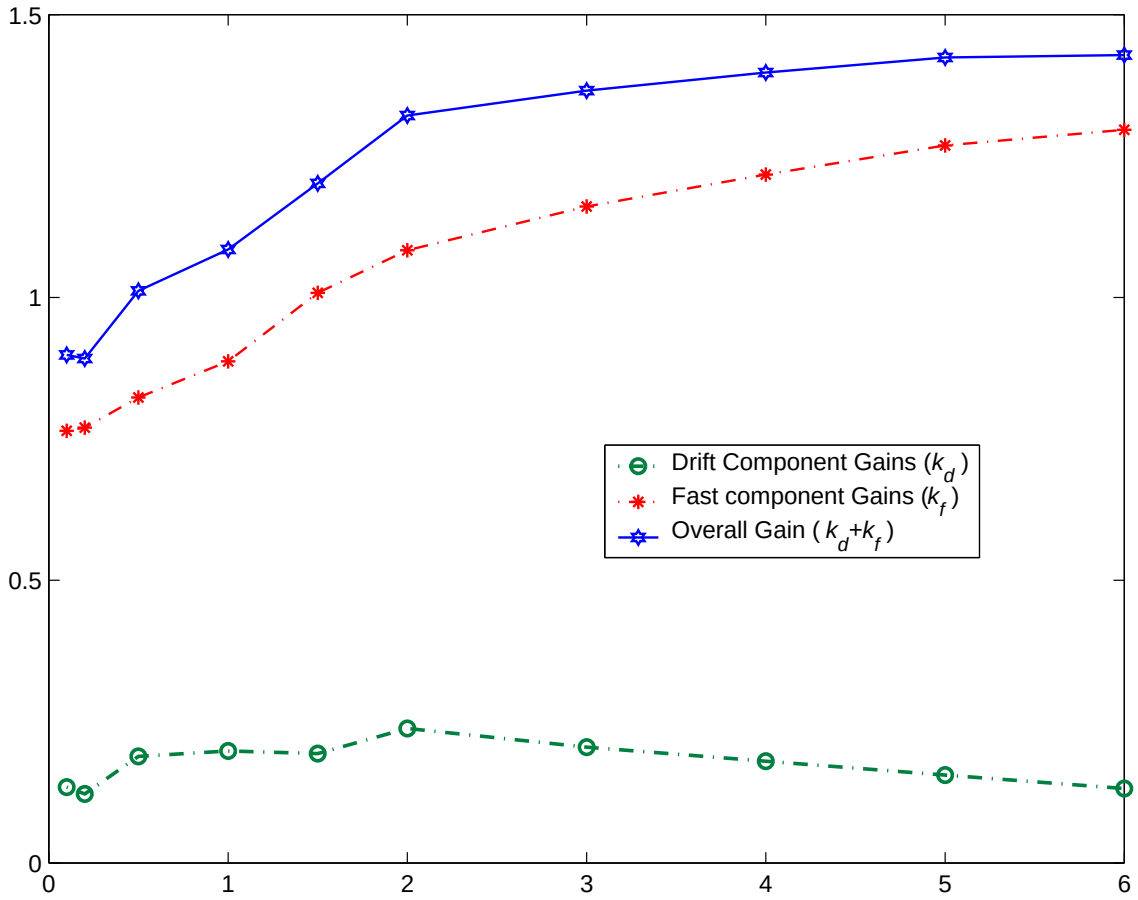

Figure 3.10. Variation of Gains of fast and slow component in response with respect to the height of the step inputs.

3.2. Cyclic/Periodic Inputs

These kinds of inputs are the most common type of inputs experienced by actuators during actual operation (during which they perform the same/similar task repetitively). Therefore it is of interest to see of any unusual behavior is observed in the response to these types of inputs.

3.2.1. Sinusoidal Inputs

Sinusoidal inputs are useful as they are smoothly varying inputs and also if the system is linear then, the response to any kind of input can be expressed as the combination of the responses to sinusoids (Fourier Transformation and superposition principles).

The nano-positioning system was subjected to sinusoidal inputs of different frequencies starting from 0.01-50 Hz (with a 3 V peak-peak sinusoid). When a linear system is excited with a sinusoidal input at a very low frequency, the plot of the output versus the input is almost a straight line. But for the hysteretic system, we see (in Figure 3.13 on page 46) that even at about 0.01 Hz (Figure 3.12 on page 45), there is a significant loop formed in the input-output plane. This loop indicates that there is a significant phase lag between the input and the output even at low input frequencies. If this system were linear, then based on the frequency response (Figure 3.26 on page 59) and the step response (Figure 3.2 on page 34) the phase lag should be almost zero (as the bandwidth of the system seems to be quite high). Hence there exists some type of nonlinearity in the system that is reflected as a phase lag in the system, even at 0.01 Hz.

One of the most well known nonlinearities that is talked about when referring to any solid state actuator (especially a piezoelectric material), is the Hysteresis effect. It has been generally agreed upon explanation that hysteresis is physically caused due to the delay in the response of the dipole domains in the piezoelectric actuator to a change in the direction of the applied electric field. This delay would be reflected as a phase lag in the response of the piezoelectric actuator when the input reverses direction. This phase lag is reflected as a loop (for sinusoidal inputs) in the I-O plot for the system.

Another interesting observation that could be made from Figure 3.13 on page 46 is that the width of the loop remains almost a constant for a significant range of frequencies. For a linear system the loop observed due to the linear dynamic phase lag would increase with increase in the frequency of the sinusoidal input. This is an indication

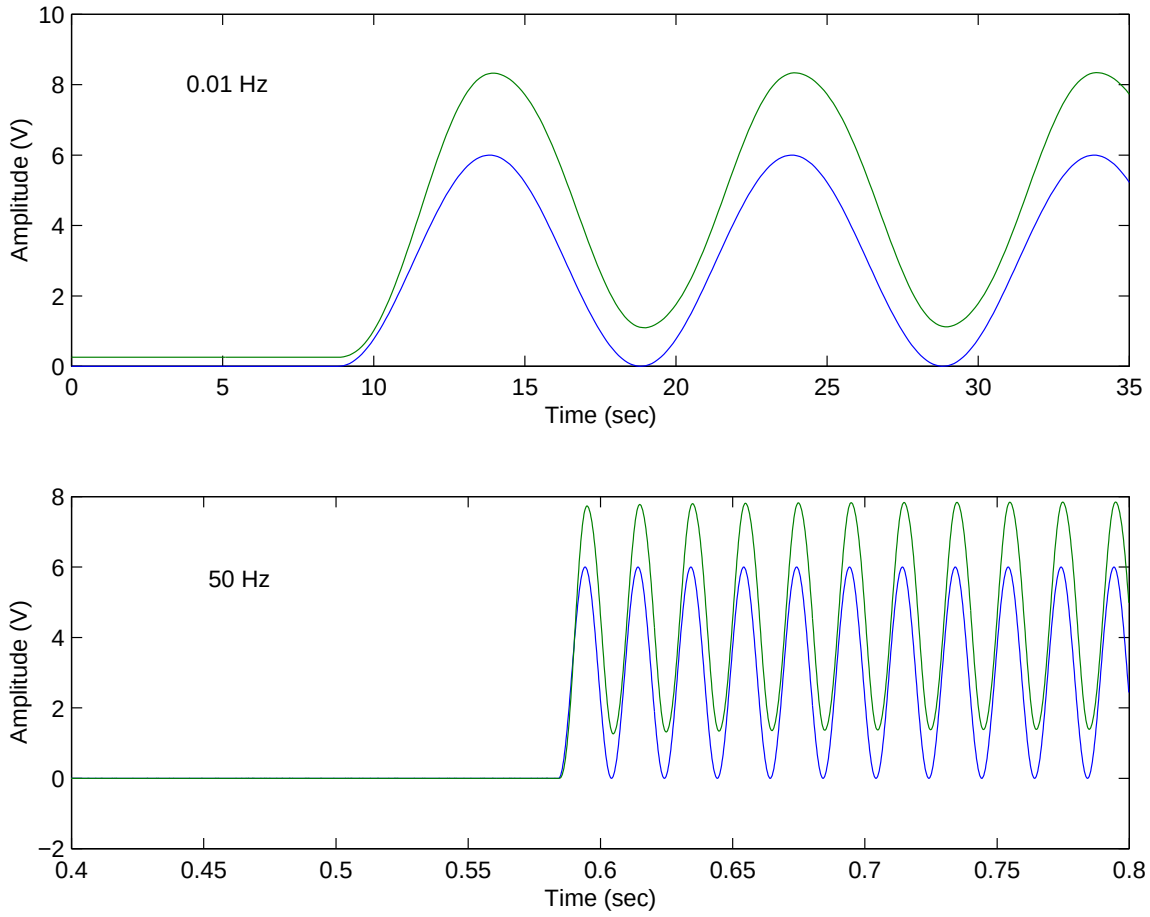

Figure 3.11. Input-Response data used for obtaining hysteresis loops at different frequencies for sinusoids.

that hysteresis appears to be a static nonlinearity (frequency/rate independent). This will be further corroborated with other tests later.

The characteristics of a hysteresis loop that are of interest are shown in Figure 3.14 on page 47.

As in the case of the empirical study of the static gain variation, tests were performed to determine any variation in the quantities of interest shown in Figure 3.14 . These quantities were computed from the hysteresis loops obtained at different frequencies. The variation of these quantities are shown in Figure 3.15 on page 48.

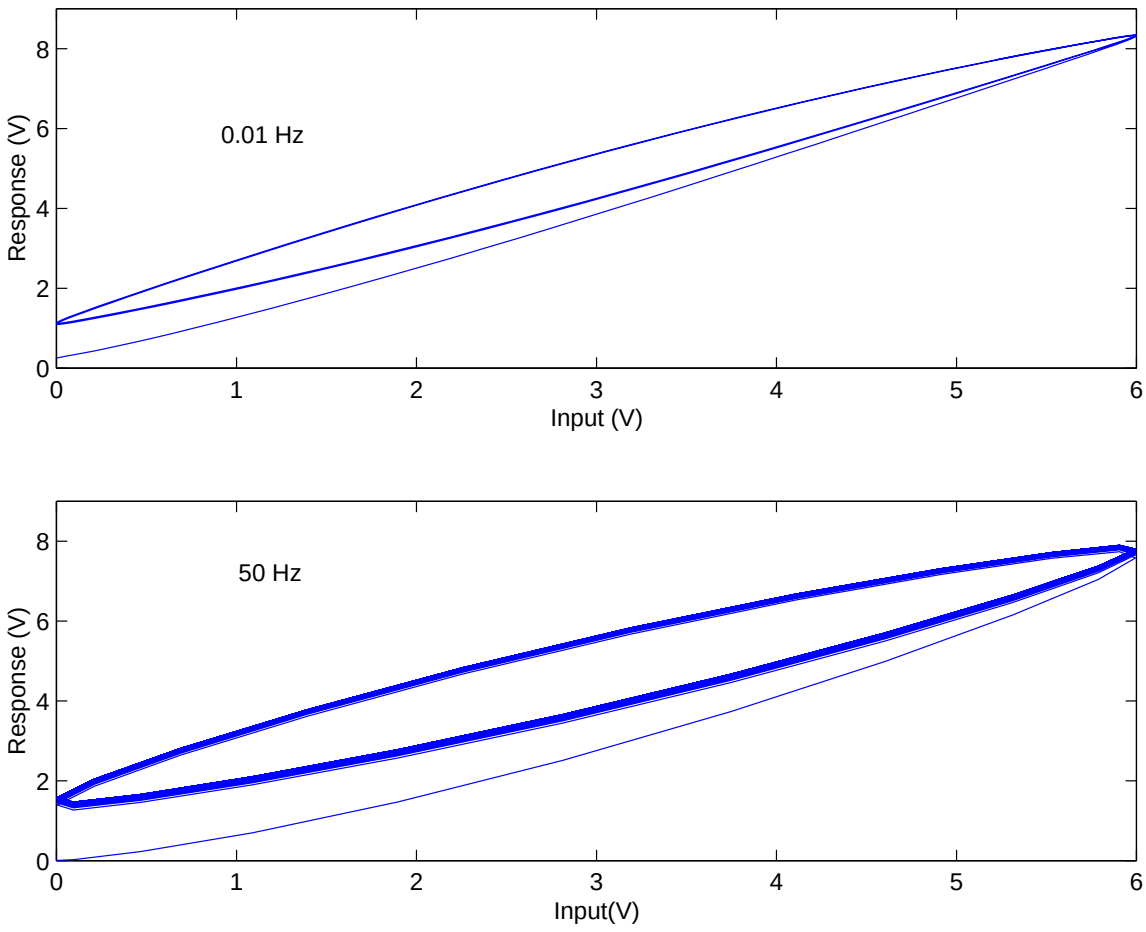

Figure 3.12. Hysteresis loops at different frequencies for sinusoids. (data shown is only for the first few cycles).

In addition, tests were performed in which the amplitude of the input to the system was varied (Figure 3.16 on page 49) and so was the offset (Figure 3.17 on page 50) of the input so that loops were obtained around different locations in the I-O plane. The frequency in the above tests was kept a constant at 1 Hz. These plots show that the hysteresis loops due to the inputs of the same amplitude are very similar even if they occur about different mid-points and also the smaller the input amplitude, the smaller is the distortion (loop) of the output.

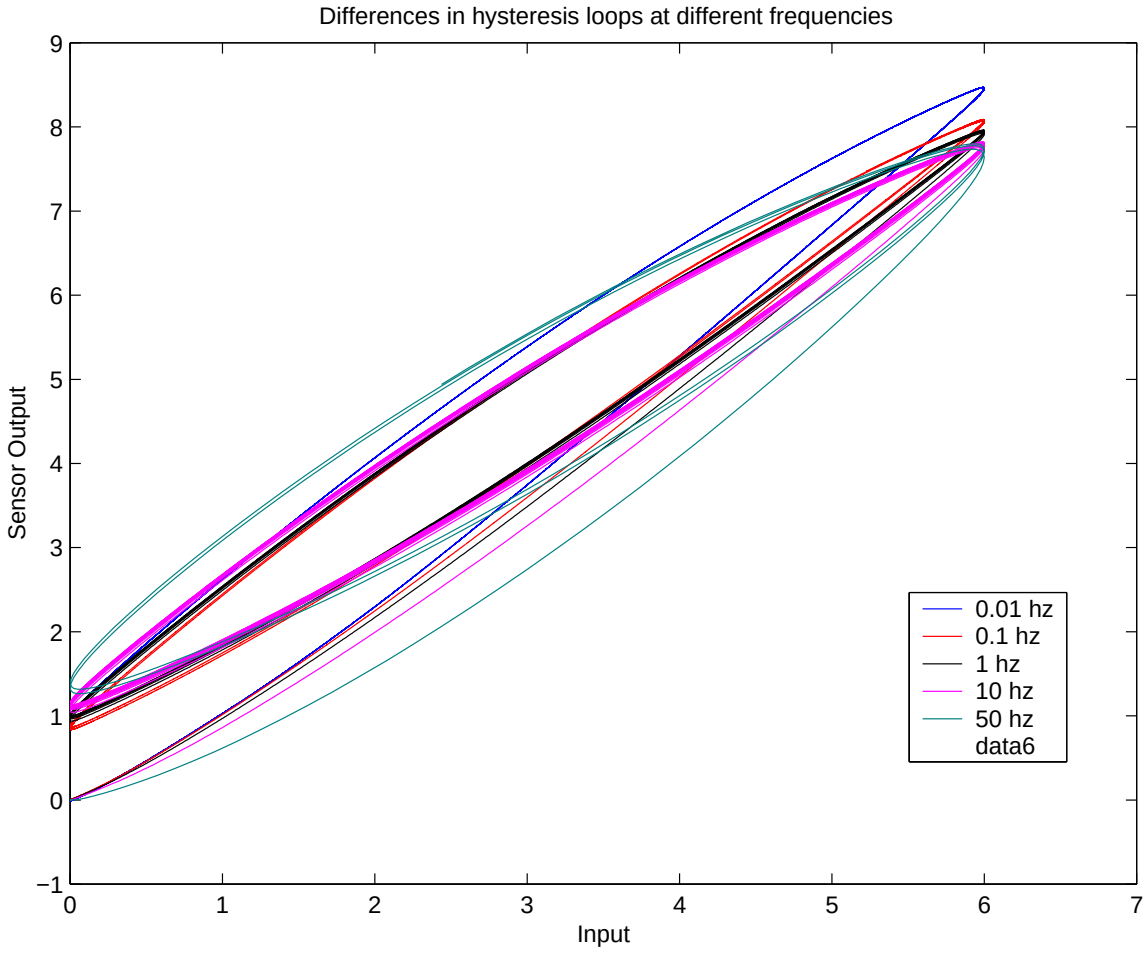

Figure 3.13. Superimposed loops at different frequencies for sinusoids.

A gradual upward shift in the hysteresis loops (as is seen in the time plots in Figure 3.18 on page 51) was also observed in these tests. When the time histories of the input and the output signals are plotted, then a shift in the mean value of the output was seen, very similar to the drift in the output of the system for a step input. In fact this drift in the mean value could be thought of as the response of the system to the offset in the input signal (DC value of the input signal is non-zero).

A detailed experimental study of this relation between the drifts is not performed in this study.

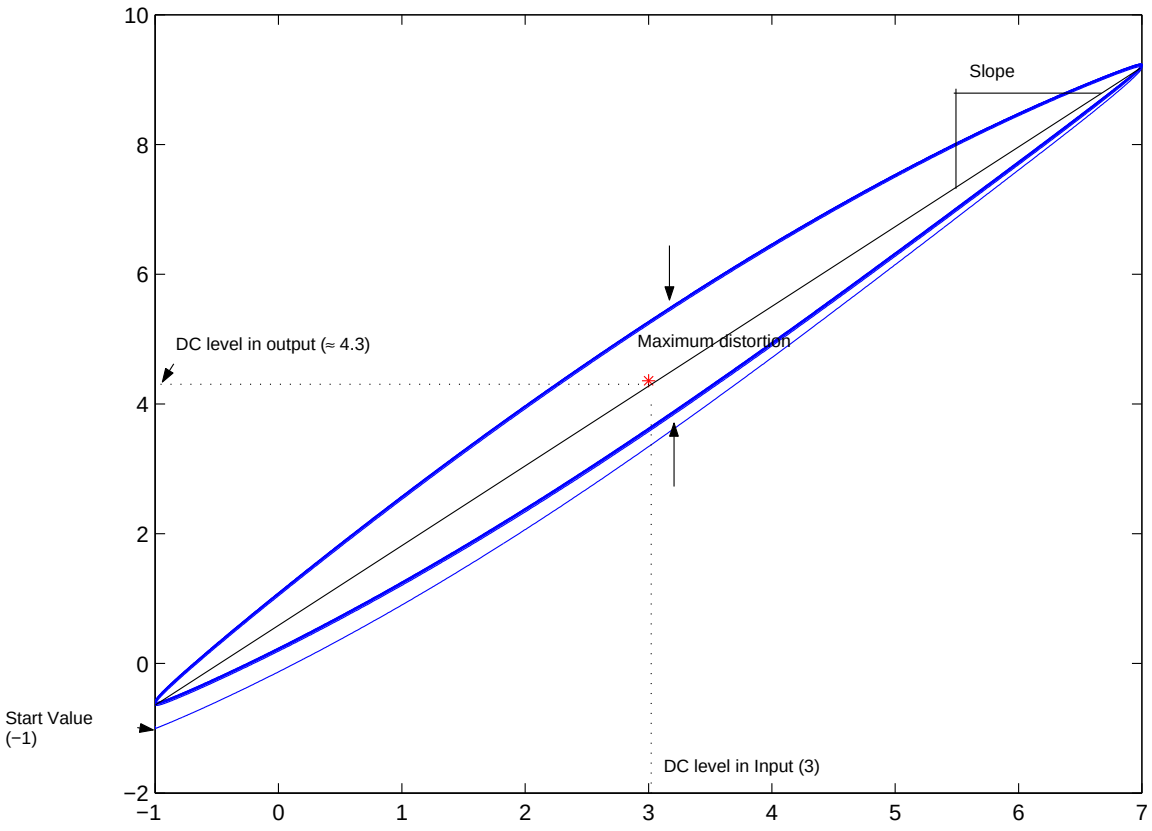

Figure 3.14. Characteristics of hysteresis loops being studied.

3.2.2. Triangular Inputs

In previous research work, many authors have assumed that hysteresis is a rate independent phenomenon (Celanovic and Goldfarb [15, 28]; Adriaens et al. [16, 22]). This assumption probably came about from the basis of the models that they used to capture the effect of hysteresis. The easiest method to verify this would be to vary the rate of the excitation input and compare the outputs. Since the rate of change of a sinusoidal signal is not a constant, it was decided that triangular inputs would be used to verify any rate (in)dependence. The amplitude of the inputs was chosen to be a 6V (peak-peak) triangular input. This would result in a significant distortion which can be observed easily. The velocity would then depend on the frequency of the

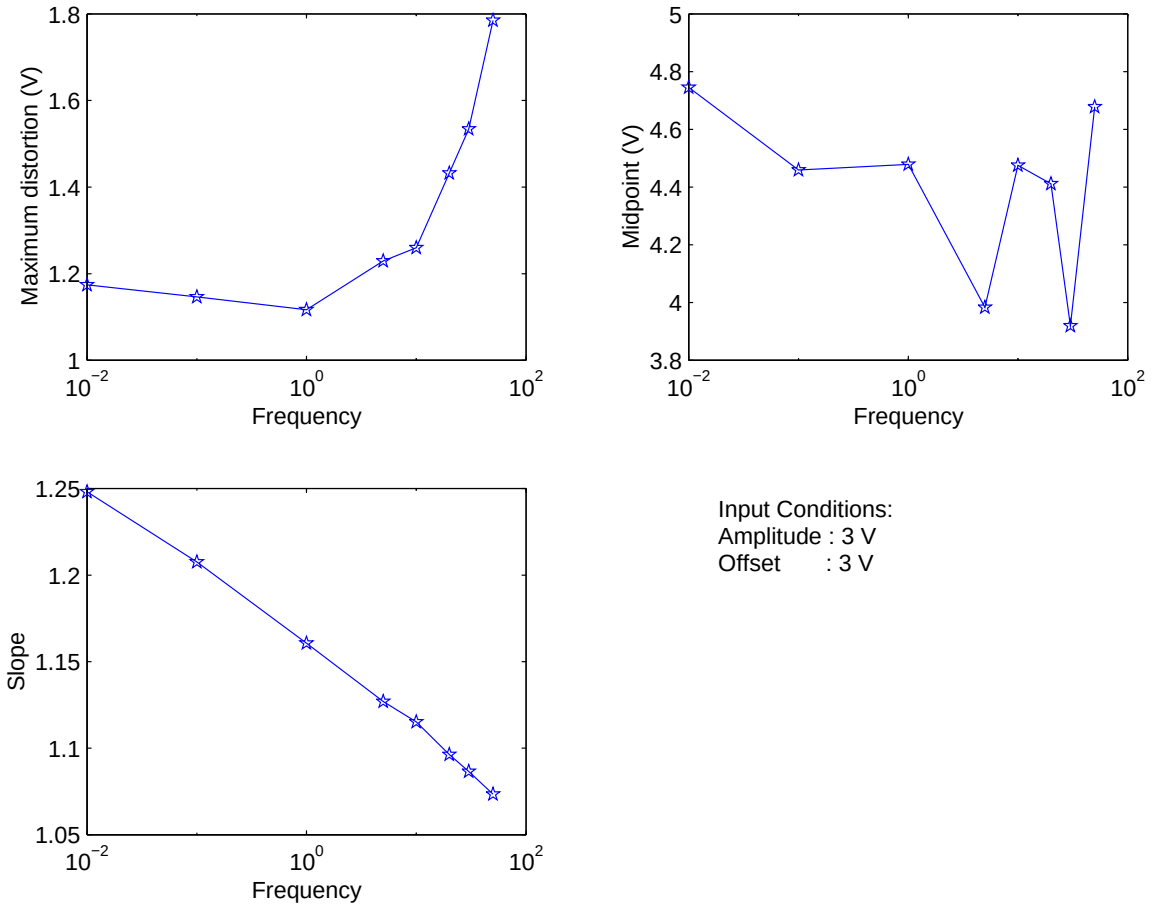

Figure 3.15. Trends seen in hysteresis loop characteristics with frequency variation.

input (for a given amplitude). Three different frequencies were used: $\frac{1}{12}\ Hz$, $\frac{1}{6}\ Hz$, $\frac{1}{2}\ Hz$. The plots of the time histories and the response versus the output can be seen in Figure 3.19 on page 52. Only the steady state loops are shown in Figure 3.21 on page 54. The drift in the output can be seen in Figure 3.20 on page 53.

Figure 3.21 on page 54 shows the comparison at the different velocities. The loops are very similar with a downward shift in their mid-points with an increase in the velocity. The maximum distortion in the loop remains the same with an increase in the velocity.

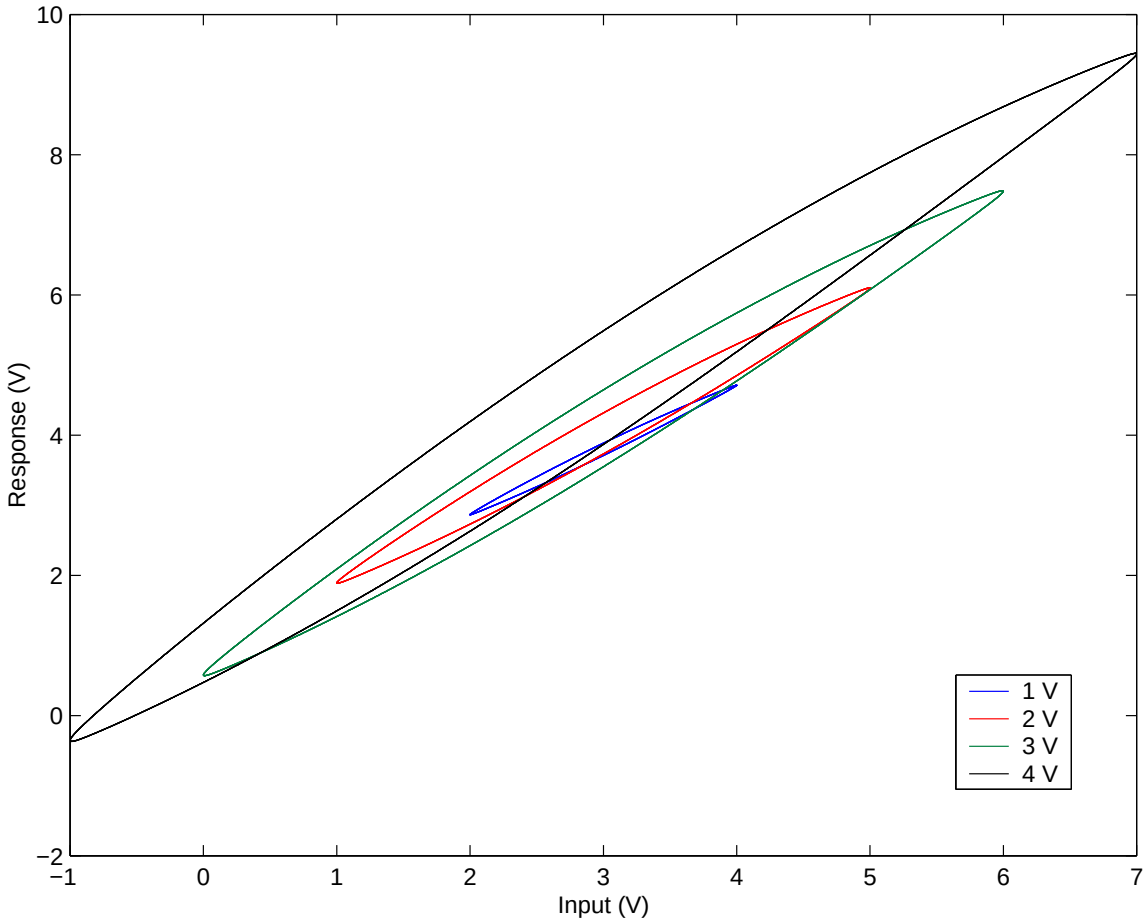

Figure 3.16. Steady-state hysteresis loops at different input sinusoid amplitudes (the different loops shown are at different input amplitudes).

The behavior of the stage observed in the tests conducted above clearly shows the presence of hysteresis and drift which are nonlinearities. The results of characterization and modelling reported in the literature on piezoelectric materials and actuators almost uniformly agree that piezoelectric materials in addition to exhibiting the above nonlinearities, also has a linear component to its behavior. Celanovic et al. [15] and Adriaens [16] have used the same overall set of equation describing the electromechanical behavior of the system. One of the component equations is a linear, dynamic, relationship between the charge developed on the electrodes of the

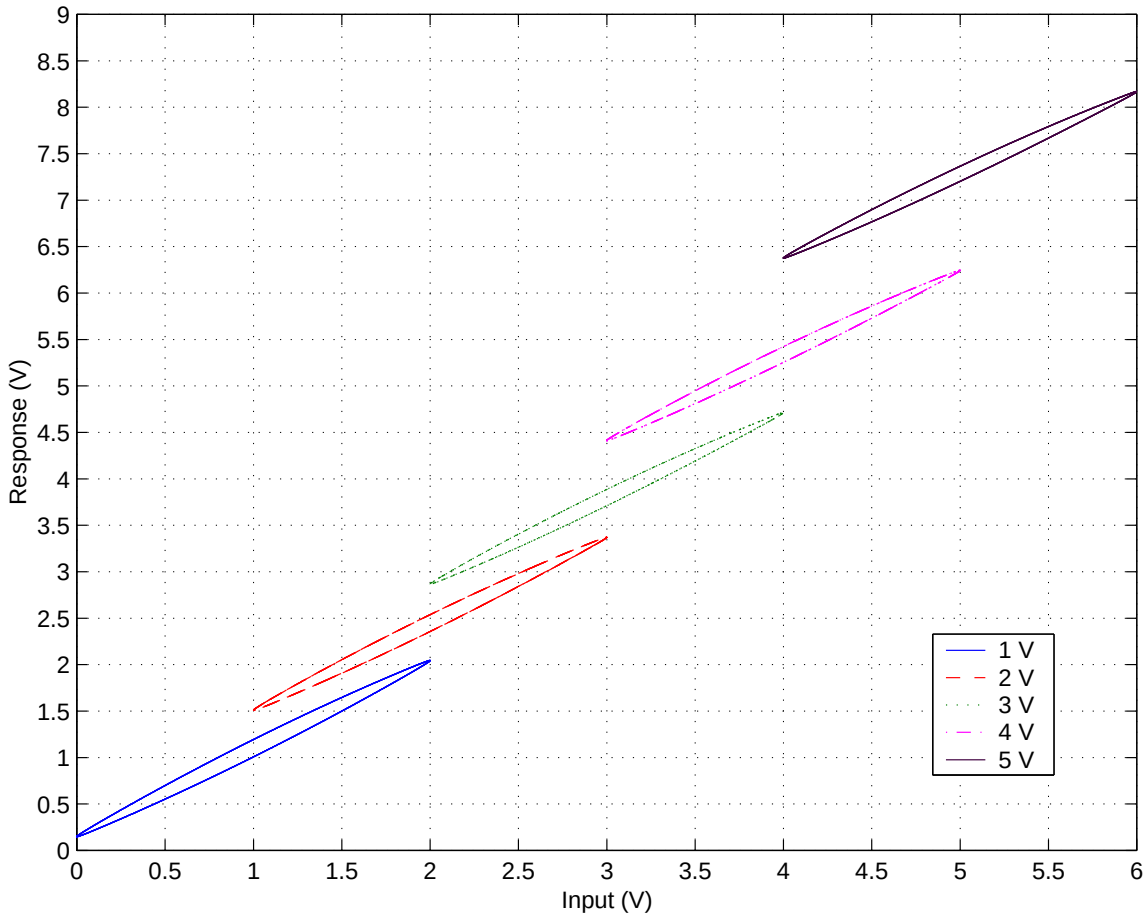

Figure 3.17. Steady-state hysteresis loops at different input offsets.

actuator to the displacement of the actuator. The next section is aimed at "isolating" the linear subsystem and to determine its characteristics.

3.2.3. Linear Characteristics

As noted from the step response, the overall system seemed to be a first order dominated system with no observable overshoot/oscillation. Analytical results by Adriaens [16], however, indicate that piezoelectric actuators tend to behave like second order dominant systems. To explain the discrepancy, it is necessary to look closely

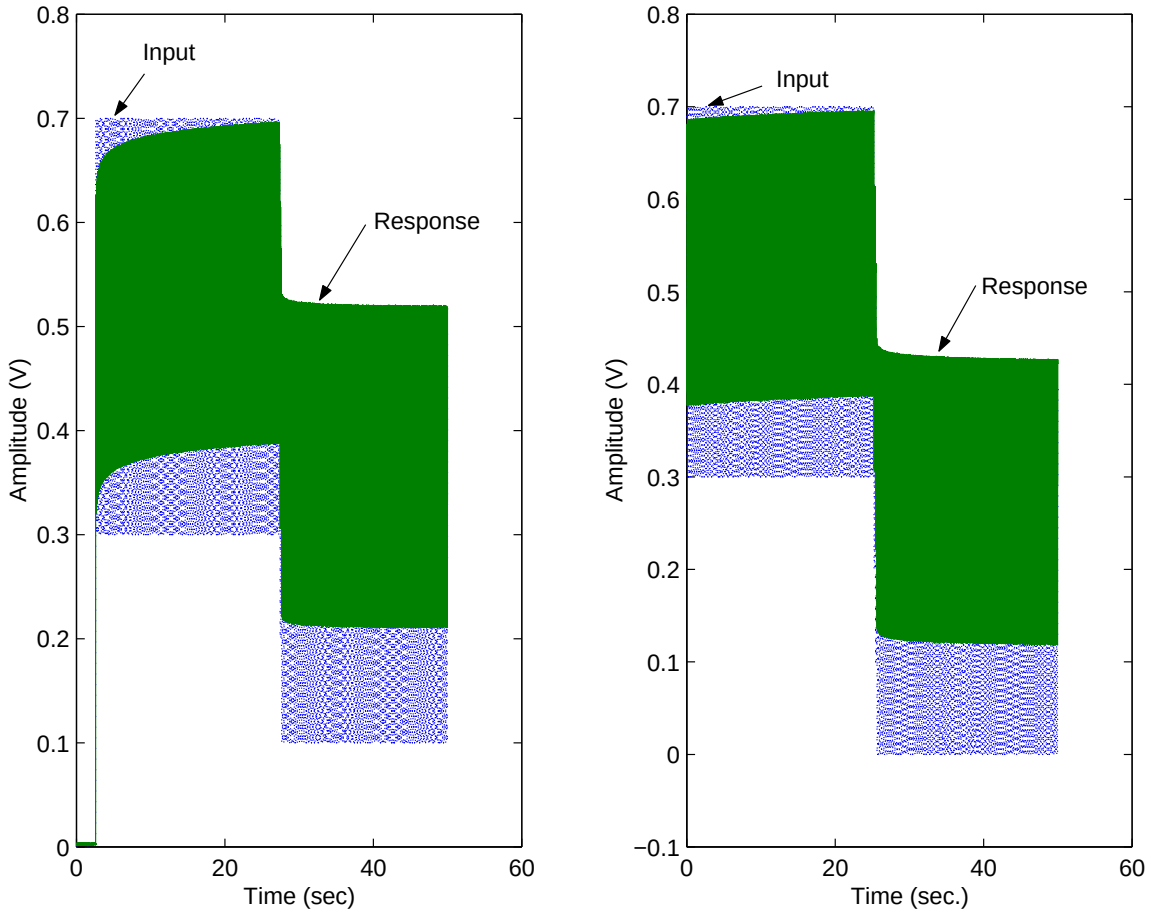

Figure 3.18. Plots to indicate the drift in the output to an offset sinusoidal input signal (darker band corresponds to the response).

at the step response of the system (see Figure 3.3 on page 35). When sampled at 50 kHz, the response does reveal an oscillatory behavior as expected. The reasons that the oscillatory behavior is hardly observable in the step response are: (a) The bandwidth of the actuator is large enough that the transients die down within about 4 msecs. (from Figure 3.3 on page 35). (b) The natural frequencies of the actuator is not excited sufficiently due to a step input (again due to the high bandwidth).

The observed step response is actually the open loop step response of the entire open loop plant as discussed in Chapter 2. To deduce the behavior of the nano-

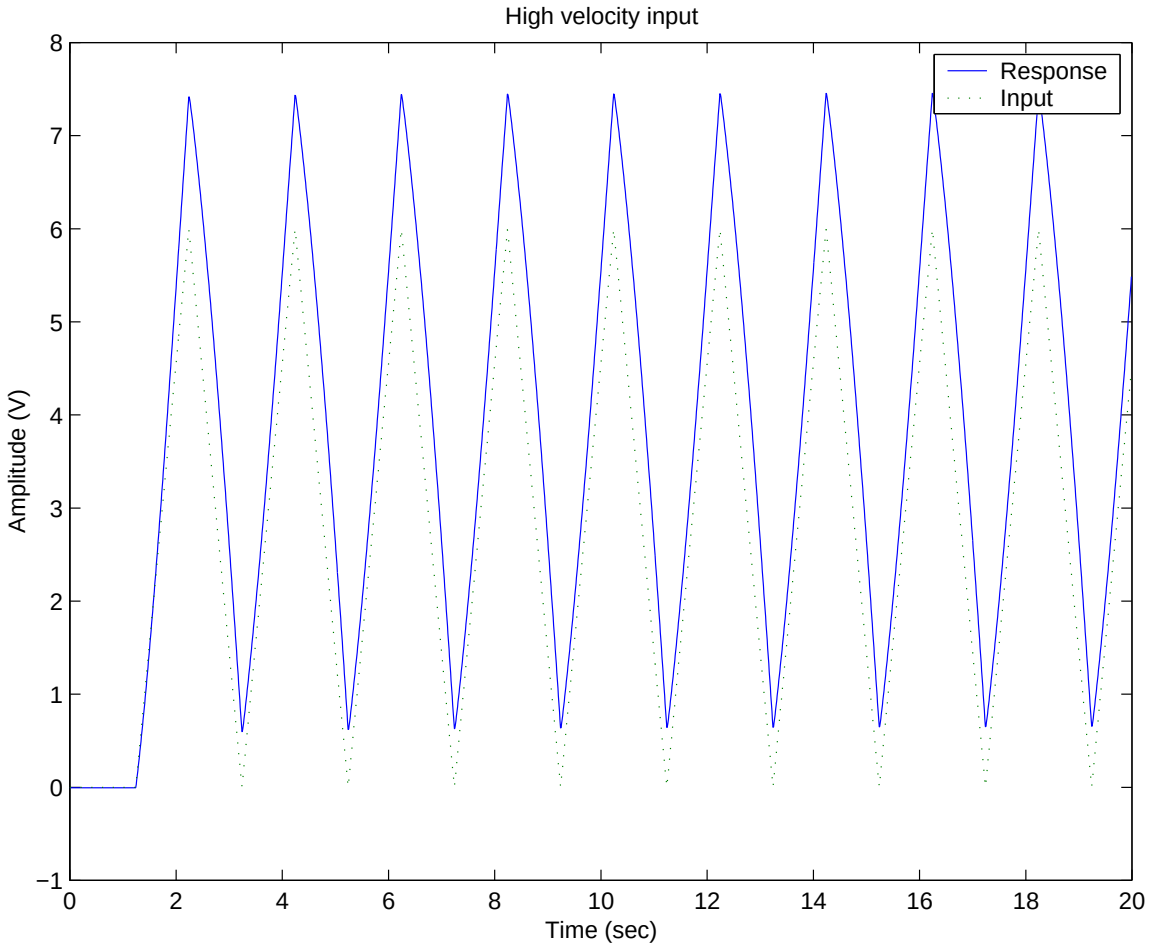

Figure 3.19. Response for triangular inputs.

positioning stage alone, the characteristics of the other components have to be known. The first one is the amplifier. The amplifier as any physical system has a finite bandwidth depending on the amplitude of the input signal (see Figure 2.12 on page 29). To ensure that the amplifier by itself does not posses any other significant dynamics, the frequency response of the amplifier was generated by monitoring the output from the amplifier. The frequency response of the amplifier did not contain any significant resonances (Figure 4.4 on page 71). As expected it rolls off at higher frequencies (for a given amplitude of the reference input signal). The amplifier's output is affected

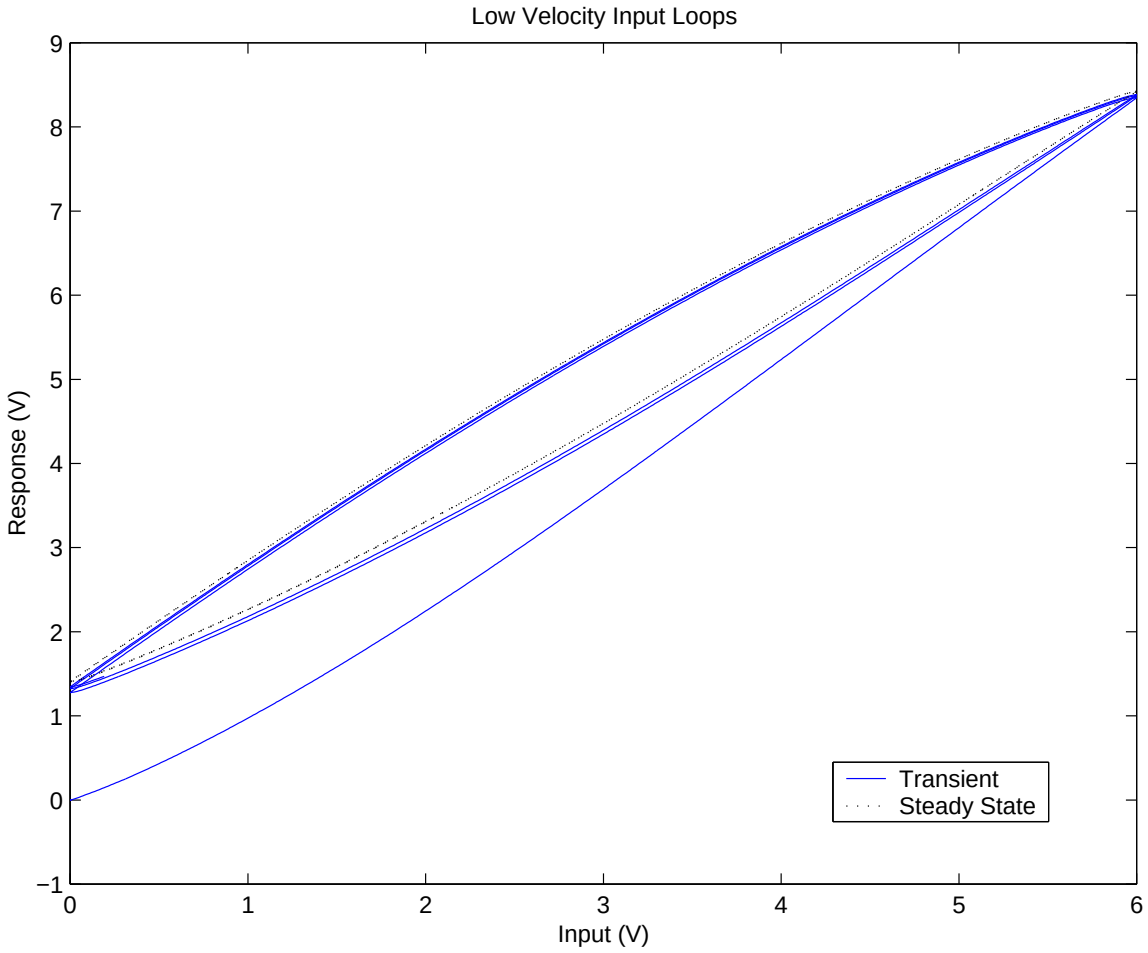

Figure 3.20. Transient and steady-state loops for triangular inputs.

by a slew-rate limiting circuit to ensure that too much current is not drawn (which might damage some of the electronics). This might cause a nonlinear behavior of the amplifier.

The other component in the loop is the capacitive sensor. The capacitive sensor is specified to have a bandwidth of 10 kHz, which is higher than the first resonant frequency of the stage. Hence we can conclude that the frequency response that is obtained with the sinusoidal sweep is almost entirely due to the positioning stage.

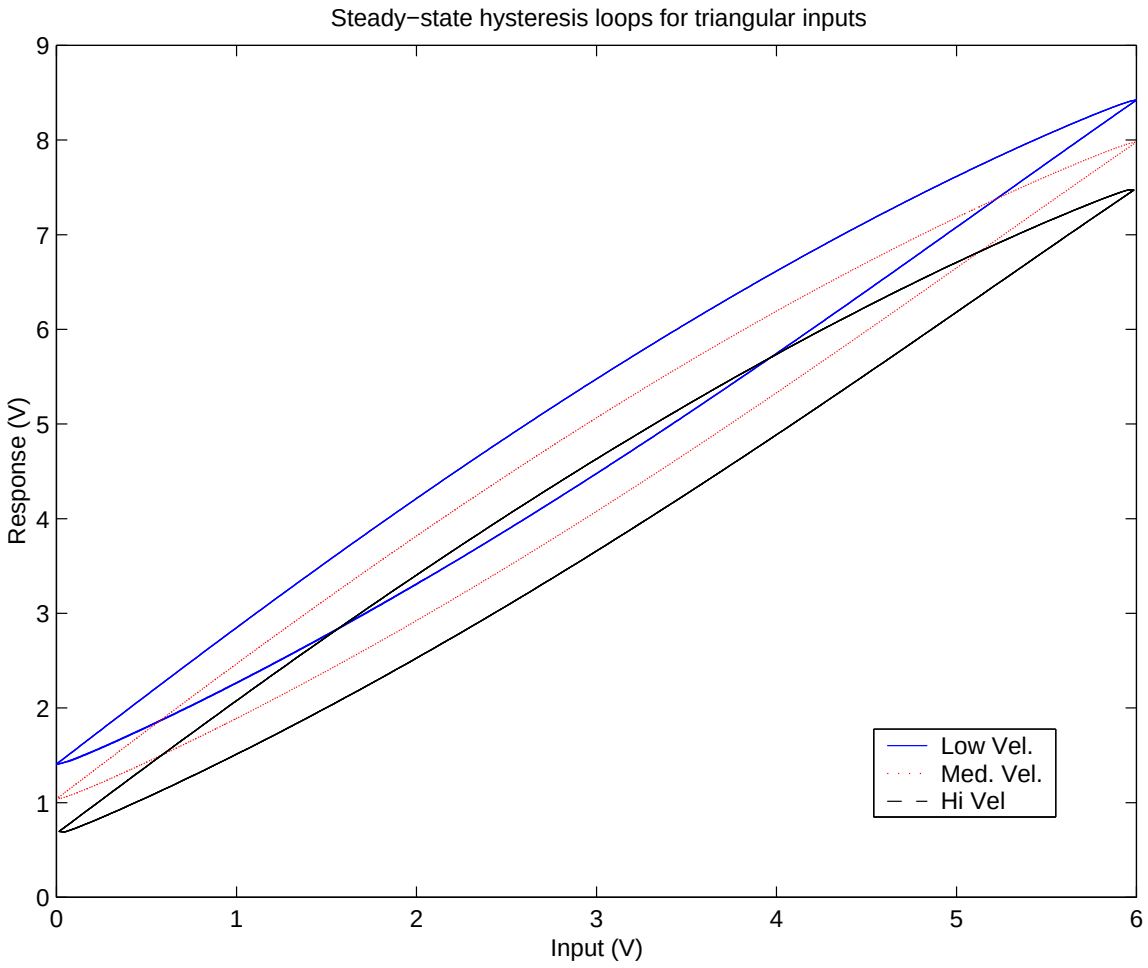

Figure 3.21. Hysteresis loops at different frequencies for **triangular inputs** (data obtained after about 2 minutes of cycling).

Looking at the input-output behavior of the system (see Figure 3.22 on page 55), it appears that for periodic inputs, the significant effect of the nonlinearities is that there is some DC offset in the output of the system. The output of the system is still periodic at the same frequency as of the input but there is an additional phase lag in the output (for a 1 V amplitude sinusoidal input 1Hz, the phase lag is $\approx 10°$ deg). From the earlier sections of this chapter, these distortions can be attributed to the nonlinear gain, drift and the hysteresis effect encountered in piezoelectric actuators.

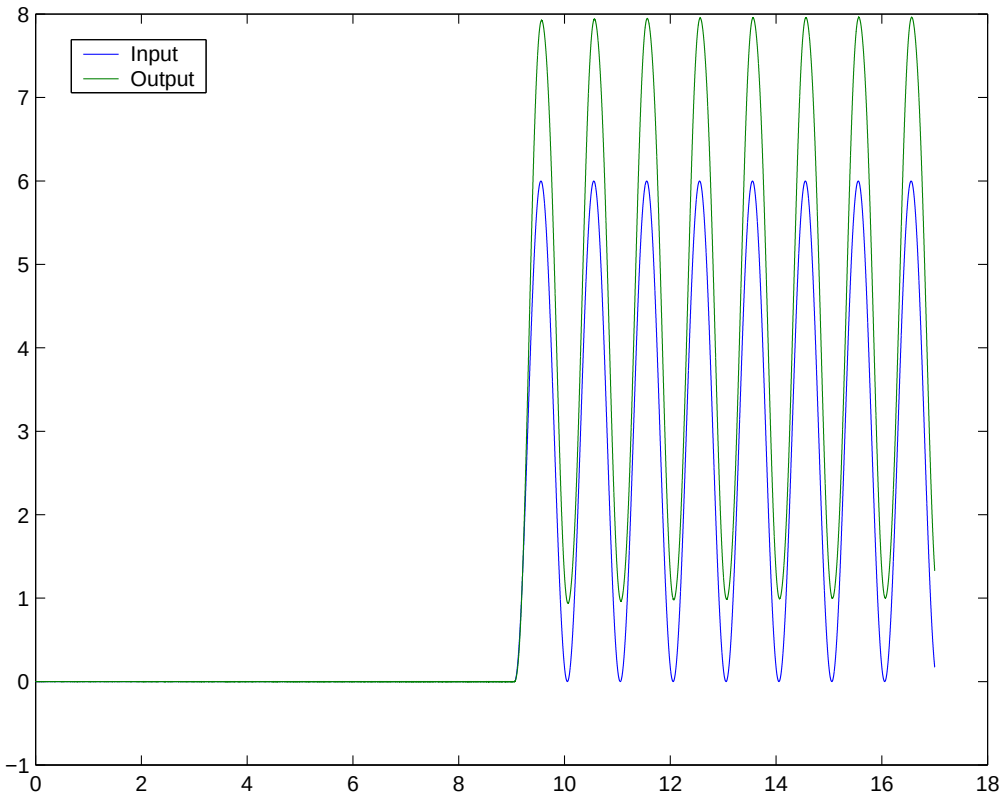

Figure 3.22. Input-Output behavior for periodic inputs.

One way to reduce the effect of these nonlinearities is to reduce the amplitude of the inputs as they all seem to be input magnitude dependent (from tests conducted with the positioning system). The Figure 3.23 ndicates the distortion due to nonlinearities at low amplitudes and low frequencies. One can notice that there is a much smaller distortion than those input at large amplitudes shown in the earlier sections on Hysteresis. Hence if one were to determine the frequency response using a swept sinusoidal signal, to reduce the effect of hysteresis and the nonlinear static gains, small input amplitude should be used, which is the basis of the experiments performed and results presented in this section.

Since the aim is to determine the parameters of the linear subsystem, the input signal used for system identification should first of all excite the system modes. Ac-

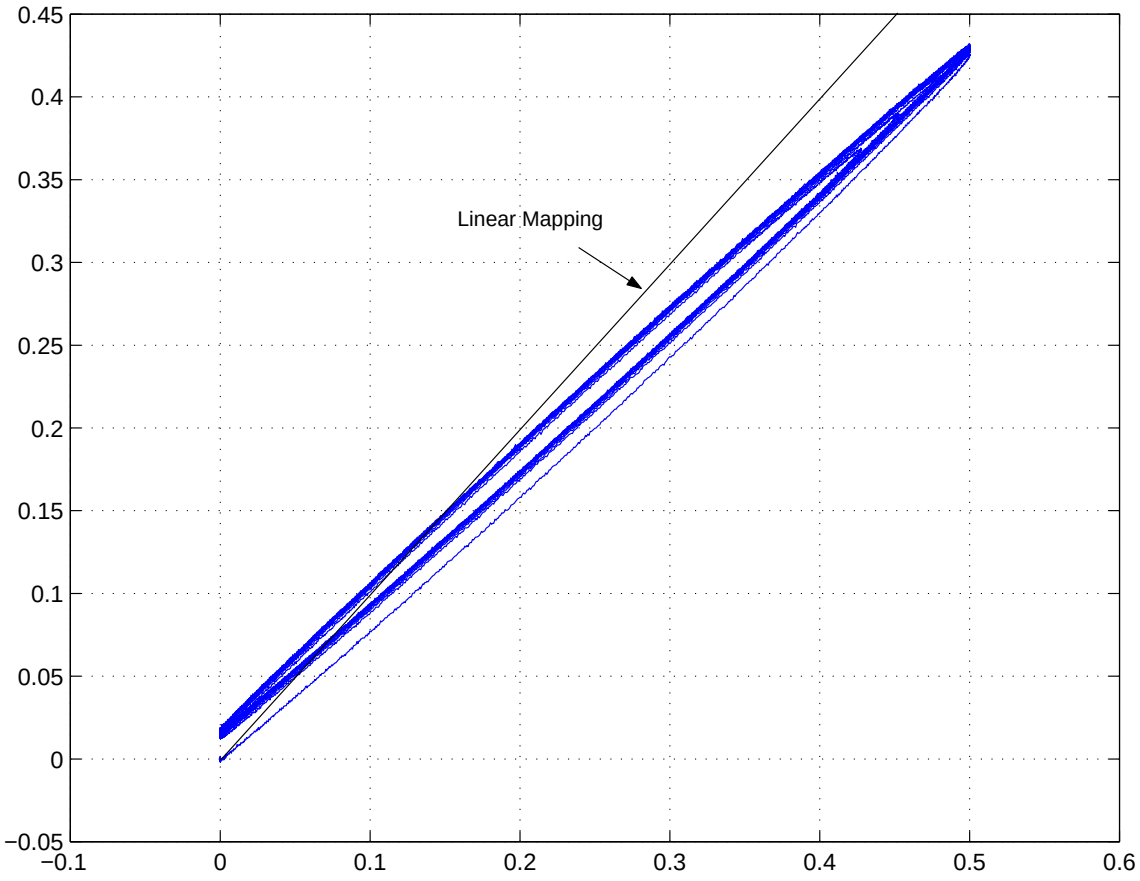

Figure 3.23. Hysteresis loop for a low amplitude (0.25 V amplitude; 0.25 V offset; 1 Hz. frequency) sinusoid; The line indicates static gain of the actuator and the sensor.

cording to the specifications on the actuator the lowest resonant frequency of the actuator is around 5 kHz. Hence the input signal should have frequency content greater than 5 kHz. To verify the presence and probably dominance of any other resonant frequencies close to the fundamental resonant frequency, the frequency range of interest for a preliminary experiment was chosen as 0–12.8 kHz. Also, to ensure that the nonlinear effects are insignificant in the response, the amplitude of the input signal should be low so that the maximum distortion due to hysteresis (15 – 20% of full range travel) is within the sensor resolution (and hence could be considered

as noise). For the tests performed on the system under consideration, the amplitude was restricted to a maximum of 30 mV (which corresponds to a full range of $30 \times 10^{-3}V \times 12\mu m/10V \approx 36nm$. The maximum hysteretic distortion here is about 72 nm (assuming a 10% distortion) which is around the noise resolution of the sensor.

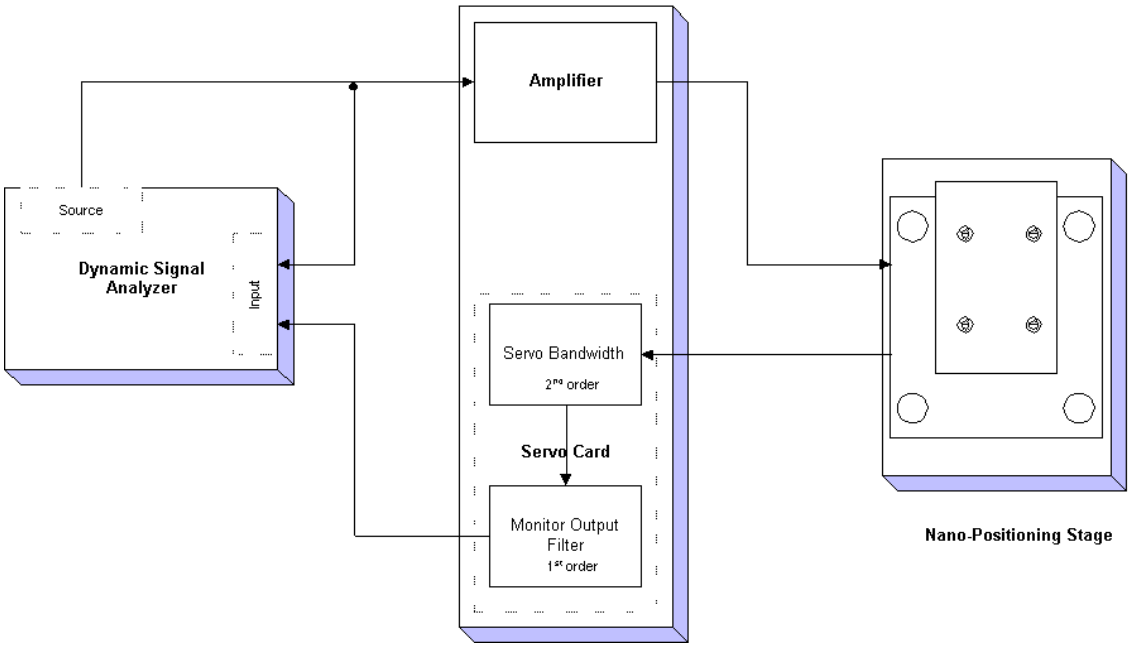

Figure 3.24. Schematic of connections for the frequency response determination test.

A HP dynamic signal analyzer is used to obtain the bode plots for the system. The excitation signal used is a sinusoidal sweep with a frequency range from 0–12.8 kHz. It is generated using the in-built source of the dynamic signal analyzer. The experiment is repeated at different offsets (-1, 0, 2, 3 V) of the input signal and also different input signal amplitudes (5, 25, 70 mV) to ensure that there are no significant nonlinearities affecting the output of the system. The resultant frequency

response is seen in Figure 3.25 on page 58 (with offsets of 0,1,2,3 V) and Figure 3.26 on page 59(with amplitudes of 5, 25,70 mV). If the system were perfectly linear then the bode plots obtained at different DC offsets of the input should be the same (at different offsets).

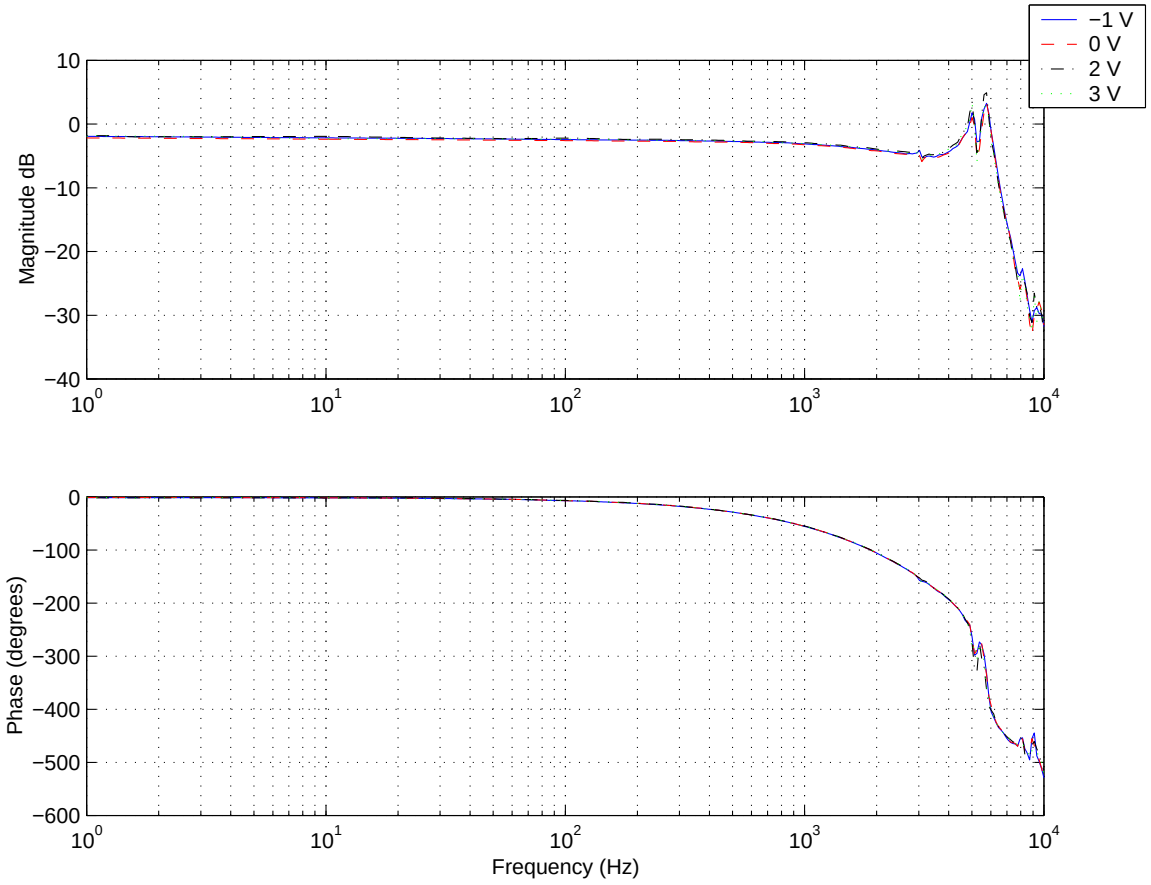

Figure 3.25. Frequency response of the Positioning system at different offsets of the excitation sweep signal.

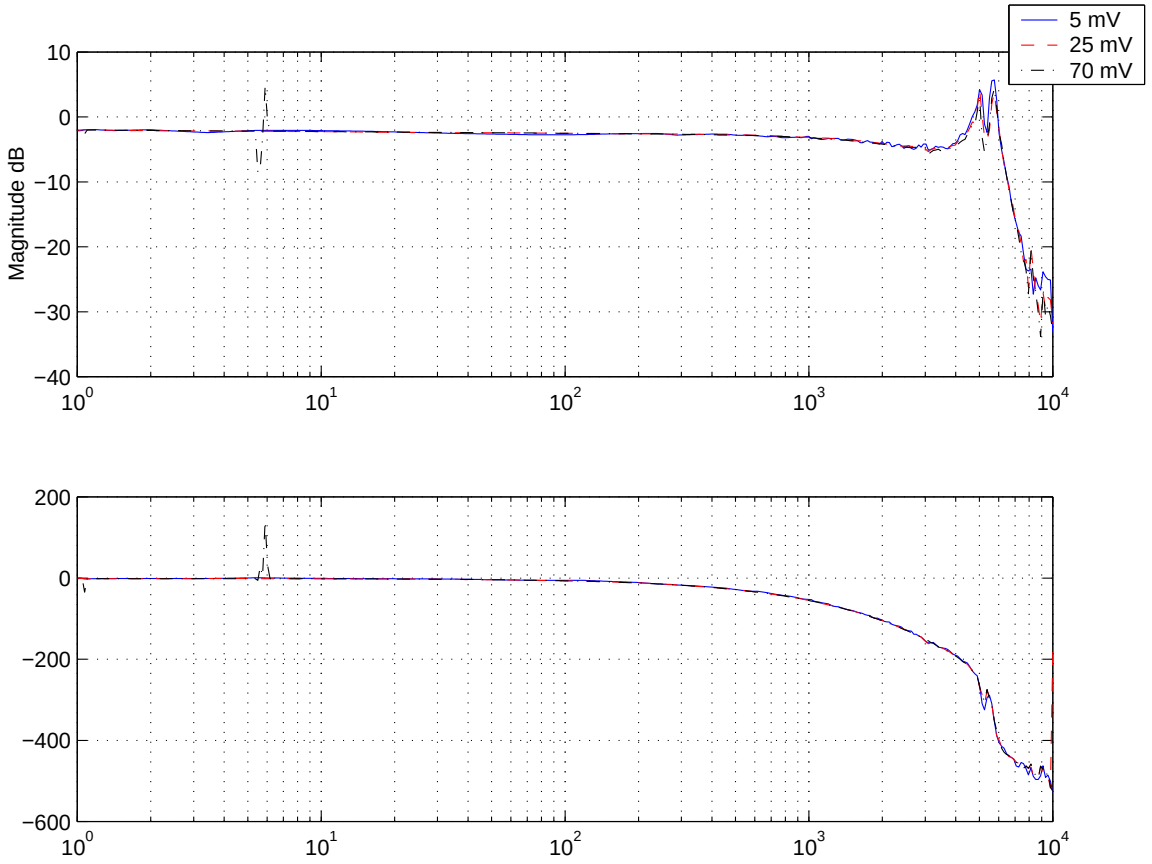

Figure 3.26. Frequency response of the Positioning system at different amplitudes of the excitation sweep signal.

It can be seen that the bode plots at different input voltage offsets are very similar, especially in the high frequency range. Hence the frequency response plots are to be used to gather information about the high frequency behavior (gain and the phase) of the actuator, and the tests with quasi-static inputs are to be used to characterize the low frequency behavior of the system.

3.2.4. Friction

One significant nonlinearity in most mechanical systems is the presence of friction between the moving platform and any of its supports. According to the specification by the manufacturer, there is no sliding action anywhere in the 'transmission' of the nano-positioning stage. The motion of the tip of the stack actuator is transmitted to the flexure guides directly. These guides support the entire weight of the moving platform and any other load on the platform. To actually verify this simple experiments were carried out. They are described below.

To test whether friction is truly a concern in the positioning system, experiments had to be performed due to a lack of knowledge about the construction of the positioning stage. In these experiments, the control input applied to the amplifier is slowly ramped up (at the rate of 0.005 V/s) and the time taken for the stage to start moving is noted. When a load is added onto the stage, the normal force at the contacting surfaces (if any) should increase and hence the threshold for the frictional forces also increases. Hence the control input required to move the stage should also increase. If the ramp-up rate is maintained a constant, in the presence of static friction, it should take more time for the stage to start moving. But from the experiments performed with 5 different loads from no load to approximately 9 kgs (even though this is much higher than the maximum allowable load, it was used as at the time of the experiments, the manufacturer's specifications were incorrect), no appreciable difference in the time lag was noted (for the platform to move). When a similar set of experiments were performed but with step inputs of different heights, it was noted that a step of

1.4 mV in magnitude induced measurable deflection in the stage. These observations could be the result of two factors:

- The sliding surfaces do not support the weight on the moving platform, i.e., the flexures take up the entire load on the moving platform. As a result, the change of load has not much effect on coulomb friction.
- The voltages required to make the stages move is due to the stiction force, and the stiction force is large compared to the coulomb friction component.

The former is in agreement with the specification of the manufacturer. Hence for the initial approximation, the friction is neglected. Another reason that the friction could be generally neglected in typical piezoelectric systems is that the stiffness of the actuator is very high. Hence even for small voltage inputs, the deflection of the unrestrained actuator is sufficient to produce enough force (if restrained) to overcome the frictional force.

4. LINEAR MODEL & CONTROLLER: IDENTIFICATION AND EXPERIMENTS

Linear design models for plants are very popular choices due to their simplicity in formulation and ease of use in analysis. Hence a tremendous amount of research effort has been focussed on this area. This resulted in fairly well established methods designing controllers and analyzing their stability and performance in the case of linear plants. In this chapter, a linear model for the piezoelectric positioning stage is proposed and experiments to deduce the parameters of the system are performed. Based on the linear model, a simple linear compensator is designed. The designed compensator is shown to outperform the servo controller obtained with the positioning system, in terms of attainable closed-loop bandwidth (hence trajectory tracking accuracy), with experimental data.

In reality most physical systems are never completely linear. They possess some elements that introduce nonlinearities in their behavior. Even the simple mass spring damper system (even though this is a used as a 'linear' approximation for many real-life systems) is nonlinear if the spring's nonlinear stiffness is considered (under large deflections). Also the friction between the mass and the surface is nonlinear. If the mass moves at low velocities, then dynamic friction is a very significant contributor to the nonlinear behavior of the system; at higher velocities it is either the coulomb or the viscous friction that is dominant, depending on the condition of the sliding surface. Thus whenever a linear model for a system is used to study its behavior it has to be kept in mind that the model is an approximation of the system and it works best under restrictive assumptions on the operating conditions.

4.1. Linear Plant Model

The standardized IEEE model for the piezoelectric effect in materials can be summarized in the two equations,

$$S_p = s^E_{pq} T_q + d_{kp} E_k \tag{4.1}$$

$$D_i = d_{iq} T_q + \epsilon^T_{ik} E_k \tag{4.2}$$

where S: Strain tensor; s^E: Elastic compliance matrix; T: Stress Tensor; d: Piezoelectric constant matrix; E: Electric field vector; D: Electric displacement vector; ϵ^T: Permittivity of the material measured at a constant stress level.

Equations 4.1 and 4.2 state that the strain and the electric displacements are linear combinations of the mechanical stress (due to the external load and the constraint on the inverse piezoelectric effect). If the material is not constrained, then the nett stress is due to only the external load.

When an electric field is created in a piezoelectric material (by applying a voltage across electrodes as in a piezoelectric actuator), it causes the material to develop a strain (i.e. an expansion or a contraction). This effect is termed the inverse-piezoelectric effect (because it is the converse of the piezoelectric effect that was first discovered). If the material is constrained, it develops a force on the constraining mechanism. This force, from the IEEE formulation, is therefore linearly dependent on the applied voltage. This force causes the displacement of any external load placed on the actuator. Thus the whole system can be approximated by a force being applied onto a mass (the external load)-spring (the stiffness/elasticity of the piezoelectric material)-damper (material damping) system (see Figure 4.1 on page 65). The model is usually parameterized in the following manner: the mass is the effective lumped mass of the stack actuator; the spring constant is the stiffness of the actuator under nominal closed circuit conditions and the damping constant is a lumped term that accounts for the losses in the system. Since all the losses are represented by a lumped linear term, this model can be though of as incorporating the linearized model for the hysteresis in the system.

This linear formulation has been the basis for many models and controllers for piezoelectric actuators (Kim and Nam [11, 12],Xu et.al. [50]). Some variations of this formulation have been employed by Croft el.al. [40] and Garcia et.al. [51, 52] where it was assumed that the hysteretic effect could be treated as a nonlinear operator which distorts the output of the linear dynamics of the piezoelectric actuator. Even when nonlinear effects like hysteresis and drift have been modelled, the dynamics of the piezoelectric actuator has always been assumed to be a linear second order system by most authors.

The piezo-ceramic actuator in the P753.11C is fabricated by bonding ceramic disks in a stack-like fashion (hence the name "stack actuator"). The electrodes to apply the electric field are deposited onto the face of each of the disks to a thickness of the order of a few microns. Though the ceramic disks are bonded together it can be assumed for an initial approximation that the entire stack is made up of the material of the piezo-ceramic.

The mass-spring-damper model implicitly assumes that the entire mass is concentrated at a point, i.e., the position of the entire mass can be described with one variable. However, in the actuator the mass is not concentrated at a single point. It is distributed along the length of the actuator. Therefore it possesses an infinite number of degrees of freedom (unlike the lumped model which has two degrees of freedom). To describe the motion of such a system accurately it is required that one uses partial differential equations.

Adriaens [16] has performed a detailed analysis of the distributed model of the actuator and derived an equation of motion that involves the use of partial differential equations. The solution of this equation of motion is obtained by using the method of separation of variables. From the solution and analysis in [16] it can be seen that the distributed model of the system has infinite number of natural frequencies corresponding to the various modes of longitudinal vibration of the stack actuator.

The analysis in [16] also indicates that the higher natural frequencies of the actuator can be neglected as:

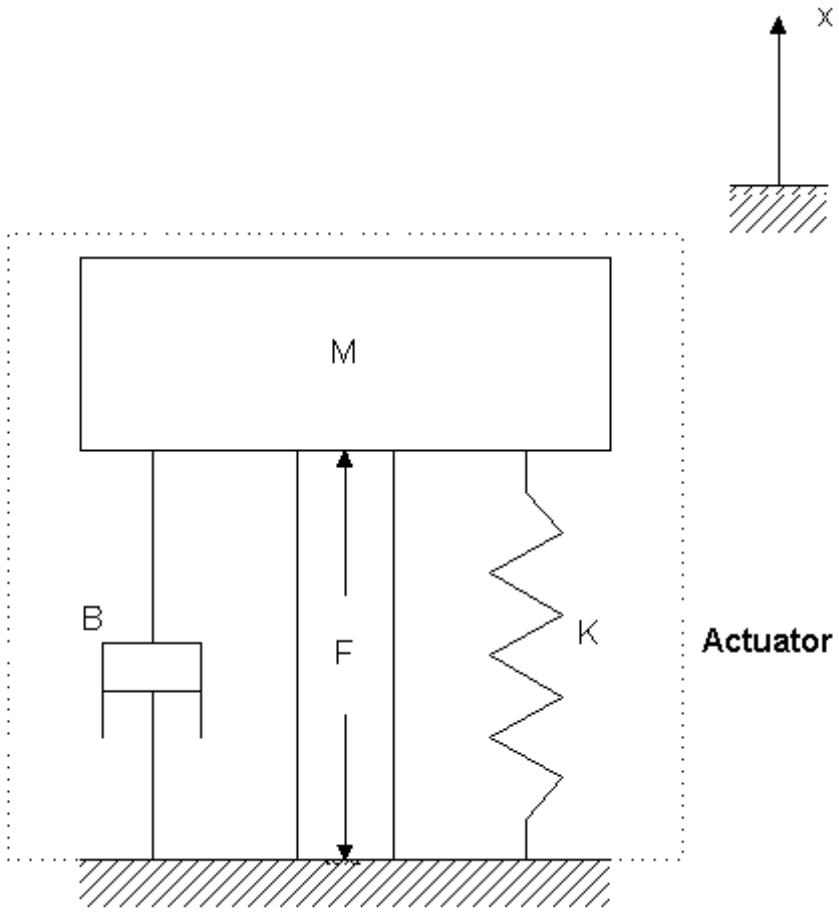

Figure 4.1. Schematic of linear dynamic model of the Actuator. Actuator is assumed to be an ideal force transducer with stiffness and damping.

- The higher resonant modes appear at much higher frequencies which are usually not excited in typical applications.
- Even if those frequencies are excited, the gains at these frequencies are too low for the mode to show up in the response.

It also showed that upon addition of any load to the actuator, the fundamental resonant frequency decreases to a large extent. This property is useful when the system is to be controlled with a digital controller due to the limitation on the maximum sampling rate possible. For practical purposes, the second order model which results due to the mass-spring-damper approximation is parameterized in this manner, The mass is usually chosen to be the nett effective load on the stage (as the mass of the stack is usually negligible). The stiffness of the spring is chosen so that the resonant frequency of the mass-spring system matches the fundamental frequency of the positioning system. The damping ratio is chosen so that the resonant peaks for the fundamental resonant frequency have the same magnitude. The resonant frequency and the peak magnitude can be easily determined from a bode plot which can be obtained experimentally as described in Chapter 2.

4.1.1. Determination of Model Parameters For Overall System

A convenient method to determine the parameters of a linear model is to use the frequency response method to determine the transfer function and transform the coefficients of the transfer function polynomials back to the parameters of the linear differential equation model.

The frequency response of the positioning system (includes the amplifier, the positioning stage, the sensor electronics) was obtained as described in Chapter 2 in the section on Linear Dynamics. To verify the presence of any nonlinearities, the amplitude and the offset of the excitation signal (a swept sinusoid) was varied and the frequency responses were compared. The frequency responses obtained were very similar with variations of less than 0.4 dB in the gain and less than 5-10 degrees in

the phase plots (Figure 3.25 on page 58 and Figure 3.26 on page 59). The input dependent nonlinearities discussed in Chapter 3, apparently, had very little effect on the frequency response of the system. This probably due to the small amplitude of the excitation signals.

From the magnitude plot of the system, it can be seen that near the peak in the magnitude there are actually two peaks present with an anti-resonance in-between them. This was not due to some computation as this was consistently observed under different input conditions and also computation methods. Hence there are two resonant peaks close to each other. But due to the proximity of a resonant peak and an anti-resonant node, we can assume, for the sake of model order reduction, that they cancel out each other. As a result of this assumption, there exists only one prominent resonant peak (which is assumed to be the second one).

Based on the shape of the magnitude plot of the experimental frequency response, it can be seen that the stage is essentially an under-damped second-order system. Also just before the resonant peak occurs, there seems to be a roll-off in the magnitude plot. By an iterative approach, this roll-off in the gain can be approximated by a first order term with a corner frequency at 2 kHz. After this first order term is compensated for, then using standard formulae for second order systems, a transfer function for the second order term can be deduced.

The parameters that can be obtained from the frequency response experiments are the resonant frequency and the equivalent damping ratio. From the peak of the magnitude plot, the resonant frequency can be read-off as, $\omega_r = 5.715kHz$. The steady state gain can be determined from the bode plot very low frequencies to be 0.79. Based on the static gain and the magnitude of the resonant frequency, one can determine the damping ratio to be, $\zeta \approx 0.08$. Since $\zeta \ll 1$, the natural frequency $\omega_n \approx \omega_r$ the resonant frequency ($\omega_n = 5773.4Hz$). These results for the resonant and natural frequencies are in very good agreement with the specifications by the manufacturer. The experimental frequency response and the bode plot of the model are overlaid on the same plot to check the agreement between the two

and the parameters were iterated further to provide the best possible fit (Figure 4.2 on page 68). The values obtained after this final iteration are $w_n = 5792\ Hz., \zeta = 0.08,$ and$K_{static} = 0.79$.

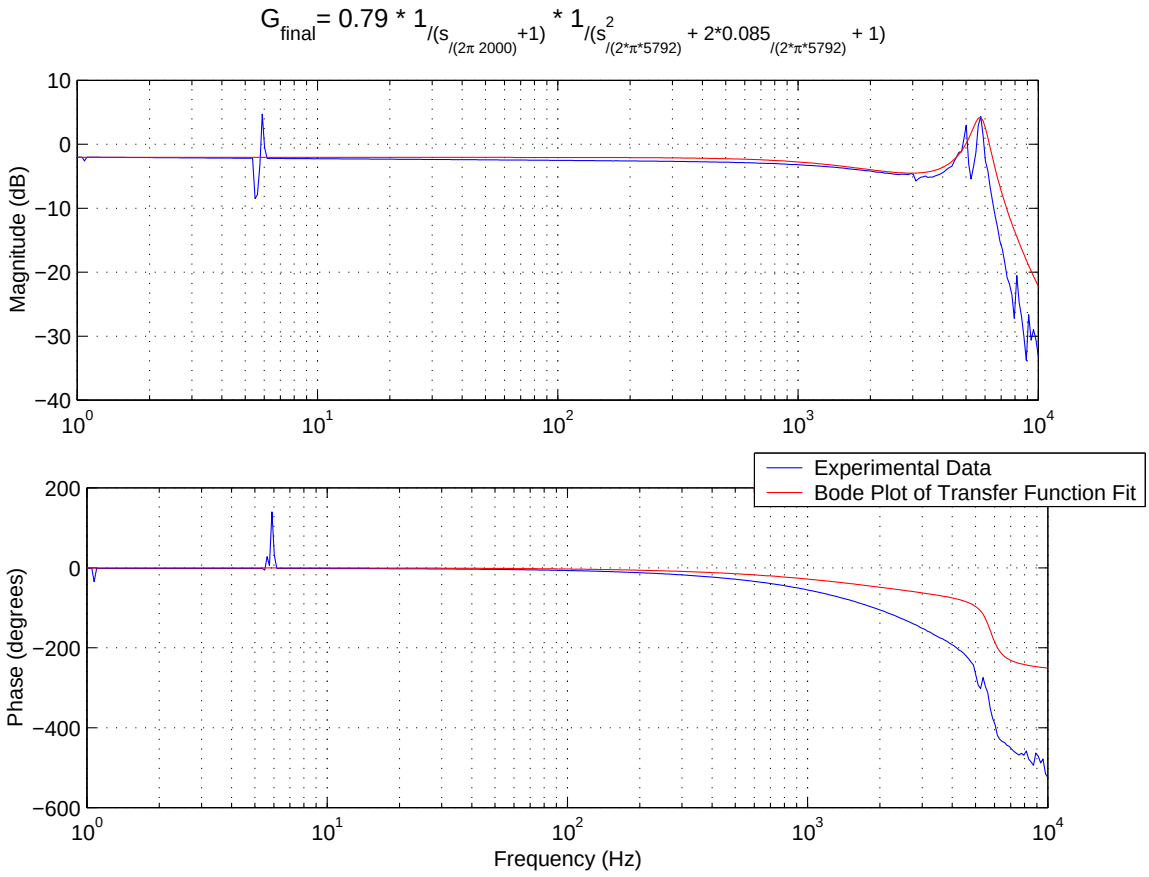

Figure 4.2. Comparison of experimental frequency response and bode plot of transfer function model.

The transfer function model for the entire system (amplifier, positioning stage , sensor) is:

$$G_p(s) = \frac{1}{\frac{s}{2\pi\,2000} + 1} \times \frac{0.79}{\frac{s^2}{(2\pi\,5792)^2} + \frac{2\,0.08}{2\pi\,5792}\,s + 1} \tag{4.3}$$

In Figure 4.2 on page 68, even though the magnitude plots match well, there is a large discrepancy in the phase plots, especially at higher frequencies. When the

phase discrepancy was plotted against the frequency, a linear variation was observed (Figure 4.3 on page 69). A linear drop in the phase is normally caused due to a time delay in linear systems. The slope of the discrepancy in the phase gives the value of the time delay. Hence a time delay was assumed to exist in the system and the time delay was deduced to be $T_d \approx 0.085\ msec$.

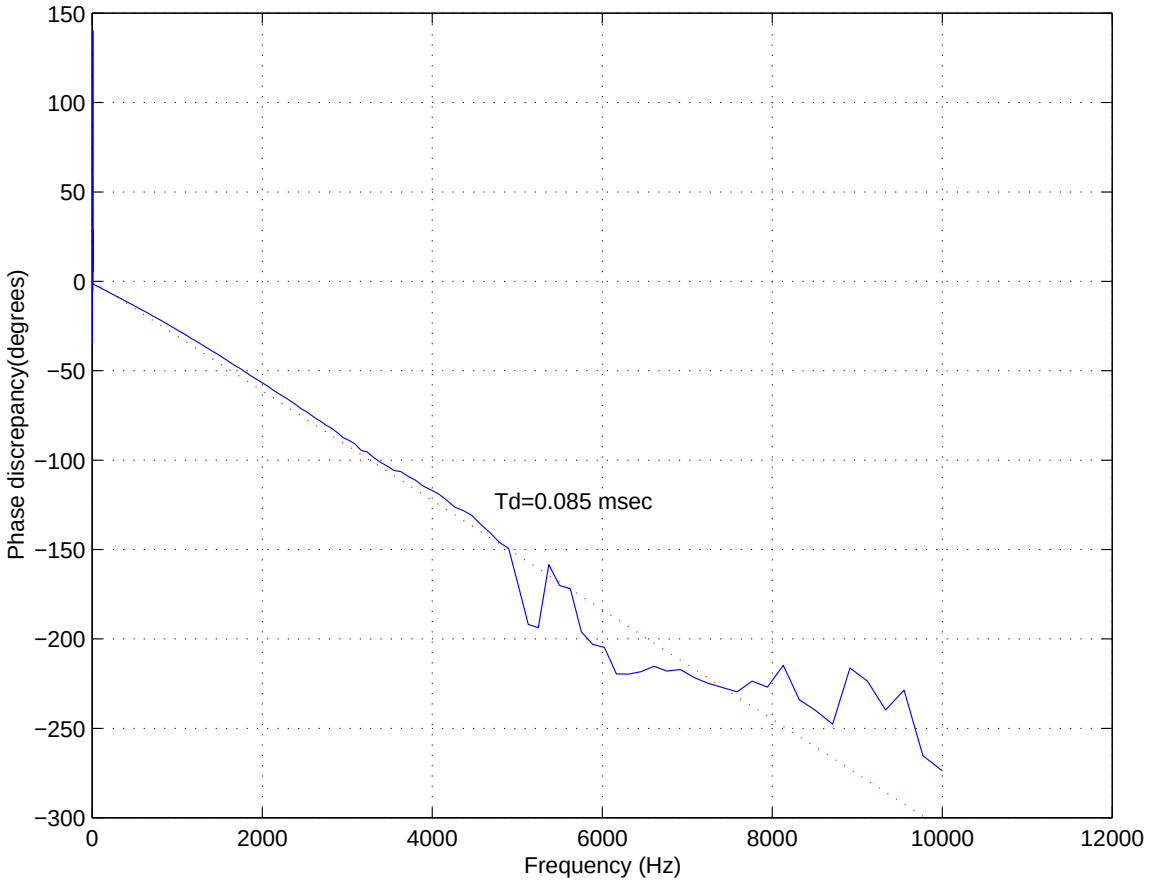

Figure 4.3. Discrepancy in phase: $(\phi_{exptl} - \phi_{tf.model})$.

Based on all the above information, the linear model of the piezoelectric positioning system is:

$$G_p(s) = e^{-T_d\, s}\, \frac{1}{\frac{s}{2\pi\, 2000} + 1} \times \frac{0.79}{\frac{s^2}{(2\pi\, 5792)^2} + \frac{2\, 0.08}{2\pi\, 5792}\, s + 1} \tag{4.4}$$

The frequency response shown is that of the overall system. It is frequently useful to identify the contributions to the frequency response from the various components in the loop. In this case they are the amplifier, the sensor and the electronics in the position control loop. This information could be useful, for example if one wants to eliminate any bottleneck on the bandwidth of the closed loop system, it would be help to know if the bottleneck could be eliminated by choice of a different amplifier, sensor or electronics. The next section presents experimental results and manufacturer specifications (when experimental data could not be obtained) on the dynamics of the different components in the loop.

4.1.1.1. Frequency Response of Amplifier

Based on the specifications by the manufacturers, it was initially assumed that the amplifier behaves as a static component in the control loop. The specified gain is 10 V/V. As illustrated in Figure 2.12 on page 29 in Chapter 2, the bandwidth of the E505 amplifier depends on the positioning stage that it drives and also the amplitude of oscillation (for sinusoidal inputs). This dependence is due to the difference in the capacitance between the stages. For the 753.11 stage, the bandwidth limitation is defined by the curve for the 1.8 μf capacitance.

Frequency response tests was performed with the amplifier in open and closed circuit (when connected to the positioning stage) mode. The results are shown in Figure 4.4 on page 71 & Figure 4.5 on page 72. As is apparent from the open circuit frequency response, the -3 dB bandwidth of the amplifier occurs around 20–30 K rad/sec (≈3–5 kHz). The phase lag also remains close to zero until about 2 kHz. This is reasonably close to what is specified as the frequency response of the unloaded amplifier (the uppermost curve on Figure 2.12 on page 29).

In the case of the closed circuit configuration (-3 dB point occurs approximately at 4 kHz). This again is what was expected as the amplitude of the input signal

used to determine the frequency response of the amplifier when connected to the positioning stage is much lower (70 mV at most). Therefore the roll-off should occur at a higher frequency than what is specified in Figure 2.12 ($\approx 1.25\ kHz$). Also the characteristics of the PZT stage seem to affect the response of the amplifier especially near the resonant frequencies. For large amplitude signals the bandwidth is expected to be much lower (based on the manufacturer's specification). *This 4 kHz corner frequency is the most probable cause for the roll-off observed in the frequency response of the overall system at approximately 2 kHz.*

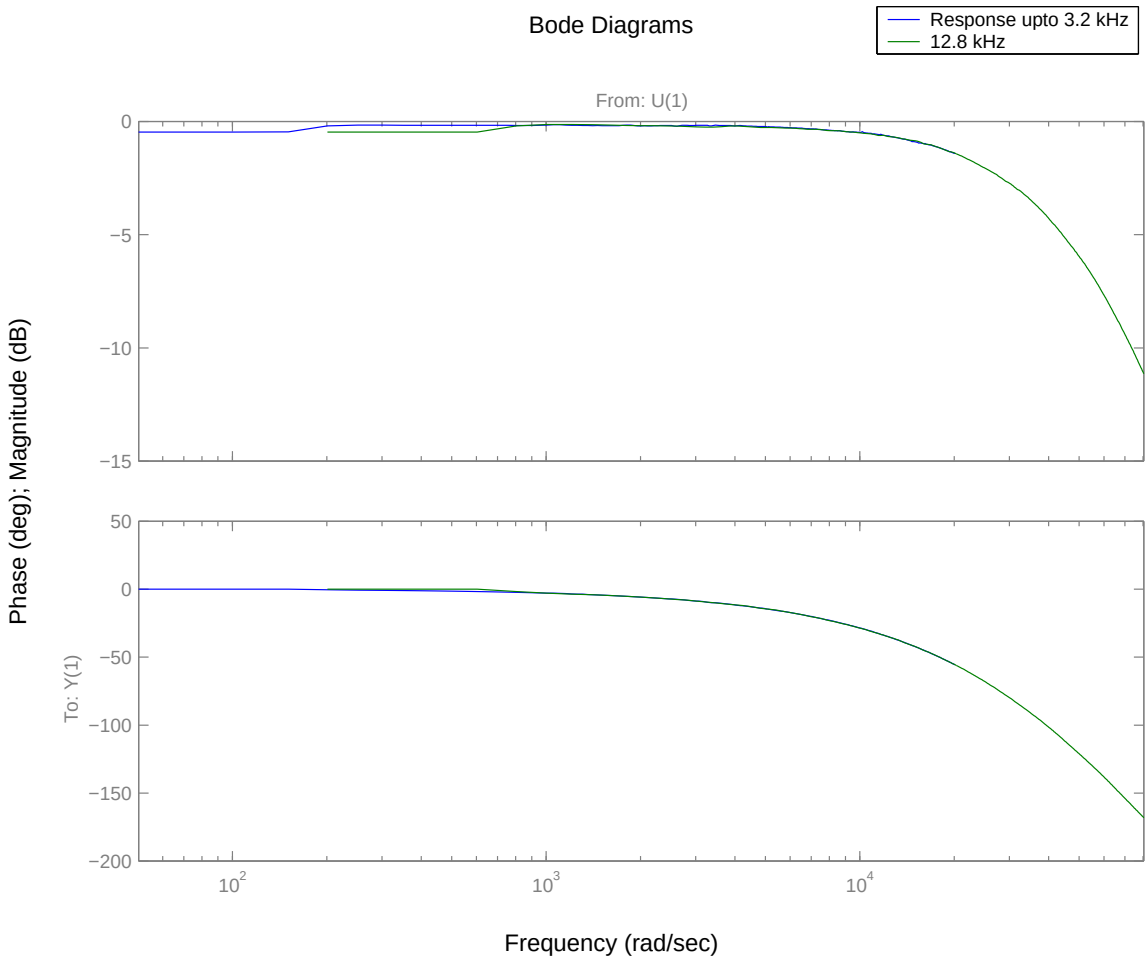

Figure 4.4. Frequency response of unloaded amplifier (in open circuit mode).

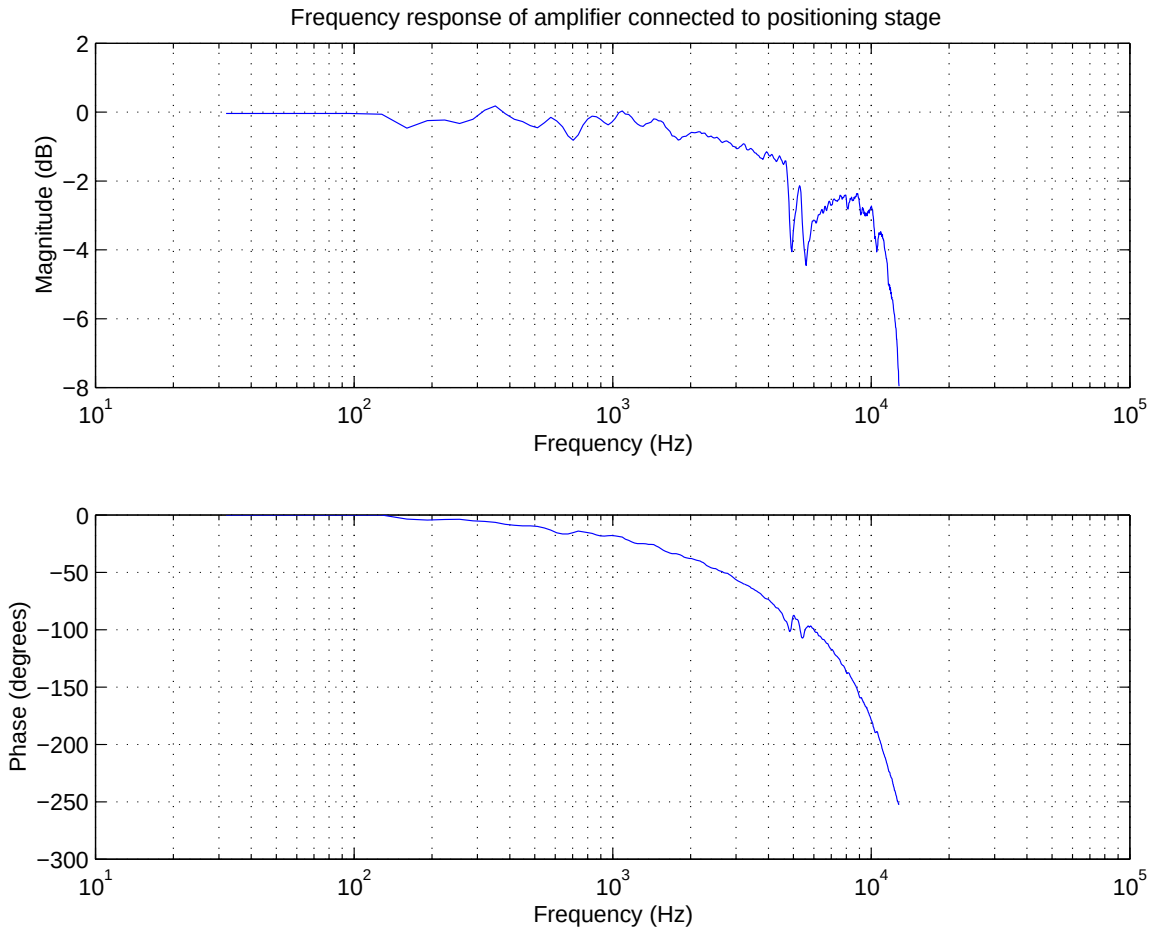

Figure 4.5. Frequency response of amplifier with the PZT load (closed circuit mode).

4.1.1.2. Dynamics of the Capacitive Sensor

The monitor output of the sensor has a range of 0-10 V for a nominal displacement of 0-12 μm of the actuator. Also inferring from the test data (as explained in Chapter 2), the sensor is assumed to be linear and has negligible dynamics in the frequency range of interest. Hence it is assumed to be a static component with a gain of 1/1.2 V/μm.

4.1.1.3. Slew Rate Limiter

One component in the electronic system which was not considered in the modelling process is the slew rate limiter. This is a nonlinear circuit which limits the rate of change of the control input (and hence the output voltage of the amplifier). If this circuit is not present then the output voltage of the amplifier will not be the same as that of the input voltage (due to limitations on the electronics of the amplifier). This hampers the reliability of the amplifier, in the sense that the output voltage does not correspond to the input and additional (nonlinear) dynamics have to be considered.

Hence to ensure that the voltage applied onto the piezoelectric stack actuator is proportional to the control input applied to the actuator, the slew rate of the input signal has to be checked. The slew rate limit is set by turning a potentiometer. The range of the actual setting is 15 V/ms to 1500 V/ms. This setting on the experimental system is close to its maximum value of 1500 V/msec. This was again verified by experiments in which the potentiometer to adjust the setting was initially set to one of its extremities. The input was then ramped up at a rate that was between the two limits (say 750 V/msec.). It is apparent that the rise of the output voltage (of either the capacitive sensor or of the amplifier) is bound to be much slower for one extreme setting of the slew rate limiting circuit. That setting would then correspond to the lower slew-limit setting.

4.1.2. Linear Controller: Performance Requirements and Design

Since the system is known to be nonlinear, it is necessary to design a controller that firstly ensures stability under the operating conditions. Hence robustness of the controller has to be guaranteed in the design stages. The specifications/requirements are given below.

4.1.2.1. Performance Requirements

The overall model for the system is a third order transfer function (with a time delay) and the system is of type zero. Hence the static error due to a constant input/disturbance is non-zero. Hence the first requirement was that the *static error due to a step input be zero.* This can be easily achieved by including a free integrator in the controller structure. Hence for the purposes of the controller design an augmented plant will be considered.

Robustness of the controller is a very critical issue, as the design plant model is a nominal one and the actual system may vary from the nominal model. Some of these variations were studied in an empirical fashion in Chapter 3 (Nonlinear Effects). The most significant variation observed was the static gain of the system to step inputs. Based on the extrapolated experimental results (Figure 3.6 , Figure 3.8) , the *gain margin of the system (with the controller) should be greater than 2 (≈7 dB).*

As discussed in the section on Hysteresis in Chapter 3, the effect of hysteresis is an additional phase lag in the response of the system. Since the phase lag observed, in the experiments to determine the frequency response, is the total phase lag in the system, it is difficult to "separate" the phase lag caused due to hysteresis. To estimate this "phase-lag" due to hysteresis, a very low frequency sinusoidal input was used. The amplitude of this input was so chosen to obtain the maximum possible range of travel from the stage. This would correspond to a maximum sensor output (and also an A/D input limit) of +10 V. When the output is plotted against the input, for this experiment, the maximum distortion due to hysteresis is observed.

To determine the "phase distortion" that is caused by hysteresis, let us assume that a linear system is excited by the same input as that was applied to the positioning system. Since the hypothetical system is linear, the output is simply shifted by a phase. By a trial and error process, the phase lag and the amplitude of the output of this linear system can be chosen so that the distortion in the input-output plot for this linear system is the same as that for the hysteretic system. When the loops match

reasonably well, the phase lag due to the hysteresis phenomenon can be assumed to be the same as that of the linear system. A variation of this approach, also used for modelling hysteresis is called the "Phaser Model" developed by Hernandez and Cruz [53, 54].

For the positioning system a 4 V amplitude sinusoid at 1 Hz. was used to excite the system. The range of motion of the stage (at steady state conditions) for this input was pretty close to the maximum range of output motion possible.

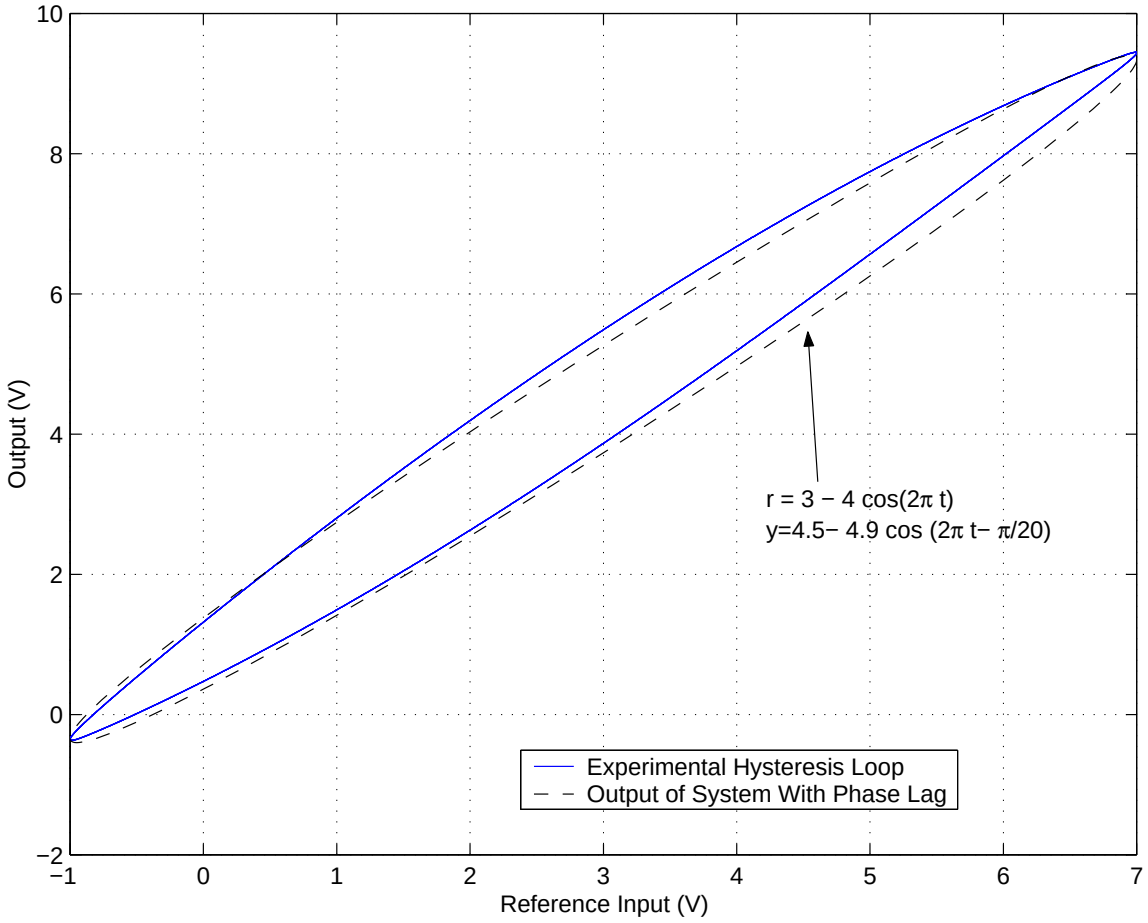

Figure 4.6. The Input Vs. Output plots for the hysteretic system and the hypothetical linear system.

From the above plots we can assume that the maximum phase distortion caused by hysteresis is 9 degrees. Therefore, the *phase margin that is needed is 60 degrees*, in order to ensure robust stability and also a reasonably good settling behavior.

The bandwidth of a system is usually a good indicator of its speed of response. Hence the final requirement is that the *maximum possible closed loop bandwidth be achieved*. For reasons similar to those stated for the phase margin, this is translated into achieving the *largest gain cross-over frequency* for the closed loop system. The desired closed loop bandwidth is in the worst case to be equal to the bandwidth of the system with the servo controller provided by Polytec PI. This is determined experimentally to be 200 Hz. from the frequency response of the closed loop system with the servo-controller card in Figure 4.7 on page 77.

4.1.2.2. Controller Design

The bode plot of the plant model augmented with a free integrator (augmented plant model) , is shown in Figure 4.8 on page 78. It can be seen that by using a *simple proportional controller (with a gain of 2300 of* $\approx 65dB$*) for the augmented plant*, the bandwidth can be increased to that of the servo card from Polytec PI. This would also provide a gain margin of $\approx 18dB$ and a phase margin of 76 degrees. The gain cross-over frequency (ω_{gc}) for this case is $\approx 1393\ rad/sec.(220\ Hz)$. If this gain cross-over frequency is unsatisfactory, then the proportional gain can be increased further, but this would decrease the phase margin. Hence a better controller structure, preferably a dynamic structure, is needed.

Simple forms of dynamic compensators are Lead and Lag compensators.

Lead Compensator When a lead compensator was used, it was seen that even though lead compensators are used to increase the bandwidth and phase margin, in this case, they do not meet the gain margin requirement. As a lead compensator increases the high frequency gain, it causes the peak in the fre-

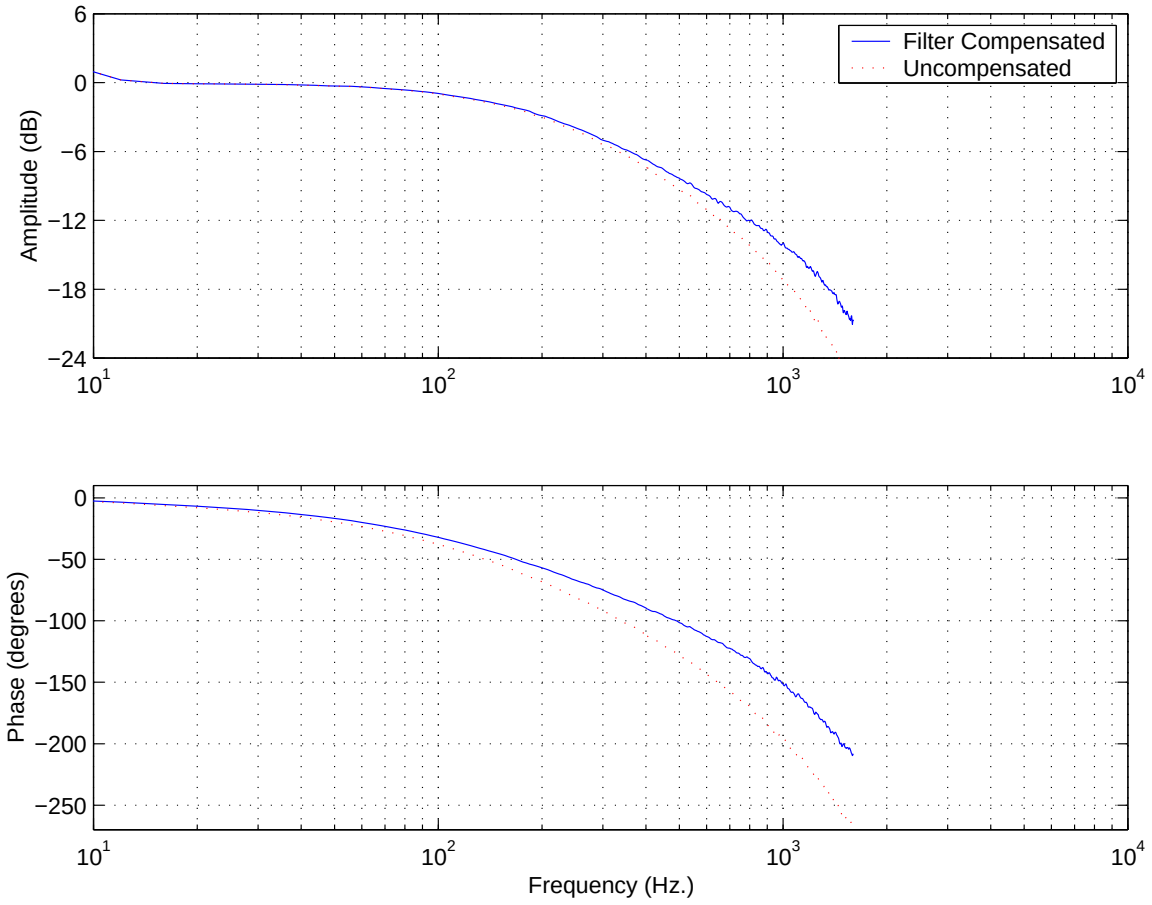

Figure 4.7. Frequency response of closed loop system with Polytec's servo card.

quency response to go close to the 0 dB line. Hence the gain had to be decreased to such an extent that the gain cross-over frequency was only about 165 Hz. Therefore lead compensators were not used.

Lag Compensator Lag compensators are typically used to increase the low frequency gain. But the shape of their frequency response is such that if the static gain is chosen to be 1, they attenuate the gain at higher frequencies (thereby reducing the gain crossover frequency). Since the gain crossover frequency of the plant can be increased easily using a gain in the loop, the desired gain crossover

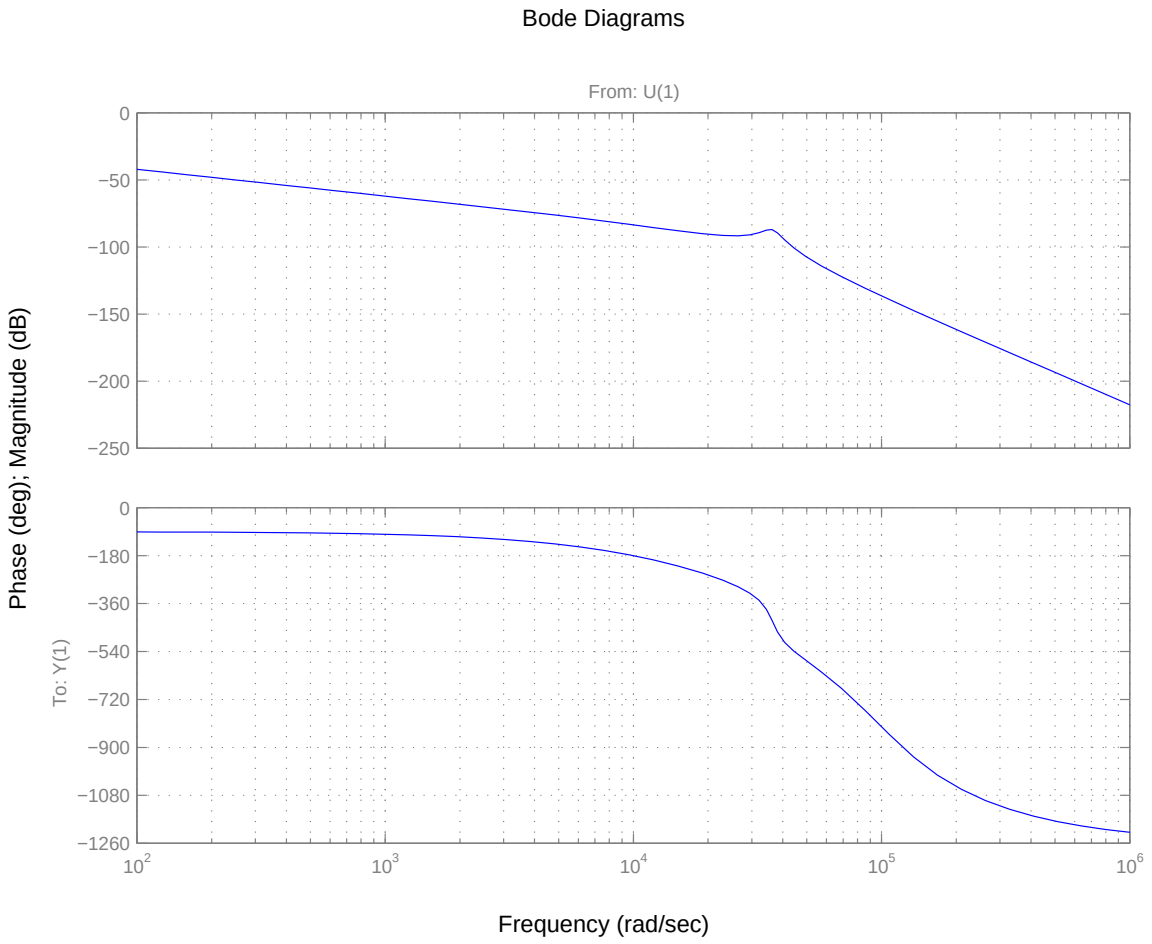

Figure 4.8. Bode plot of **plant** augmented with a **free integrator**.

frequency (hence desired closed loop bandwidth) can be attained using the lag compensator with a large enough gain.

The lead compensator designed yielded a gain margin of about 11 dB, a gain crossover frequency of about 3300 rad/s and a phase margin of 60 degrees. The resulting closed loop bandwidth was around 6000 rad/sec ($\approx$ 950 Hz). As is apparent, the lag compensator design is a better choice than the Lead compensator. The only drawback of this design is that the phase margin is not large enough to guarantee a very good settling behavior in all cases.

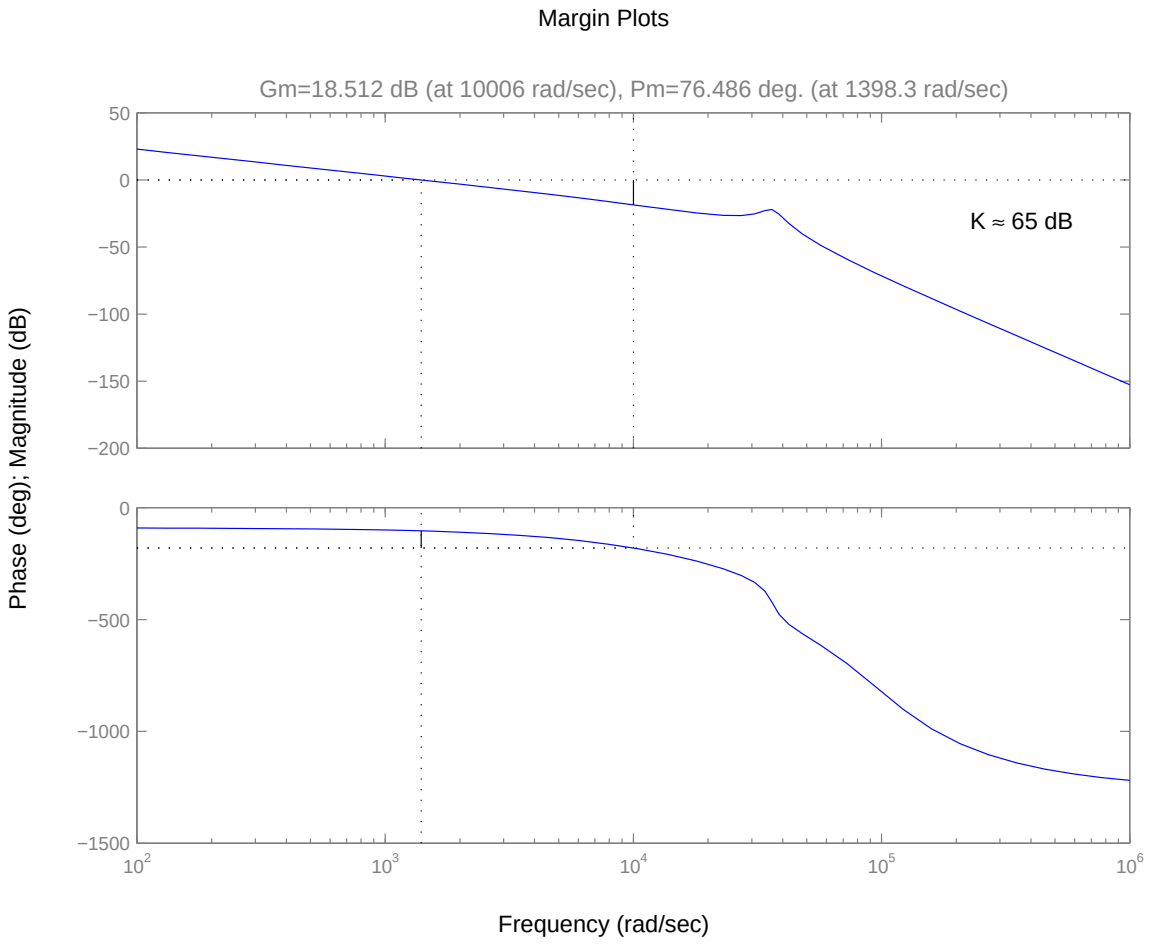

Figure 4.9. Margins of **plant augmented with a free integrator and a gain** ($K \approx 1770$).

Combined Lead and Lag Design This approach effectively seeks to combine the advantages of the lead design (i.e. good settling behavior) with that of the lag design (good gain margin and bandwidth). When designed, the resultant system achieves only a marginally better performance compared to the lag compensator alone (in terms of bandwidth and phase margin).

From the problems encountered when designing a Lead compensator, it would seem logical that a notch filter with a non-unity static gain would effectively increase

the bandwidth and still meet the gain and phase margin specifications, when the notch is tuned for the fundamental resonant frequency that degrades the gain margin. The problem with this approach is that when an external load is added on the stage, the resonant frequency changes significantly and the notch filter (which is tuned for a specific frequency) introduces uncancelled zeros in the loop. Whereas when a lag compensator is used, then even though the system performance is degraded, the system still remains stable (until the mass is increased beyond a certain extent).

After consideration of the above factors, it was decided to use the Lag Compensator as it provides the best compromise between the robust stability, bandwidth requirements and still provides a reasonably good settling behavior along with a simple structure for real-time implementation.

The Lag Compensator used is:

$$G_{lag}(s) = 10000 \times \frac{(s+1)}{\left(\frac{s}{0.398}+1\right)} \tag{4.5}$$

The bode plots of the open loop system (with the nominal, linear design plant model) and those of the closed loop system with the lag compensator are shown in Figure 4.10 on page 81 and Figure 4.11 on page 82 respectively. From the theoretical bode plot of the closed loop system it is apparent that the lag compensator does indeed achieve a higher closed loop bandwidth than the servo controller purchased from the manufacturer. The simulated step response with the Lag compensator is shown in Figure 4.12 on page 83. It should be noted that the simulations are performed in Simulink where all the quantization and sampling effects are accounted for.

The simulation results shown in the above figures were performed using MATLAB's "*step*" command. This does not account for the effects of A/D & D/A conversion, sampling and the slew rate limiter present in the actual system. To simulate and check the performance in the presence of these effects, a SIMULINK model was used (see figure Figure 4.14 on page 85). The performance shown in figure Figure 4.13 on page 84 indicates that the "real" performance is very similar to what was expected from the MATLAB simulations (continuous time simulation without sampling and

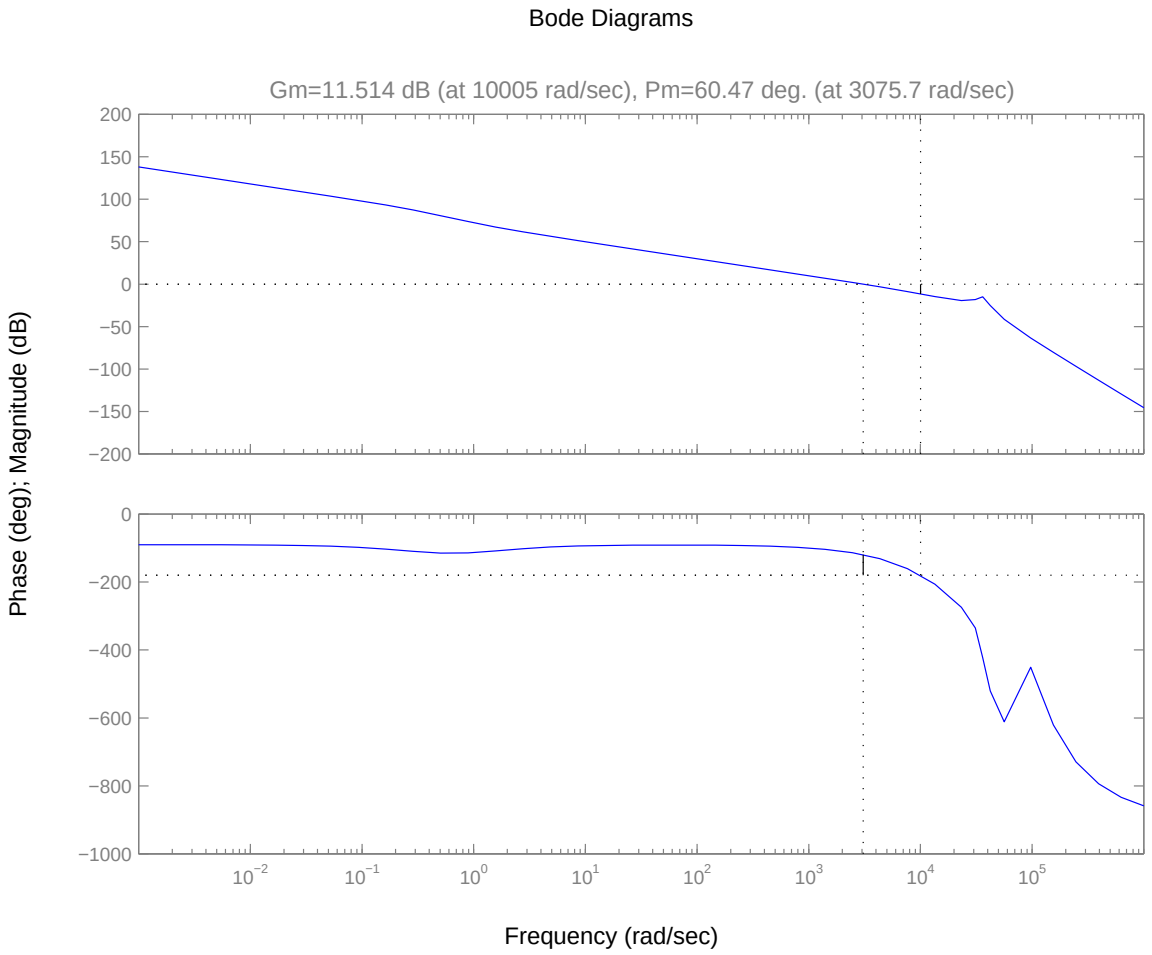

Figure 4.10. Bode plots for the open loop system with the designed Lag Compensator.

slew rate and saturation effects). This is also a measure that the linear design model used is a good approximation of the system behavior and that sampling at 50 kHz (which is the sampling rate used for the discrete simulations) does not degrade the performance of the controller.

The following conventions are adopted for the plots showing the performance of the system with the designed controller:

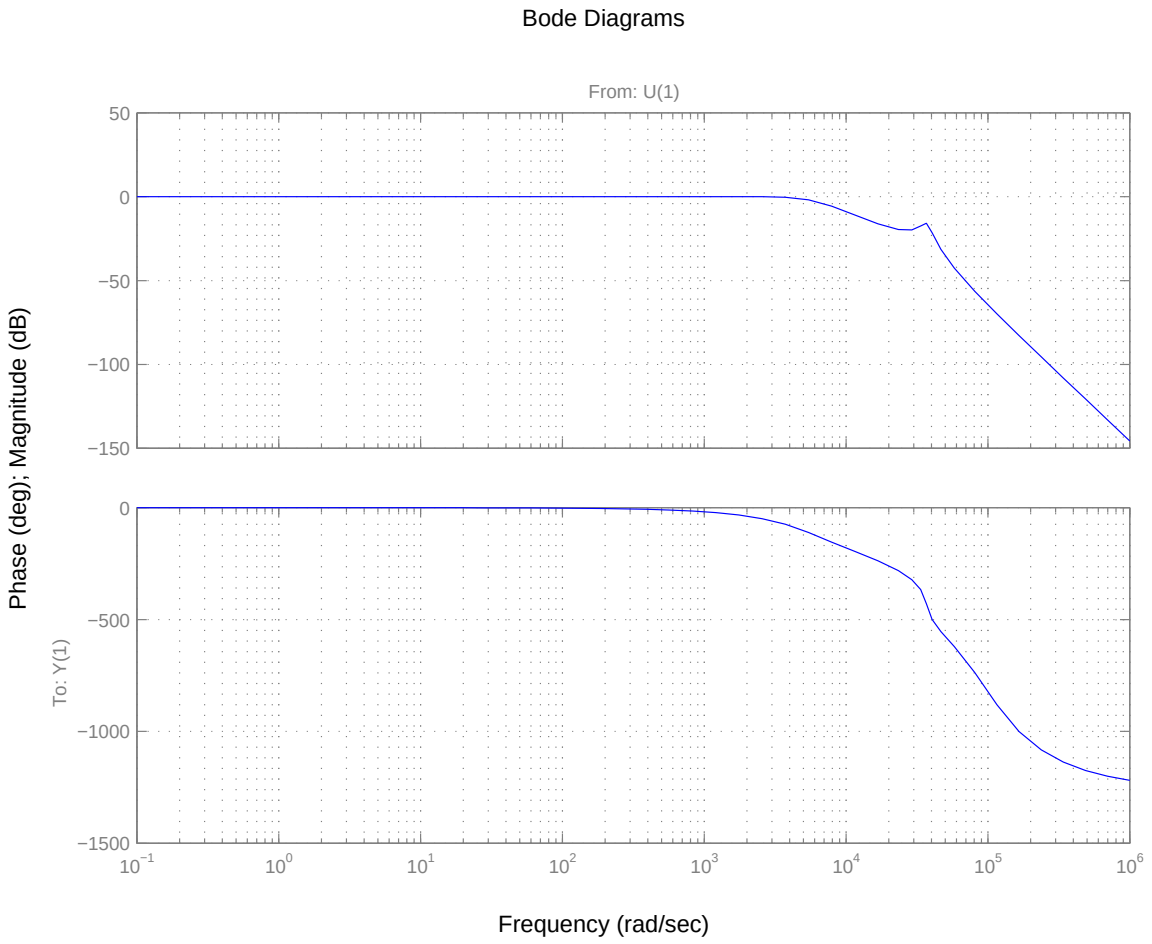

Figure 4.11. Bode plots of the closed loop system with the designed Lag compensator.

r: Reference Trajectory (trajectory to be tracked)

y: Output of closed loop system

e: Tracking error (=r-y)

u: Control Input (to the plant)

$T_{s-x\%}$: x% Settling times

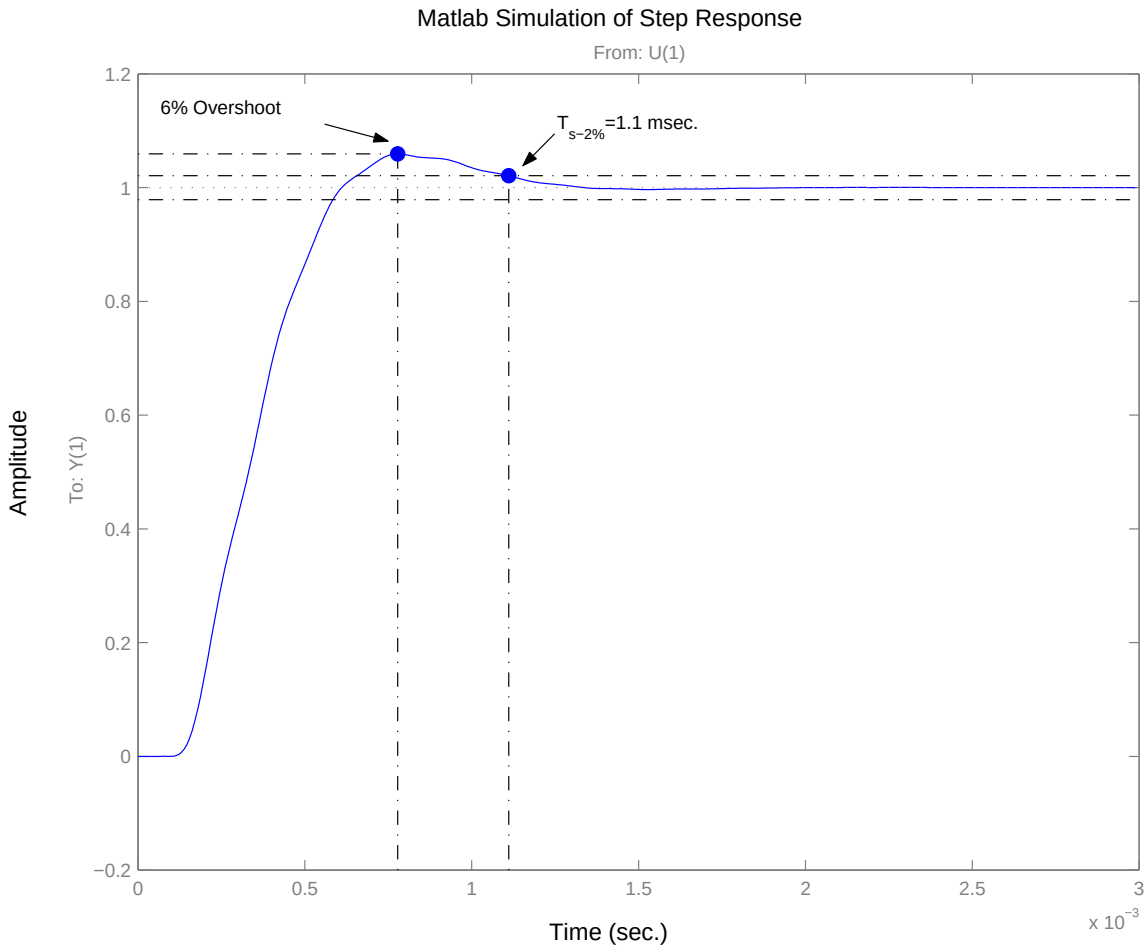

Figure 4.12. Simulated response (continuous time; in MATLAB) to a step input of closed loop system with Lag compensator.

4.1.2.3. Performance of Controller

Once the simulations showed good performance of the overall system with the compensator, the controller was implemented using the dSPACE system. A sampling rate of 50 kHz was used for the real time control loop. The actual response to a square wave (step input) can be seen in figure Figure 4.15 on page 86. The values for the settling time and overshoot compare very well with the simulation results.

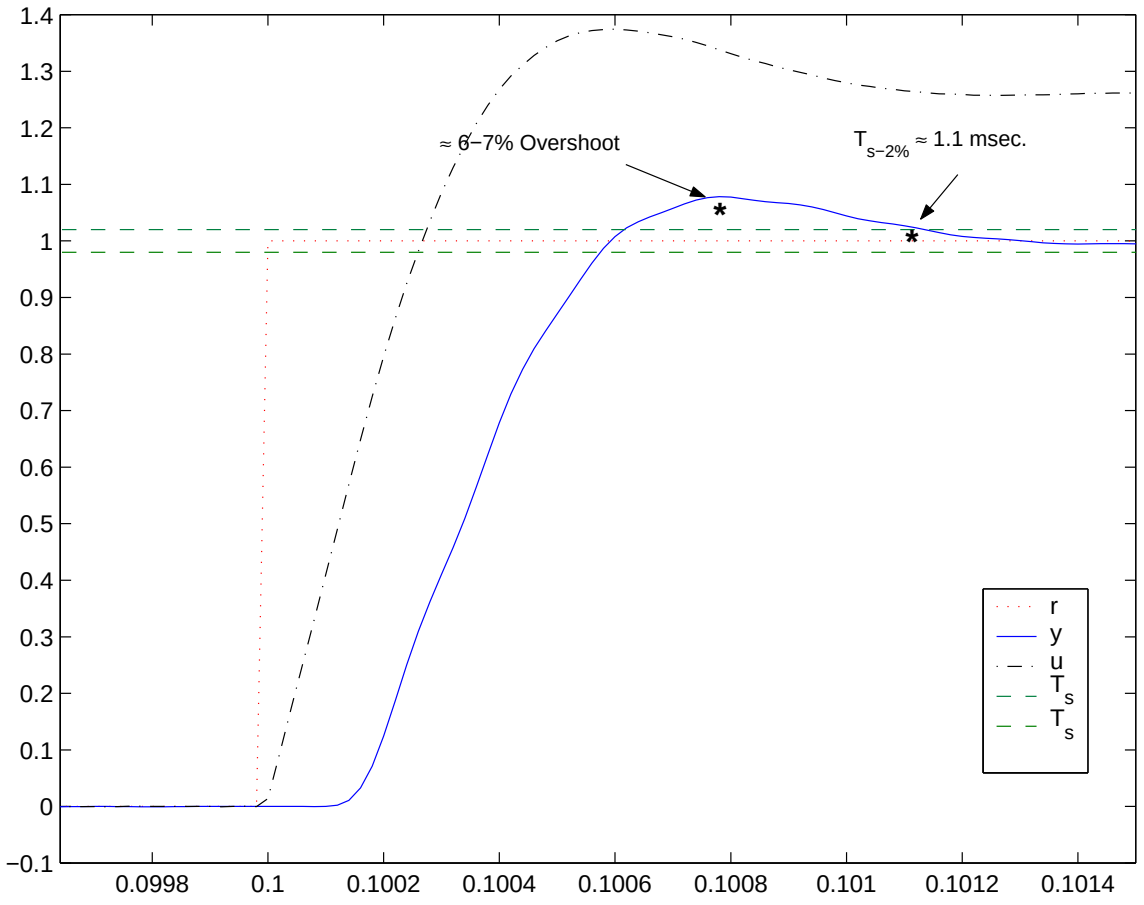

Figure 4.13. Results of simulation performed using SIMULINK.

This is another indication of the validity of the linear design/simulation model for the positioning system.

Also comparing the results in Figure 4.15 on page 86 and Figure 4.16 on page 87, we can conclude that the controller achieves better performance in terms of the achieved bandwidth when compared to the servo card even in real implementation. Even though the overshoot is considerably higher for the controller designed, this overshoot behavior could be attenuated by designing a suitable pre-filter (feed-forward compensator) and a suitable trajectory planning algorithm.

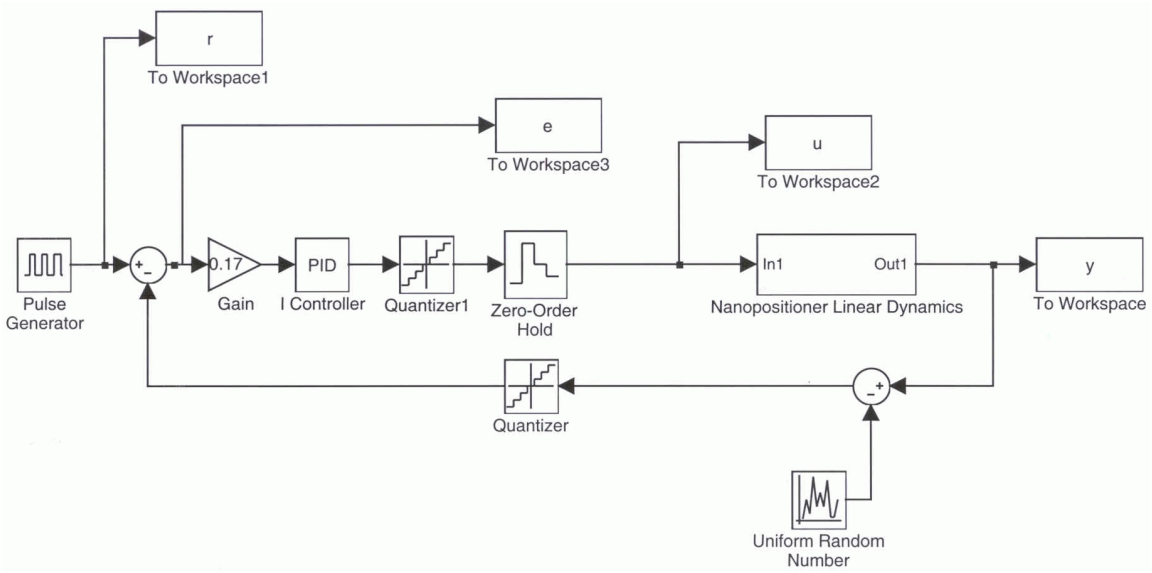

Figure 4.14. Linear simulation model in Simulink. (Block showing PID controller is a representation of location of Controller).

4.1.2.4. Pre-filter Design

Once the feedback controller has been designed, it ensures that the system is stable and achieves nominal tracking performance for any given reference trajectory. The tracking performance of the closed loop system can be improved by increasing the bandwidth of the closed loop. But this frequently causes stability problems and amplification of noise. The solution to improving the tracking performance without using large gains is to use a two degree-of-freedom control structure. This involves the use of both a feedback controller (to stabilize the system) and a pre-filter (to improve the tracking performance). This idea is used for the closed loop piezoelectric positioning system with the lag compensator.

If one can invert the dynamics of the closed loop system in the pre-filter then the dynamics of the closed loop system can be cancelled out and perfect tracking would be achieved. But frequently, inverting the closed loop system would lead to

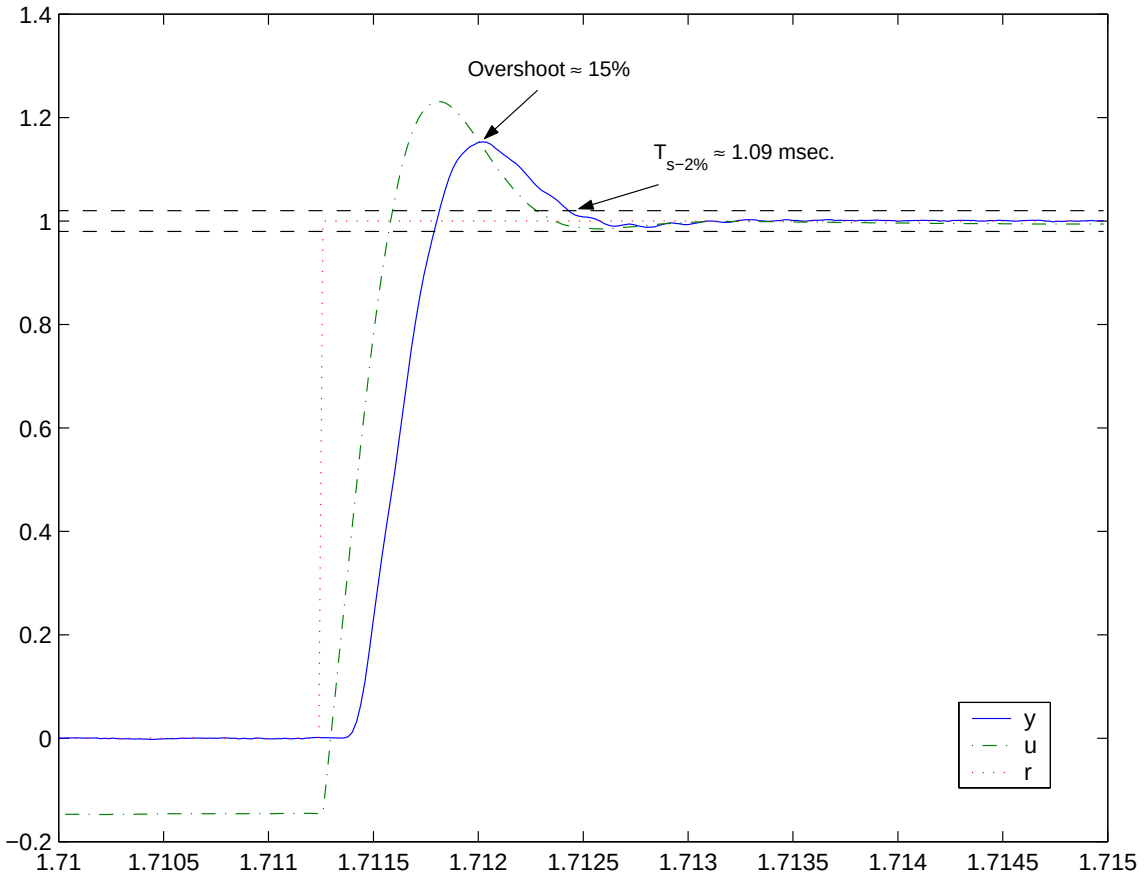

Figure 4.15. Step response of closed loop system with Lag Compensator.

improper transfer functions which cannot be implemented without prior knowledge of the reference trajectory and its derivatives. If these quantities are known in advance then this information could be used to implement this improper transfer function. The information about the reference trajectory is known if one designs the reference trajectory (*Trajectory Planning*), starting from the derivatives and integrating to get the reference trajectory.

For the piezoelectric positioning system with the free integrator and the lag compensator, the closed loop transfer function is a fifth order transfer function with one zero. An inverse of this would therefore contain 4 zeros in excess of poles. Therefore

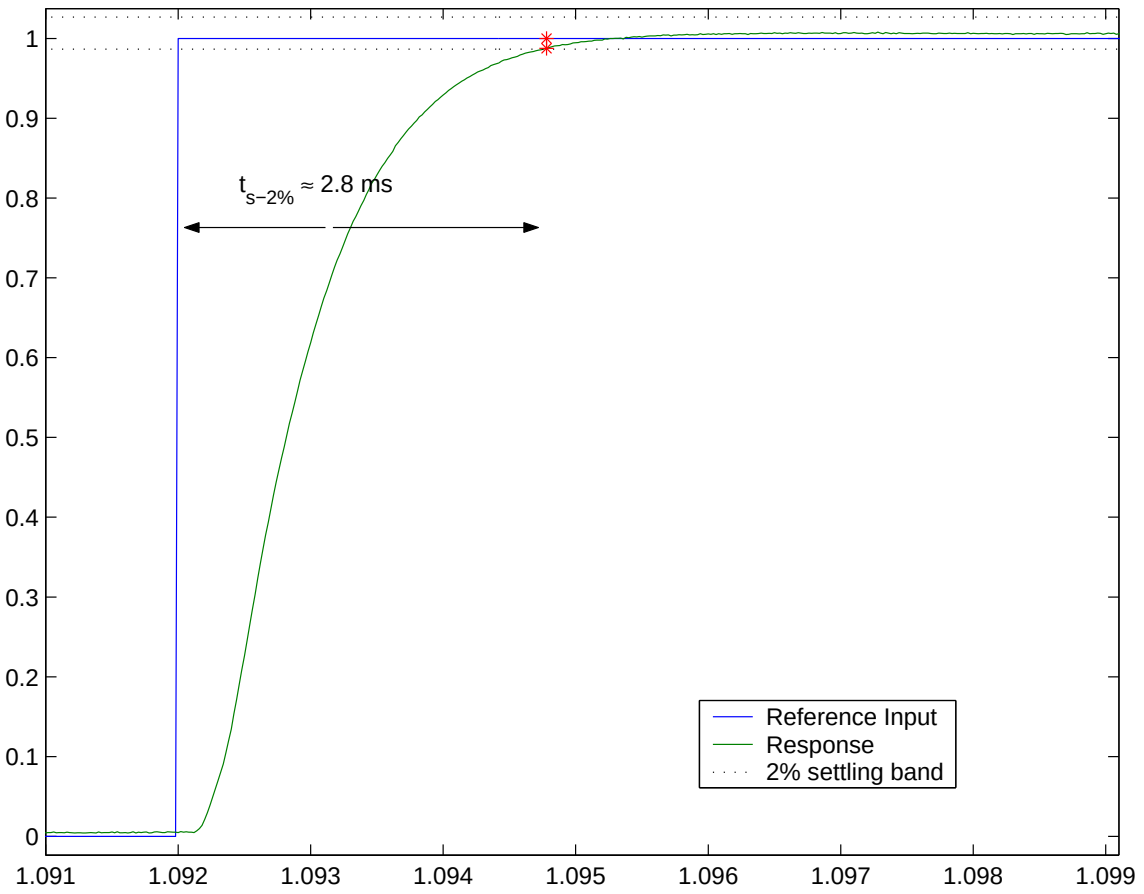

Figure 4.16. Step response of closed loops system with Polytec PI's Servo Card.

to "plan a trajectory" for this system we need to start from the fifth order derivative of the reference trajectory and work down to the zeroth order derivative. This is a very cumbersome process and relying on this approach guarantees (almost) perfect tracking performance to only those trajectories which have been "planned". This is a frequently useful approach and is used widely in robotics where all the path information is known beforehand.

But in other applications this finds little use as one does not know the trajectory in advance. Reliance on differentiation to generate the derivative from the given reference signal amplifies the noise and hence degrades the tracking performance.

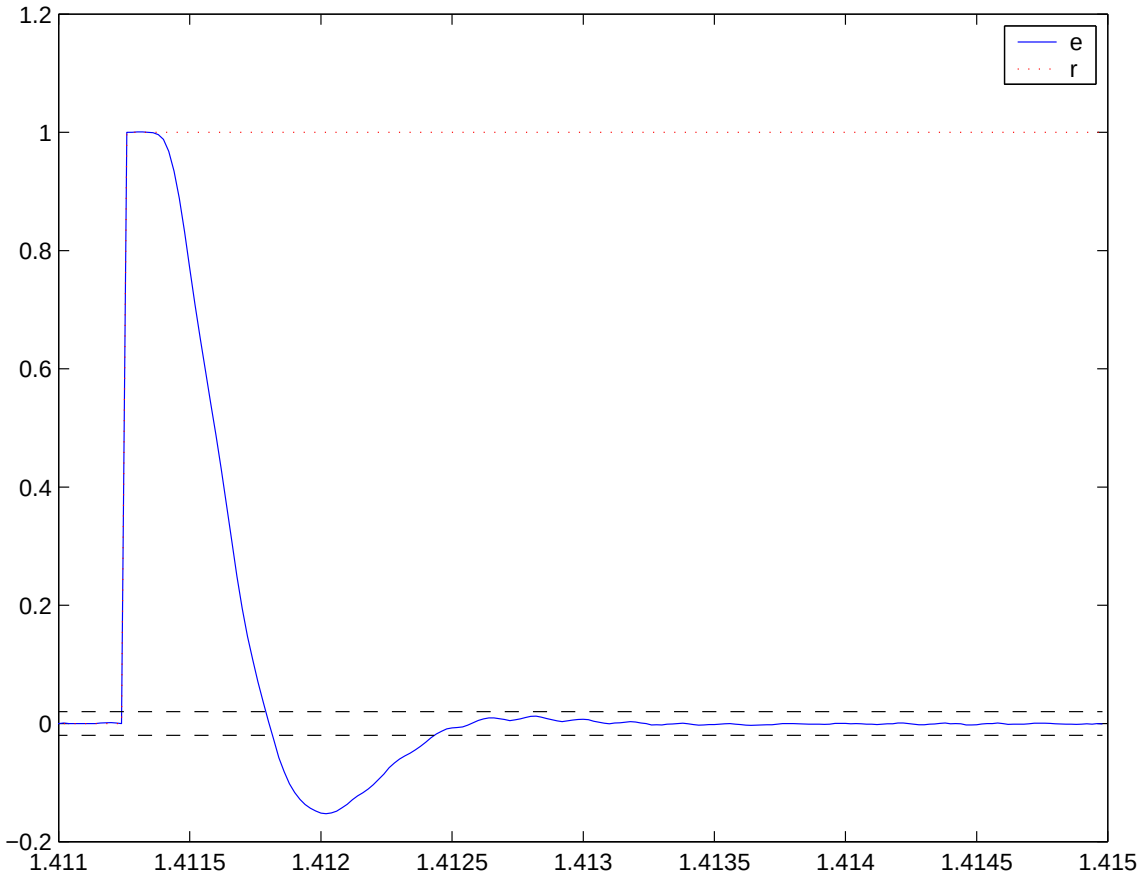

Figure 4.17. Tracking error for a step input with Lag Compensator.

Therefore a more general approach which includes both trajectory planning and pre-filter implementation is used here.

Since the inverse of the closed loop transfer function is an improper transfer function and hence un-implementable, it (the inverse) is made implementable by augmenting the denominator with enough number of high frequency poles to make it bi-proper and hence implementable without prior knowledge of reference input derivatives. This is equivalent of performing the trajectory planning with a filter so that the derivatives (filtered) are obtained from the reference trajectory.

The transfer function models of the piezoelectric positioning system is:

$$\begin{aligned} G_p(s) &= e^{(-T_d\,s)}\,\frac{1}{\frac{s}{2\pi\,2000}+1}\times\frac{0.79}{\frac{s^2}{(2\pi\,5792)^2}+\frac{2\,0.08\,s}{2\pi\,5792}+1} \\ &= e^{(-T_d\,s)}\,G_p'(s) \end{aligned} \tag{4.6}$$

The compensator's transfer function is:

$$G_c(s) = K_c\,\frac{(s+1)}{s\,(\frac{s}{0.398}+1)} \tag{4.7}$$

The closed loop Transfer function of the systems with the above plant and compensator is:

$$T(s) = \frac{G_p(s)\,G_c(s)}{1+G_p(s)\,G_c(s)} \tag{4.8}$$

The pre-filter for (4.8) is,

$$\begin{aligned} H(s) = [T(s)]^{-1} &= \frac{1+G_p(s)\,G_c(s)}{G_p(s)\,G_c(s)} \\ &= 1+\frac{1}{G_p(s)\,G_c(s)} \qquad (4.9) \\ &= 1+e^{(T_d\,s)}\,\frac{D(s)}{N(s)} \qquad (4.10) \end{aligned}$$

where,

$$L(s) = G_p(s)\,G_c(s) = e^{(-T_d\,s)}\,\frac{N(s)}{D(s)} \tag{4.11}$$

is the loop transfer function.

Since (4.10) cannot be implemented (unless the trajectory has been planned from the fifth order derivative), $H(s)$ is augmented with an additional number of poles so that new pre-filter is bi-proper. The implementable form of the pre-filter is,

$$H'(s) = \frac{1}{(\tau s+1)^4}\,H(s) \tag{4.12}$$

Let $r(t)$ be the actual reference trajectory that is specified as the trajectory to be tracked. When the augmented pre-filter shown in (4.12) is used, the reference input that is seen by the closed loop system in (4.8) is actually,

$$R'(s) = \frac{1}{(\tau s+1)^4}\,R(s) \tag{4.13}$$

Augmenting the ideal pre-filter can be treated similar to planning a trajectory starting from its derivatives. The trajectory that is to be tracked in this case, is defined by $r'(t)$ instead of $r(t)$. The other way to think about this is as if the input trajectory is filtered to make it less aggressive.

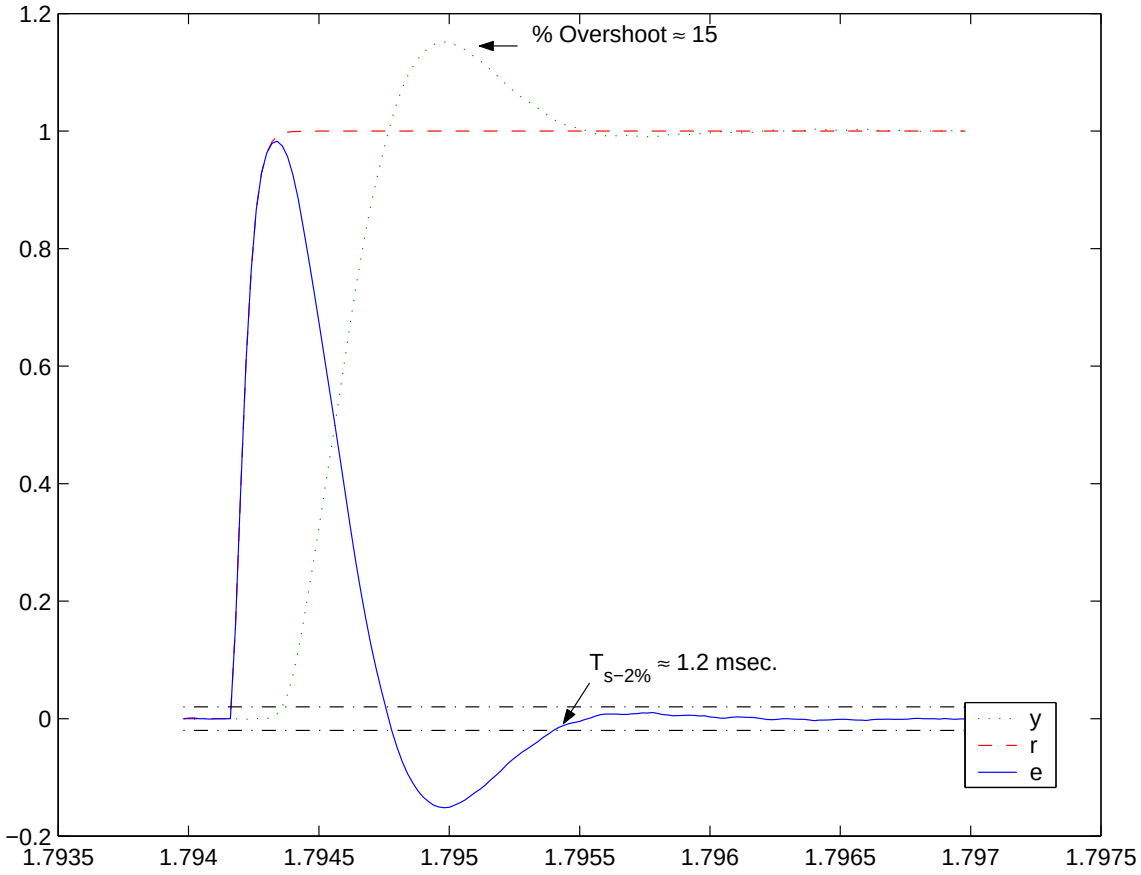

Figure 4.18. Experimental tracking performance of system with **"trajectory planning" block** and Lag feedback compensator.

This error is further reduced by including the pre-filter in conjunction with the trajectory planning block (Figure 4.19 on page 91).

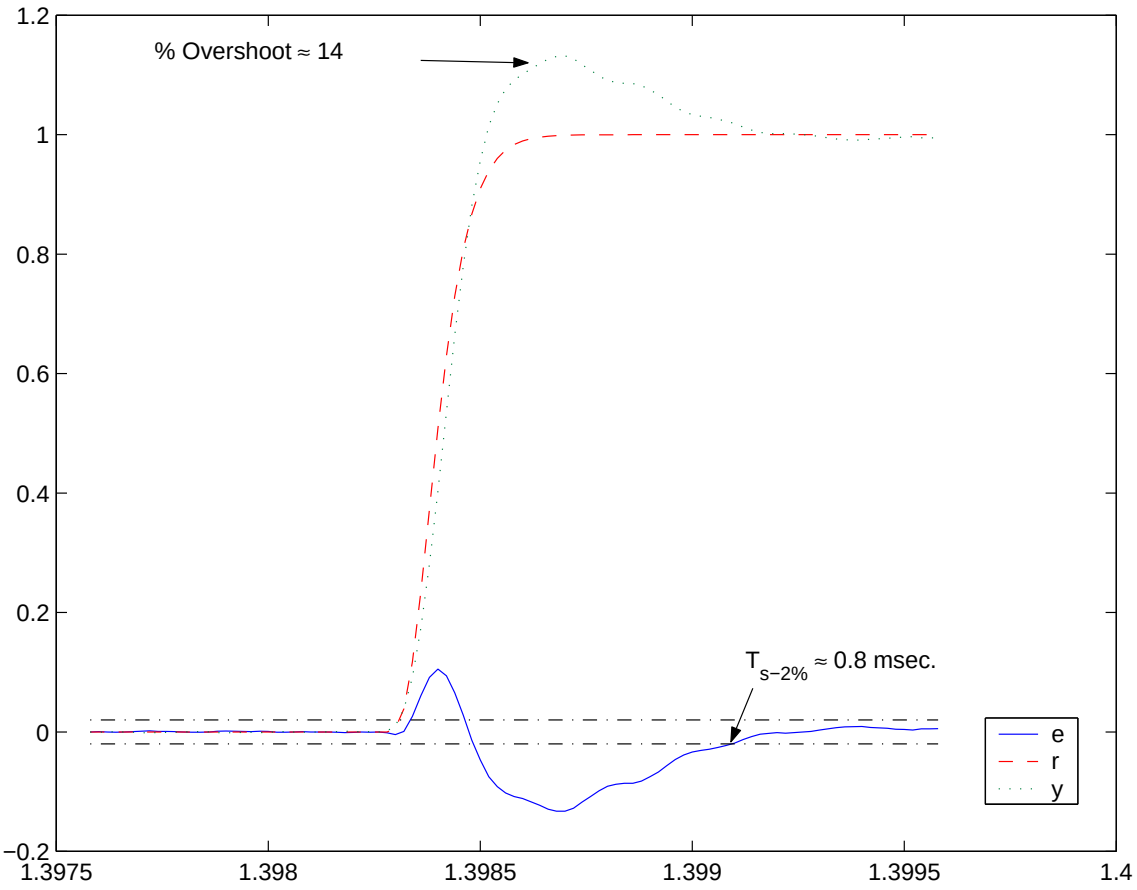

Figure 4.19. Experimental tracking performance of system with **augmented Pre-filter** and Lag feedback compensator.

5. MODELLING HYSTERESIS AND DRIFT

While the linear system model and the linear controller developed and designed in the previous chapters appear to perform satisfactorily, one should remember that the performance depends on the frequency of excitation. Since the bandwidth of the closed loop system is very high (≈900 Hz), the error due to the nonlinearities in the behavior of the plant is greatly attenuated (as they seem to be predominant only at quasi-static frequencies).

Hence, modelling the nonlinearities is the logical step ahead in effectively compensating for their effects in closed loop mode. This step is even more critical when piezoelectric actuators are operated in open loop mode (piezo tube scanners operate in open loop mode in STM's). In this mode of operation, there is no feedback loop to attenuate the nonlinearities. Therefore, feed-forward inverse compensation has to be used to achieve good tracking performance.

In this chapter the experimental results presented in Chapter 3 are used in modelling the nonlinearities. Each of the observed nonlinearities is treated individually. Models are proposed, parameterized and later verified by simulation and comparison with experimental data.

5.1. Nonlinear Static Gain

From the plots shown in Figure 3.5 on page 37 and Figure 3.10 on page 42 in Chapter 3 and Figure 5.1 on page 93, it is clear that the "static gain" to a step response or a sinusoidal input is input amplitude dependent. In general the gain seems to increase with the input amplitude and plateau's off at higher input amplitudes. This trend is to be expected as the system cannot exhibit infinitely increasing gains.

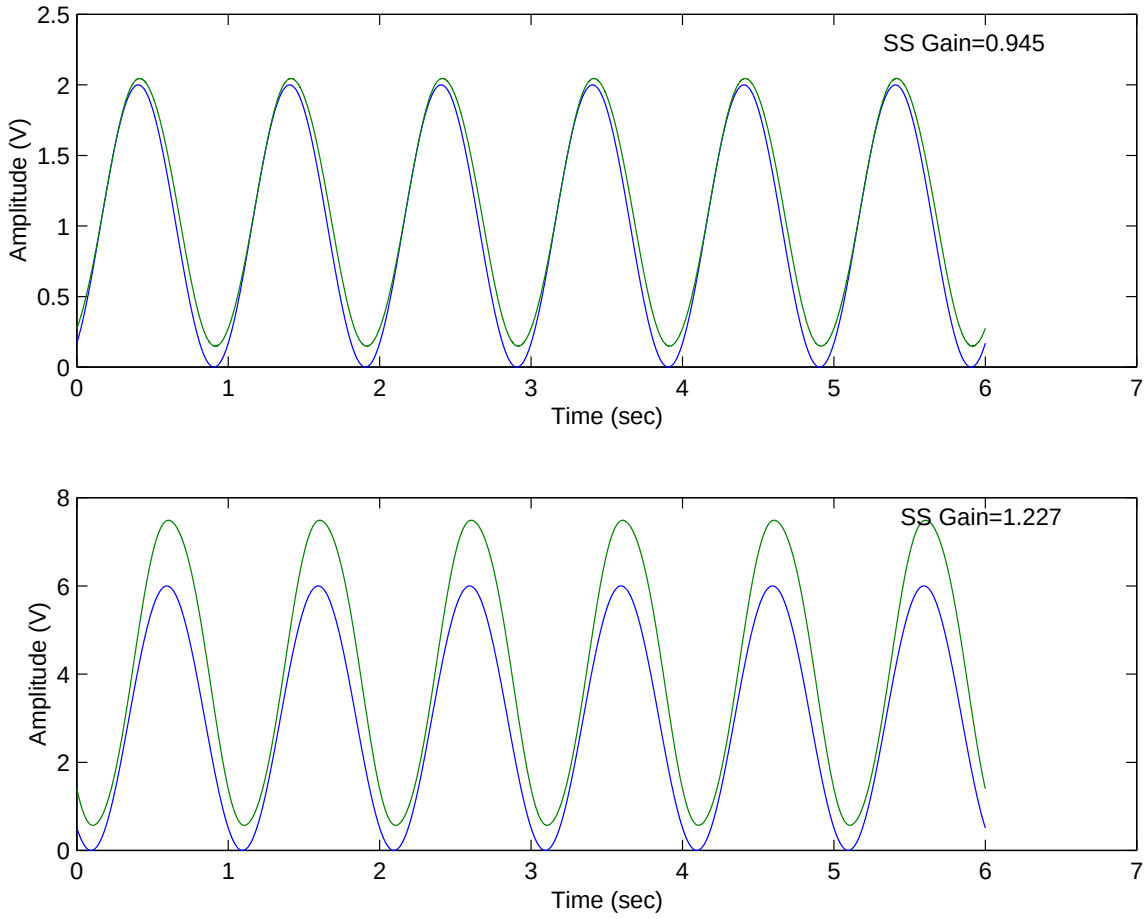

Figure 5.1. Time history plots of Inputs and Responses to sinusoidal inputs. The response shown, is obtained after cycling for approximately 2 minutes.

To capture this nonlinear behavior, it was decided that the variation seen in the "static" gain of the fast component (Figure 3.10 on page 42) will be approximated with a polynomial.

5.2. Drift

The slow component in the overall response of the positioning system can be observed in Figure 3.1 on page 33 for step inputs and in Figure 3.18 on page 51 for

offset sinusoidal inputs. This drifting behavior has been discussed in publications by Croft et al. [40] and Ge and Jouaneh [32]. In [32], the authors proposed that the drift in the midpoint of the loops observed in the case of cyclic/sinusoidal inputs was due to thermal expansion of the actuators. However, from Figure 3.18 on page 51 and Figure 3.4 on page 36, it can be inferred that this is probably not the cause. In Figure 3.18 , when the mean value of the input sinusoids was decreased, the drift in the mid-points of the response loops was also in the downward direction. If the drift is caused due to thermal expansion of the actuator, then one would expect that the drift would still be in the upward direction. Also there is a significant drift observed in the case of step inputs, where there is minimal heat generation (and consequently, minimal thermal expansion).

Chen and Montgomery [17] have explained the response of the actuators in terms of a fast reorientation of some dipole domains and the slow reorientation of the remaining. This explanation seems to be reasonable when one considers the statistical spread of the responses of all the dipoles within a given piezoelectric material. In an normal statistical distribution, there are always some dipoles which reorient almost immediately and some which take a long time. This would be in accordance with the observed behavior to a step input.

Whatever the physical reason might be behind the existence of drift, it is seen from Figure 3.4 on page 36 that the response of this component is similar to an over-damped system. Based on the observed response of the drift to a step and cyclic inputs, it was decided that this behavior will be captured by a combination of a sufficient number of first order transfer functions. The data that was used to fit the transfer functions was from the 1V step response test. After quite a few iterations of fitting the drift with first order terms, it was decided that the drift can be approximated quite well (see Figure 5.2 on page 95) with the three first order terms in a parallel combination.

$$G_{drift} = \frac{0.05}{(0.06\,s + 1)} + \frac{0.05}{(0.75\,s + 1)} + \frac{0.055}{(12\,s + 1)} \tag{5.1}$$

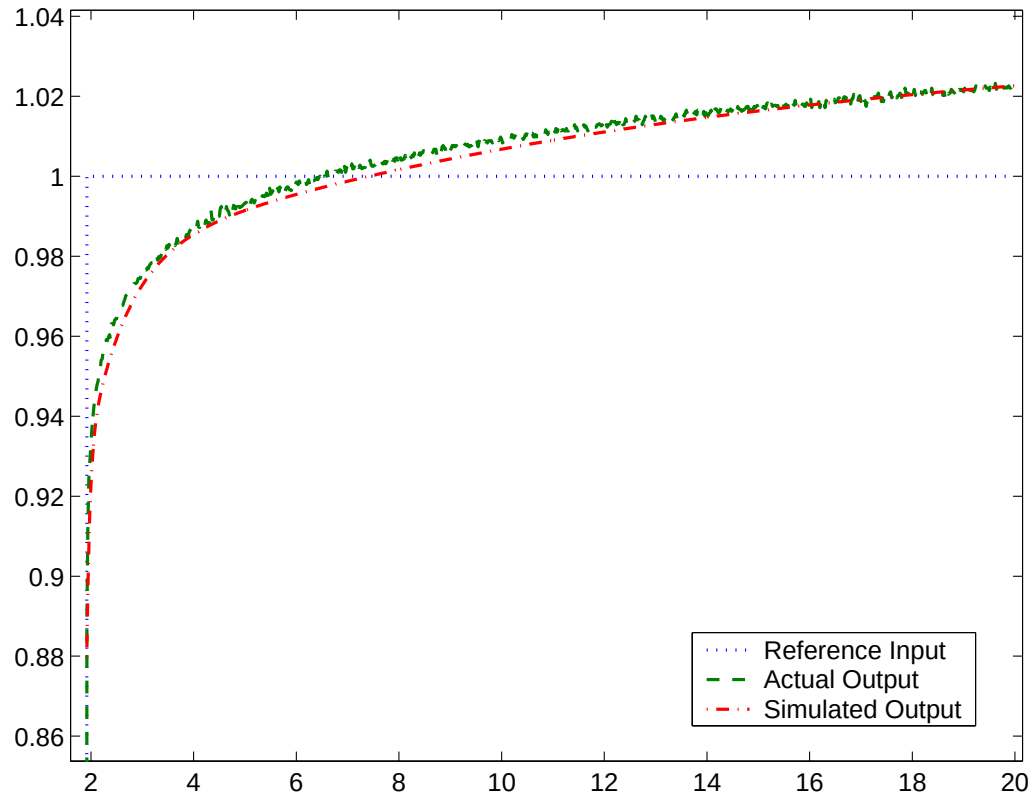

Figure 5.2. Comparison of the actual drift and the simulated response of the transfer function approximation.

This method to model the drift is also used in [40]. But, unlike [40], the gains of the first order transfer functions here are nonlinear. The gains of the static drift were calculated and results are shown in Figure 3.9 on page 41 and Figure 3.10 on page 42 in Chapter 3. These gains are based on the values of the drift, from the time that the fast component is assumed to have died down (as explained in Chapter 3) to the value at the end of the experiment (usually around 600 seconds). If this input dependent gain was not taken into consideration, then discrepancies can be seen between the simulated and the actual step responses (to different step heights) as shown in Figure 5.3 on page 96 and Figure 5.4 on page 97.

To model this variation in the static gain, the variation observed in Figure 3.9 on page 41 in Chapter 3 was approximated by a polynomial of sufficiently high order. A

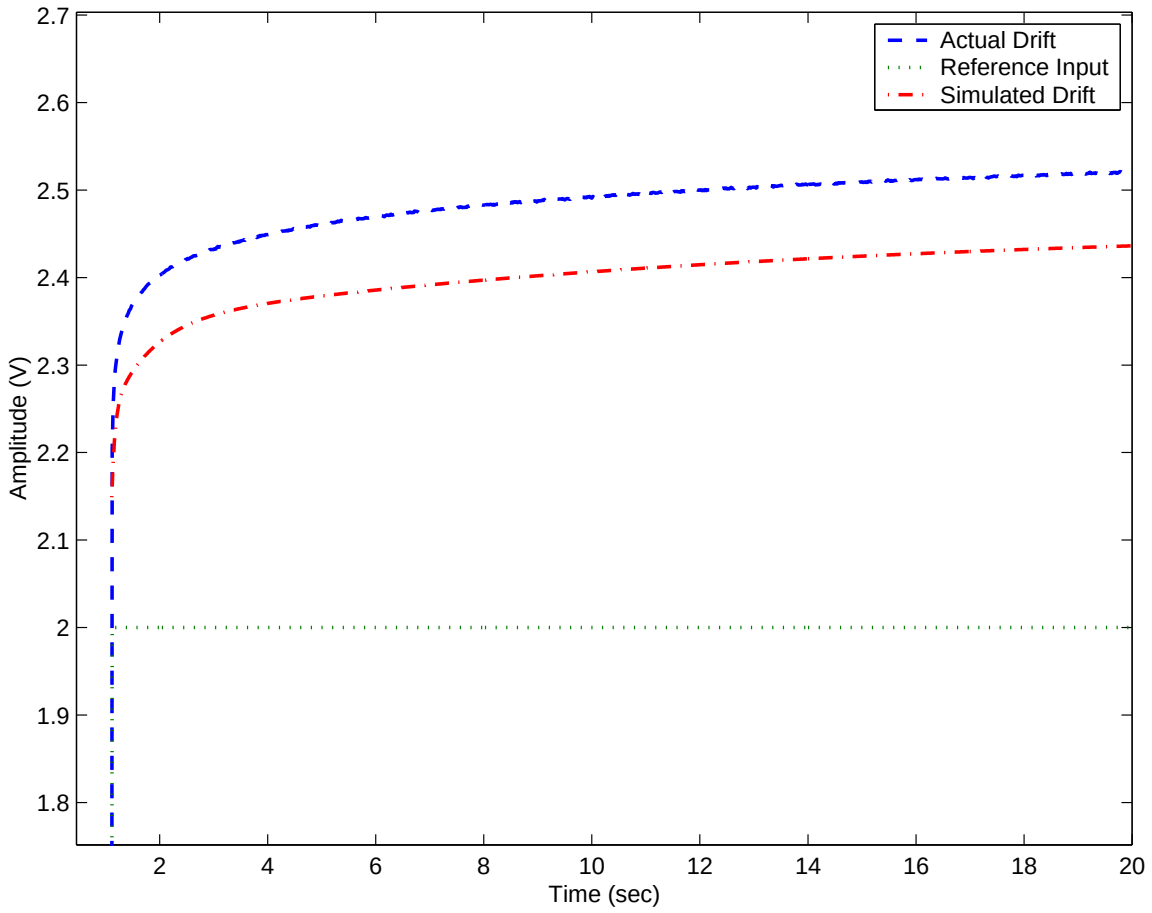

Figure 5.3. Actual and simulated drift for a 2V step input.

third order polynomial was used to approximate the gain variation. The coefficients of the polynomial were determined using the least squares approximation (Figure 5.5 on page 98). The polynomial that used was:

$$K_{drift}(u) = 0.0027\,u^3 - 0.0341\,u^2 + 0.1077\,u + 0.1204 \tag{5.2}$$

The transfer functions approximating drift (5.1) were derived using the step response to a 1V step input. Hence the polynomial above has to be normalized with the value of the polynomial for $u = 1$. The normalized polynomial gain is:

$$K_{drift}(u) = 0.0140\,u^3 - 0.1733\,u^2 + 0.5472\,u + 0.6121 \tag{5.3}$$

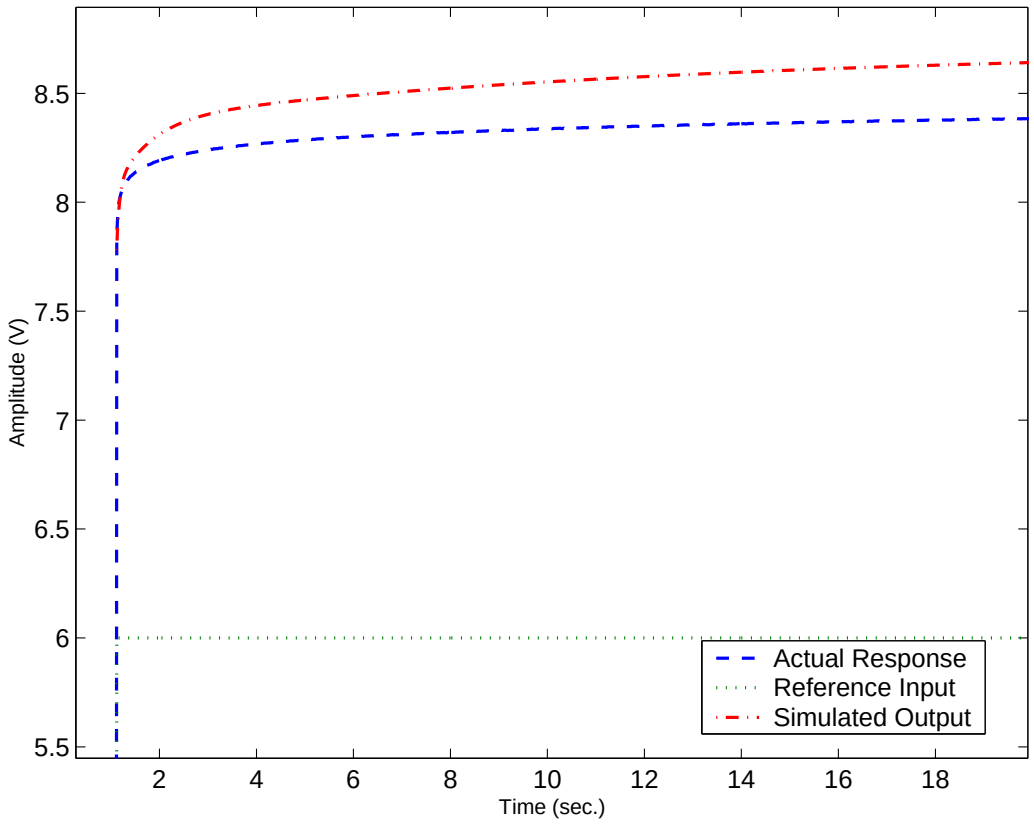

Figure 5.4. Actual and simulated drift for a 6V step input.

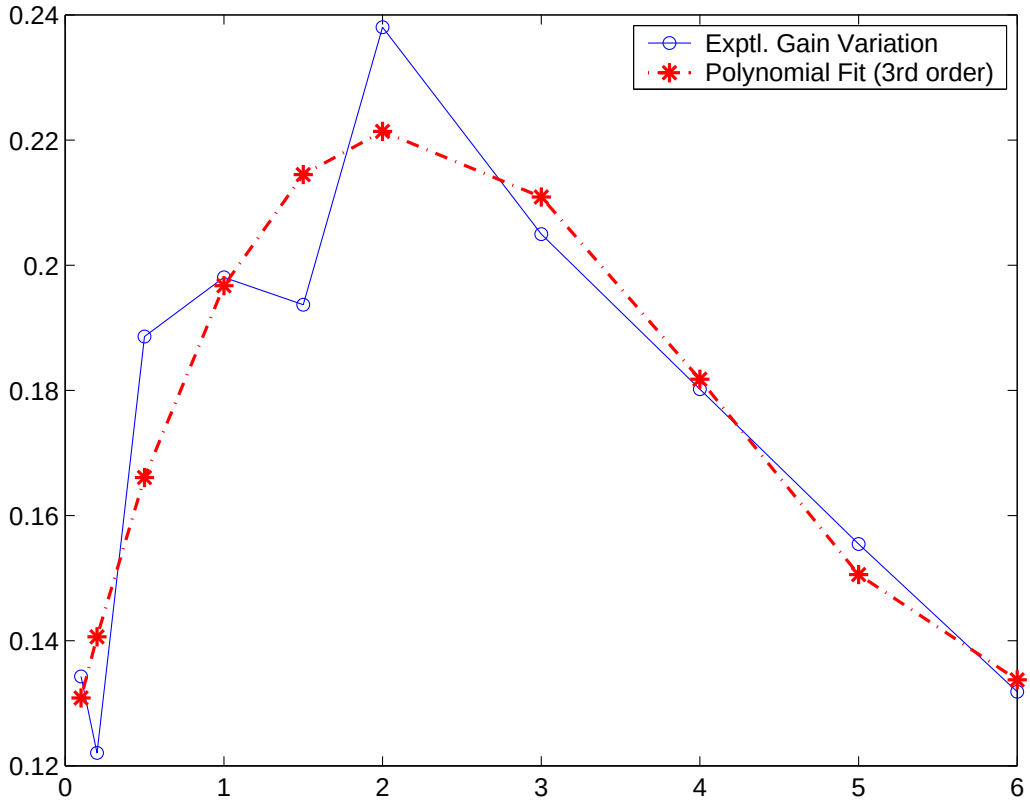

Figure 5.5. Actual and simulated drift for a 6V step input.

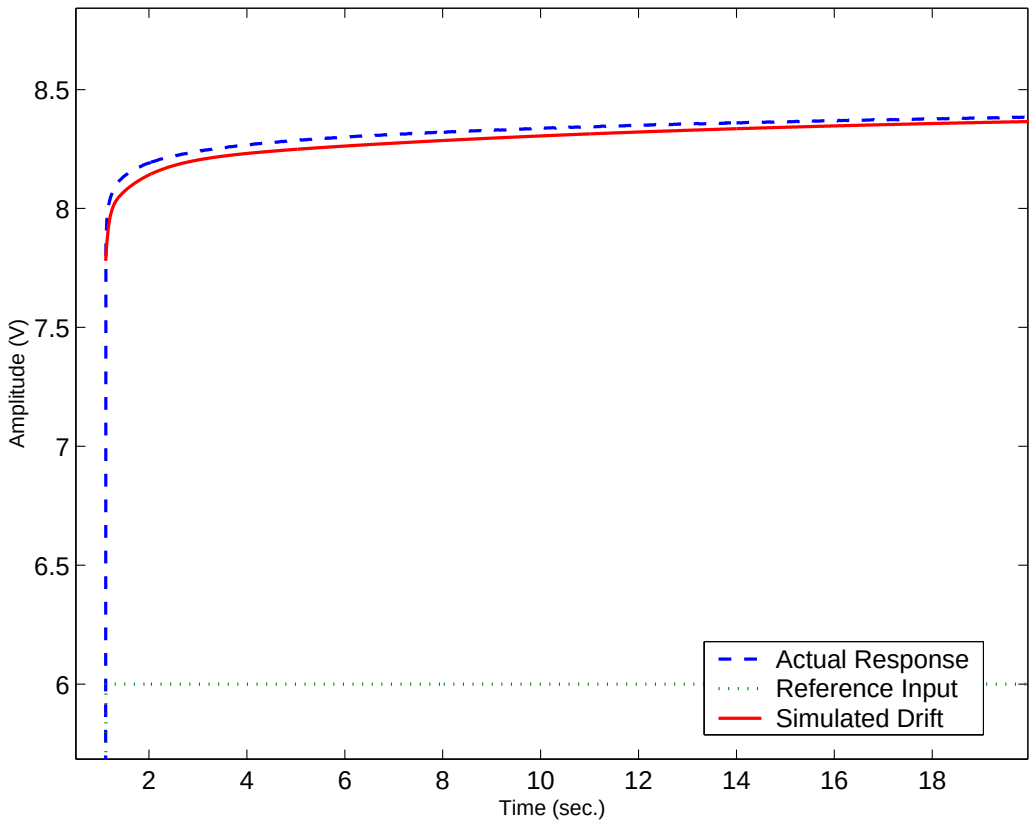

Figure 5.6. Actual and simulated drift for a 6V step input **including the nonlinear gain**.

Once the nonlinear gain (5.3) was also included, the simulated responses showed a much better agreement to the observed responses. Figure 5.6 on page 99 shows the simulated drift including the nonlinear gain. As is apparent when compared with Figure 5.4 on page 97, this is a much better approximation of the observed response. There is still some error which is the error in approximation of the gain by a polynomial.

5.3. Hysteresis

Hysteresis, literally, means *to lag*. The response of a system exhibiting this phenomenon typically lags behind the input even when the input is varied very slowly

(increased in steps while allowing the output to reach steady state at each increment). Unlike for purely linear systems, where the phase lag for sinusoidal inputs depends only on the frequency content of the input signal, the lag due to hysteresis depends on the input history; i.e. the amplitude and the type of the input.

Figure 5.7 on page 100 illustrates the input history dependence of the output. The dotted lines correspond to the different types of inputs used and the solid lines are the outputs. We can see that for the same final value (5 V) of the input signal, the steady state value of the output signals are very different (indicated by O_1 and O_2).

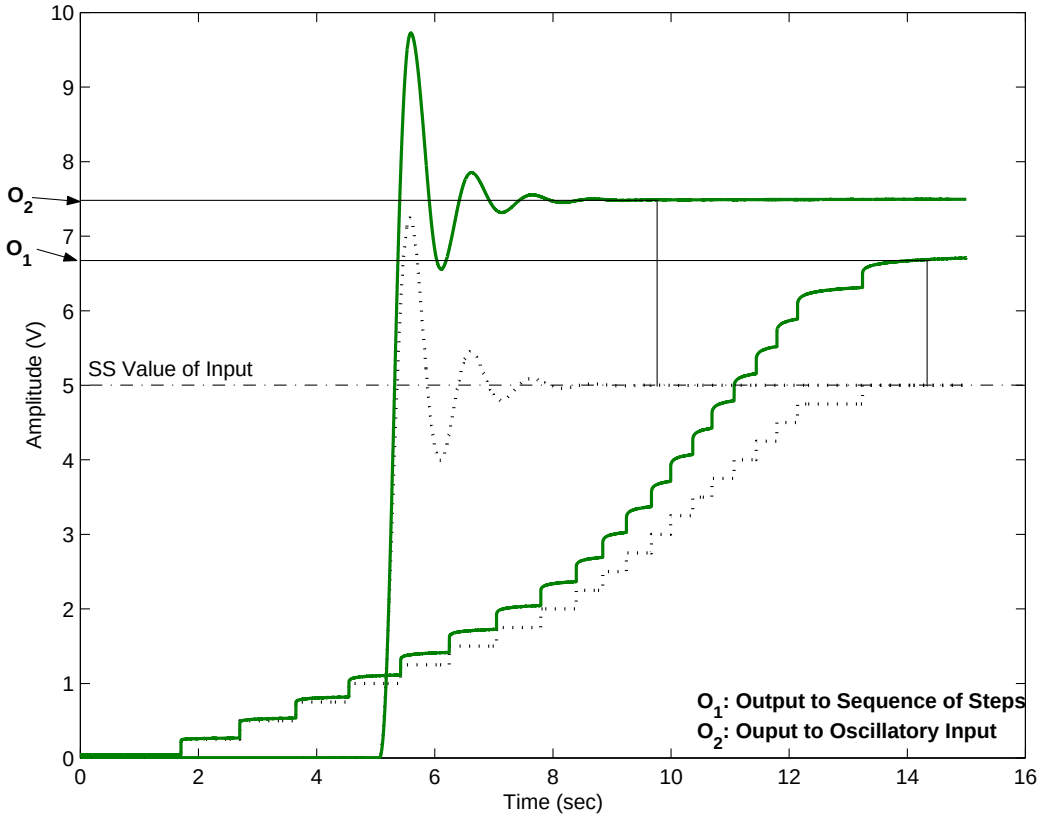

Figure 5.7. Plots corroborating the input history dependence of the output of the positioning system (solid:responses; dotted:inputs).

In addition to the reasons (for modelling the nonlinearities) mentioned above, hysteresis can cause instability if insufficient phase margin is available. This could occur either at high input frequencies or when large gains are used to get a large closed loop bandwidth.

The following conventions are commonly encountered in the literature of hysteresis modelling and will be used in this chapter:

Left Turning Points The point where $\dot{u}$ transitions from $\dot{u} < 0 \rightarrow \dot{u} > 0$.

Right Turning Points The point were $\dot{u} > 0 \rightarrow \dot{u} < 0$.

Reversal Curves The hysteresis loops on which $\dot{u} < 0$.

Rising Curve Curves on which $\dot{u} > 0$.

Major Rising Curve Rising curve associated with the largest input amplitude.

First Order Reversal Curves All reversal curves that arise from the major rising curve (indicated on the figure) and terminate at $u = 0$.

Higher Order Reversals Curves that start from the first order reversal curves before $u = 0$.

It is to be noted that the last two terms defined above are relevant for cyclic inputs only.

5.3.1. Existing Models

A survey of the existing models of hysteresis has been presented in Chapter 1. Most of these models have been derived from efforts in modelling magnetic hysteresis (Chua and Stromsmoe [55, 56]; Chua and Bass [57]) or friction. In this thesis models that were selected for use had to be simple to parameterize and implement on a real-time basis and of course should explain the behavior observed. The following models were "tried-out" to see how well they explain the observed hysteresis loops.

5.3.2. Preisach Model

This model is so named after the person who first proposed it as a suitable model to describe the hysteretic behavior in magnetic materials between the magnetization and the magnetic field. The original formulation (5.4) is a continuous model and it uses a spatial integral (in the input plane, i.e., with the maximum and minimum values of the input as axes) of the weighted elementary hysteresis operator to predict the position. The shape of the hysteresis loop that could be described by the integrals depends on the nature of the elementary operator.

$$x(t) = \int\int_{\alpha \geq \beta} \mu(\alpha, \beta)\, \gamma_{\alpha\beta}[u(t)]\, d\alpha d\beta \tag{5.4}$$

where,

$x(t)$:	Displacement at any given time t
α:	Right turning values of the input
β:	Left turning values
$\mu(\alpha, \beta)$:	Weight Function for RTP α and LTP β
$\gamma_{\alpha\beta}[u(t)]$:	Elementary hysteresis function

Here, the weight function $\mu(\cdot, \cdot)$ is unknown. In [32], Ge and Jouaneh have derived a method to determine the weight function involving double differentiation of the displacement data, which will amplify the noise greatly. Hence a geometrical approach to determine the displacement, without the weight function is demonstrated in the following. To implement this though, one needs test data for a set of first order reversal curves (Figure 5.8 on page 103). Therefore this model as such is applicable to only first order reversal curves. Ge and Jouaneh have also extended this method for higher order reversal curves.

We attempted to use this model to describe the hysteresis loops observed with the positioning system but ran into problems due to the following drawbacks of the model:

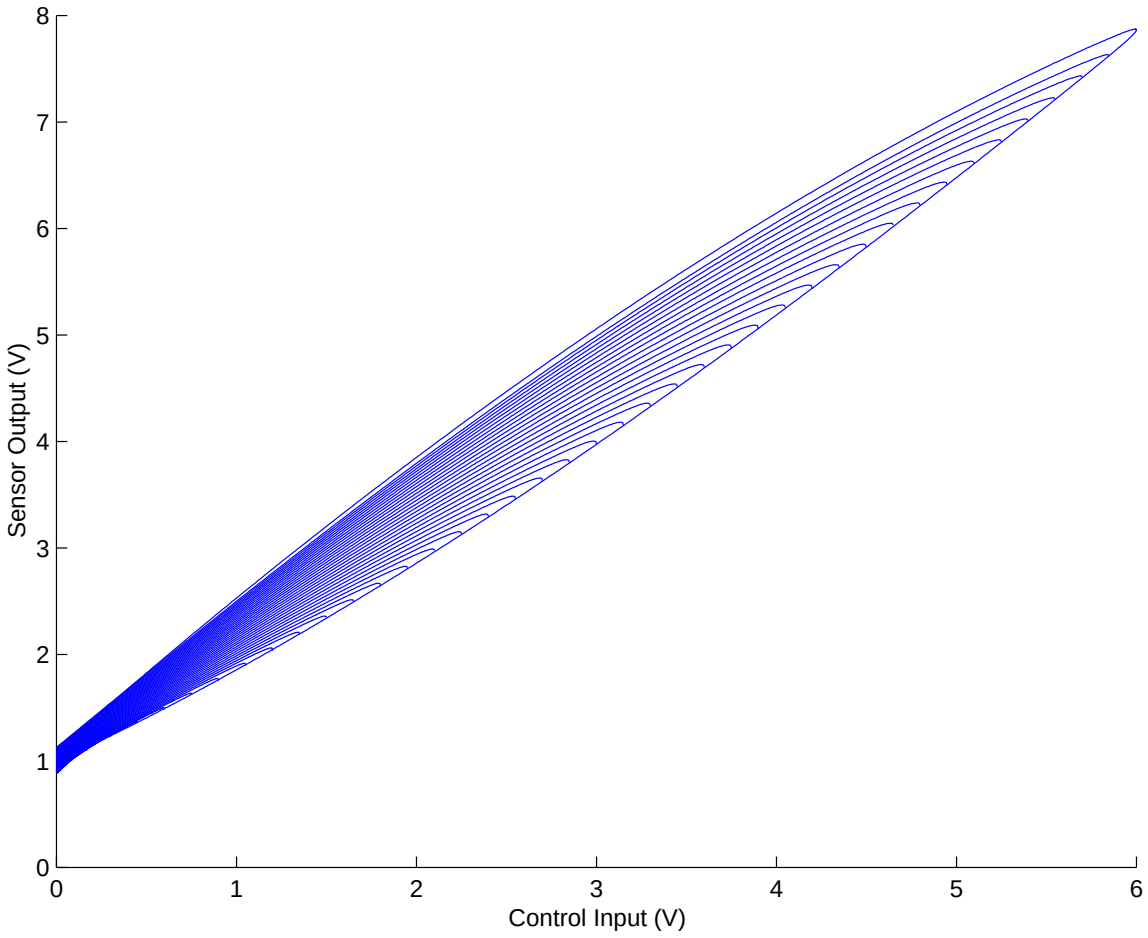

Figure 5.8. First order reversal curve set used to parameterize the Preisach model.

5.3.2.1. Drawbacks and Limitations

The Preisach model has several drawbacks. The most predominant one is that the amount of data processing that needs to be performed to parameterize the model is enormous. This has to be performed for each different actuator for which a model is being developed for.

Also in [32, 33, 34] the test data shown indicated that all the smaller loops lie within the major rising and falling curves. But during the actual experiments, it was noted that parts of some of the reversal curves actually lie outside of the major rising and reversal curves. Some of the smaller reversal curves lie entirely outside the region bounded by these two curves. Also the position (sensor output) corresponding to the zero input voltage on each of these reversal curves was different. These are illustrated in Figure 5.9 on page 105.

From the original model in [32, 33, 34], it is clear that the model allows for only one rising curve; i.e. the rising curve for all the loops are the same. But from the experimental data shown in the plots above, it is clear that this was not the case. If the experimental data was offset manually to ensure that the minimal points coincided, discontinuities occurred in the data at the maximum points and significant errors were seen at these points when the model was being used to predict the position.

Since in most practical applications, the applied input voltage never coincides with the stored values of the voltage, interpolation has to be used to determine the output position for most points in the input history. Hence this method seems to be no better when compared to the piecewise polynomial fit approach. In fact the polynomial fit method seems to be more computationally optimal with respect to the storage requirements and computational intensiveness.

The data that is used for parameterization does not account for the dynamics of the system. Hence this hysteresis model alone is insufficient to predict the displacement for dynamic inputs. It has to be encapsulated into a more general model that also takes into account the dynamics of the stack actuator. It should be noted that

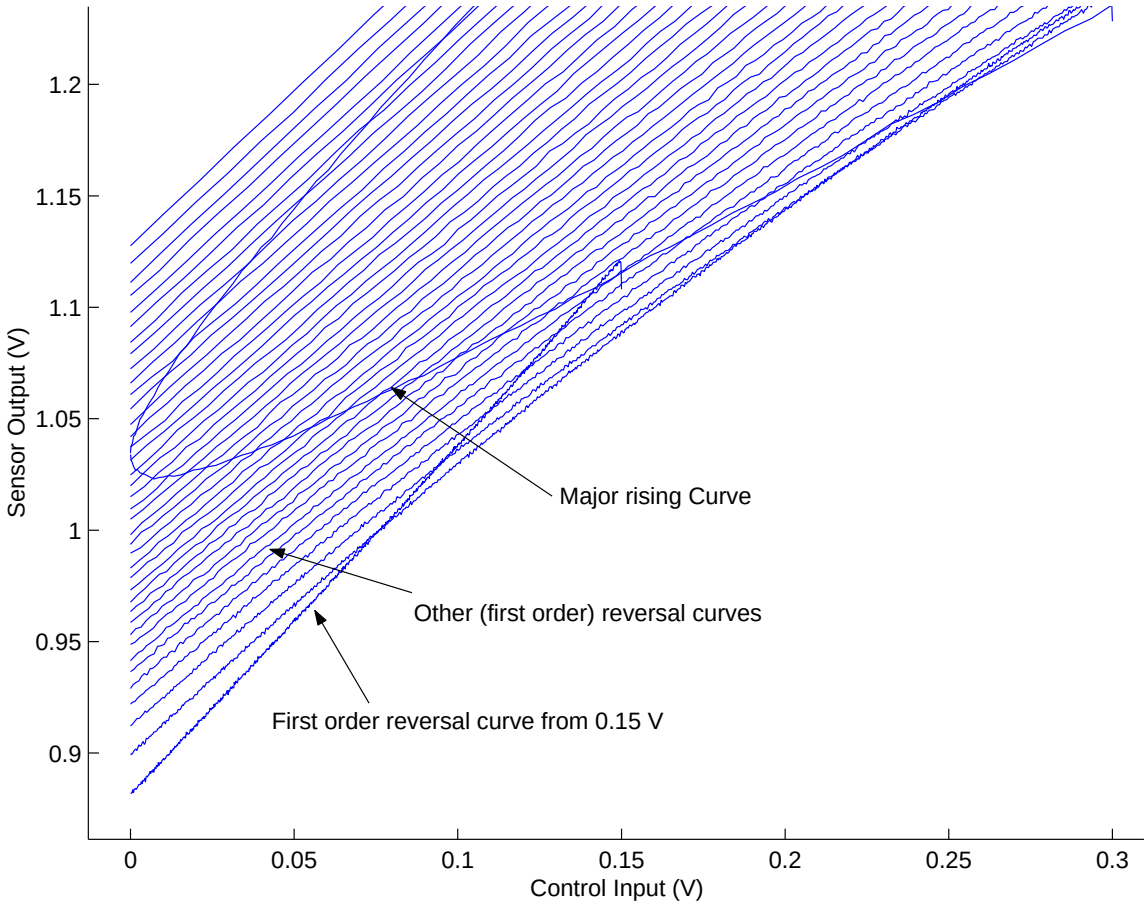

Figure 5.9. Zoomed-in view of first reversal curves used for parameterization.

most of the results shown in the publications are for slow inputs (frequencies < 10 Hz.). In the case when the dynamics are significant i.e. for a triangular input at higher frequencies, the error in the predicted position would probably be significant.

Also the amount of data that has to be stored makes it virtually useless for fast real-time implementation.

5.3.3. Maxwell's Model

As in the Preisach model, this one uses a number of elementary hysteretic systems to approximate the hysteresis behavior of the piezoelectric actuator. The origins of this model lie in the Dahl model for friction. It was observed in [20] during studies on friction that when a movable body was subjected to a slowly increasing applied force, there is a definite amount of pre-sliding displacement. When the direction of the force was reversed, the pre-sliding displacement lagged the force in reversing its direction. This is similar to the proposed mechanism for the existence of the hysteresis phenomenon, and is probably what prompted to adapt the model for friction to model hysteresis.

This model was developed by Maxwell initially and recently used in [15, 28, 58]. This model was incorporated as one of the constituent equations of a general dynamic electromechanical model for the piezoelectric actuator and was used for compensation in a feedback control scheme.

Parameterization of this model implies determination of the spring constants and the friction forces for each of the elementary hysteresis operator in the schematic Figure 5.10 on page 107. Details of how the model is to be parameterized can be obtained from [28, 15]. The simulations performed with the model show a good agreement except for random discontinuities or jumps that occur in the output of the model. This could be because of sensitivity to noise as the model uses the derivative to determine the current output of each of the elementary hysteresis operators. Hence as expected, at low velocities (e.g., at the peak values of the sinusoidal excitation),

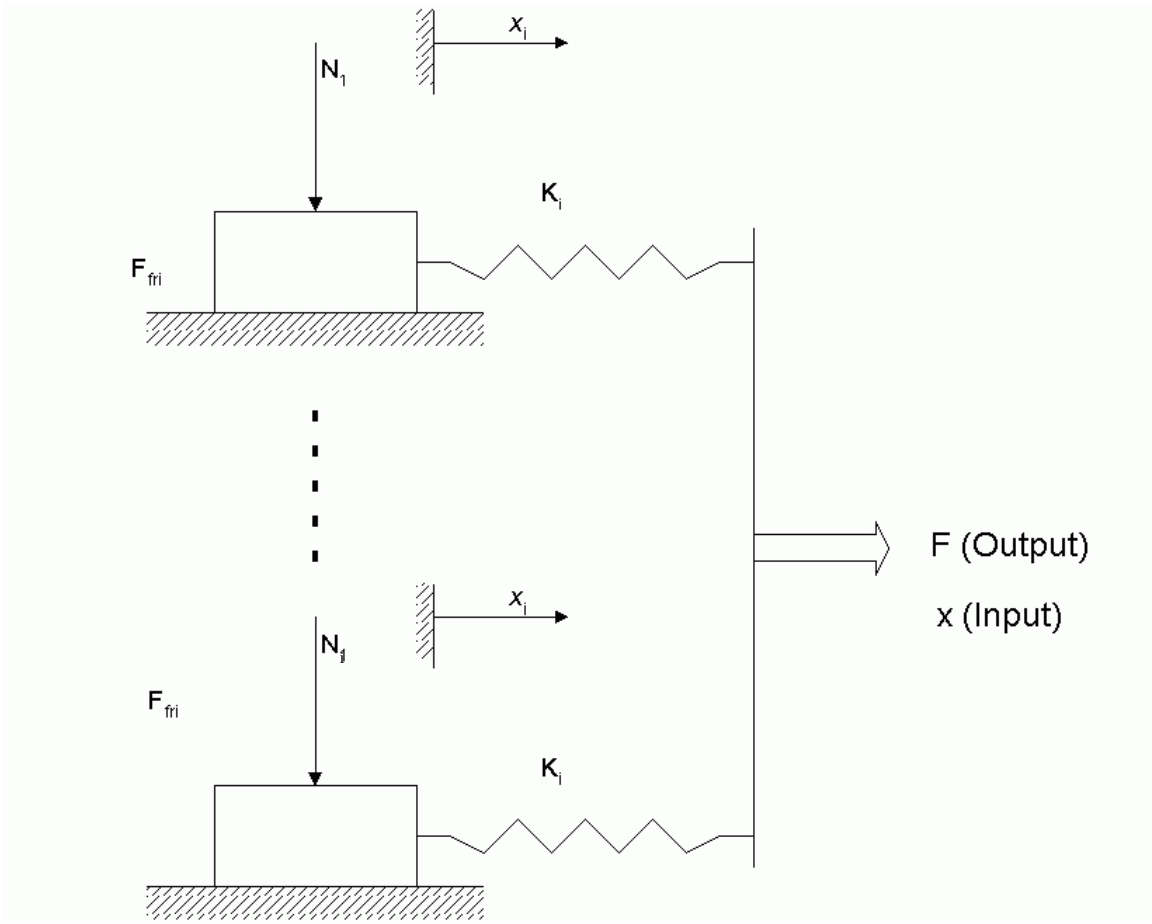

Figure 5.10. Parallel combination of elasto-sliders for Mawell's model.

the effect of the noise causes the output to chatter, in spite of averaging performed to filter the noise in the simulation program.

5.3.3.1. Limitations and Drawbacks

The principal advantage of this model is the ease of parameterization. With one set of data from the major rising curve, all the weights can be calculated. But the number of elements that is required to approximate the shape of a hysteretic loop

depends on the loop being modelled. Also the results shown in [28] are only for first order reversal curves. So it is unclear as to whether this model would still be applicable for any general hysteresis loop (as observed in the case of point to point trajectories etc).

When the model was being used in practise, since the derivative of the input was required, the model seemed to be very sensitive to the noise in the measurement. This caused large jumps in the predicted output of the system as can be seen in Figure 5.12 on page 112.

5.3.4. Polynomial Model

In this method of model formulation, the major rising and each of the reversal curves are approximated by polynomials of suitable degree. If the input reverses between two parameterization polynomials used, then interpolation is performed between the outputs on the two adjacent polynomials based on the turning point. Essentially this method is a combination of the interpolation used in implementation of the Preisach Models and a variation of the polynomial model used by Jung and Kim [24].

The first step is to obtain the data that can be used to parameterize the polynomials. This is obtained by using a low frequency sinusoid (1 Hz). The actuator is first allowed to reach steady state by sending the sinusoidal input for a period of about 2-3 minutes. The input is then cut-off and ramped down to zero at pre-specified levels of the input. The cutoff values were increments of 0.15 V from the zero input. Each time the input is cut-off and ramped down to zero, the actuator has to be allowed to reach steady state. The data that is collected is shown in Figure 5.8 on page 103.

Once the data is available, the different segments of the hysteresis loop have to be identified and the input-output data is chosen. The coefficients of the best fit polynomials are determined by the least squares method. The coefficients are then used to determine the output position given the input. Note that the actual

mapping between the input voltage and the output position is multi-valued. Hence it is necessary to track the input history to determine which reversal curve is being followed at the current time instant.

One of the properties exhibited by hysteresis loops that is used in this model is that the hysteretic distortion due to a cyclic input is unaffected by the distortion due to an input of smaller amplitude that was applied earlier. This property is termed *"wiping-out property"*(see Figure 5.13 on page 113). Hence when the cutoff values were slowly increased from 0 to the maximum value of the input, the distortion due to the larger cutoff value is assumed to be unaffected by the distortion due the previous smaller cut-off. It is also necessary that there be only one major rising curve which starts from zero; i.e. the rising curve for all the reversals is the same.

As is apparent from the data used for parameterization, this model can be used to approximate only the behavior of the major rising and the first order reversal curves. Higher order reversal and rising curves are not used to parameterize the polynomials. It is obvious that in the case of higher order rising/reversal curves the predicted displacement of the actuator will have a significant error. The plots for the data used to parameterize the polynomials and to test the model are shown in Figure 5.8 on page 103.

The following observations can be made based on the plots in Figure 5.8 on page 103 and Figure 5.14 on page 114:

1. When the input is ramped down to zero from the cut-off value to obtain the reversal curve, the output does not return to the datum value. In fact the output at zero input on the reversal curves go below the steady-state datum value.

2. Due to the above property, it can be seen that the rising curves are not the same for all the reversal curves. In fact for each reversal curve there seems to be a different rising curve. Also the smallest reversal curve lies completely outside the region bounded by the major rising and the reversal curve from the largest

amplitude. Hence the number of possible rising curves have to be approximated by one rising curve. This can be determined again by a least-squares fit but for the sake of simplicity, the steady-state rising curve was used.

3. When the input was cut-off and ramped down to obtain the reversal curve, it is seen that the maximum value of the output does not occur at a point on the rising curve. Hence there is a portion of the rising curve which is not accounted for. Therefore there is some discontinuity in the model.

4. The prediction error show in Figure 5.14 on page 114 is the discrepancy between the actual displacement and the predicted displacement. This is a result of the discrepancy mentioned above. But when compared to the maximum value of the distortion (1 V), the prediction errors are small in magnitude (0.05-0.1 V).

The disadvantage of this model is that it is very time consuming in terms of parameterization. For every new actuator that has to be modelled, large amounts of data have to be collected from experiments that generate the curves and coefficients of the best fit polynomials have to be determined for each reversal curve.

One surprising result was observed in the case of a triangular input signal. The predicted hysteresis loop seems to be off by a DC value as shown in Figure 5.15 on page 115 and in Figure 5.16 on page 116. This static offset can be compensated for easily in the controller by using some type of integral action. The peak error (without the DC mean component) is about $\pm 0.15V$. This is small in comparison to the actual distortion which is approximately 1 V.

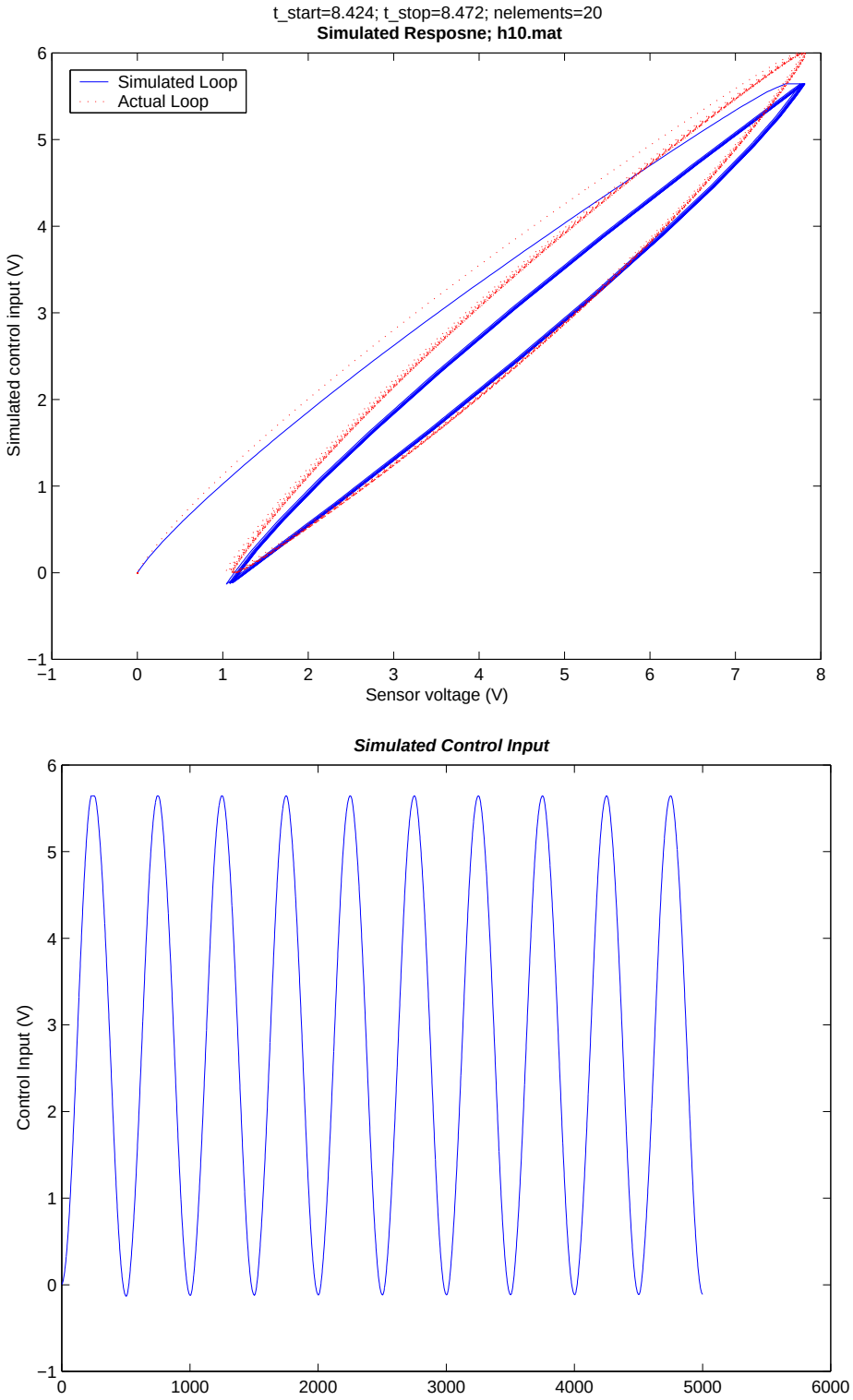

Figure 5.11. Simulation results with Maxwell's model for 10 Hz. sinusoidal input.

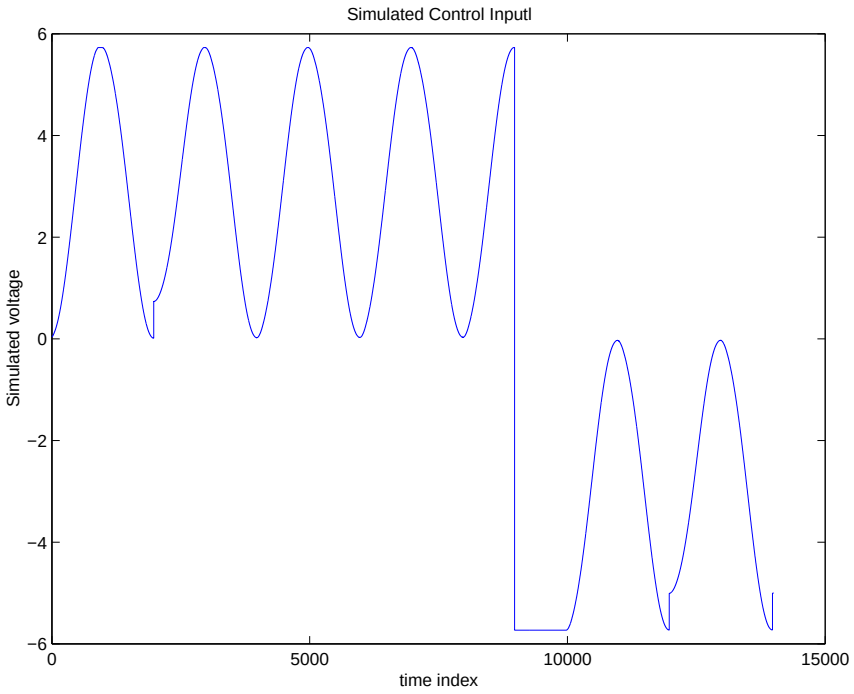

(a)

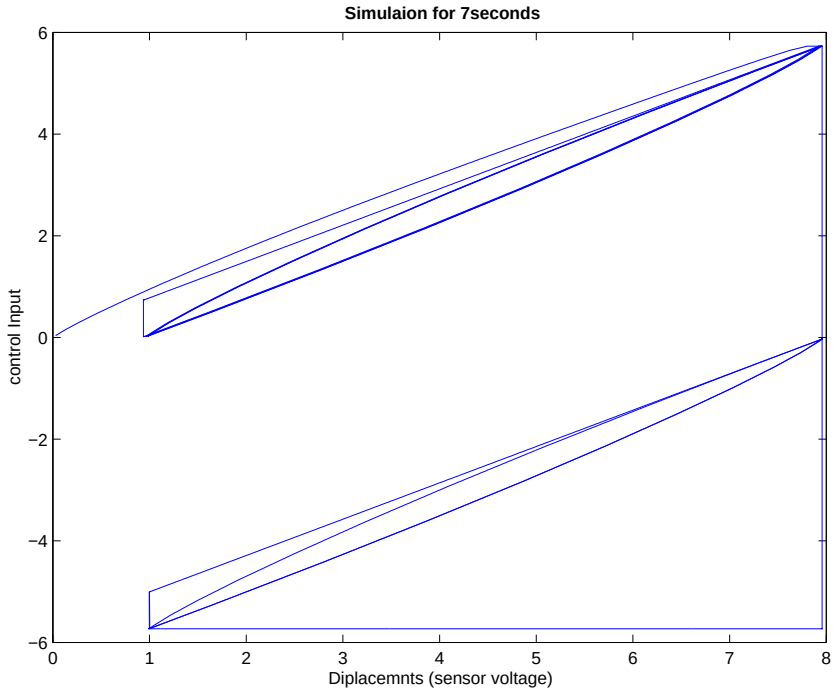

(b)

Figure 5.12. Irregularities and discontinuities seen in the simulated control input for low velocity inputs (1Hz sinusoid).

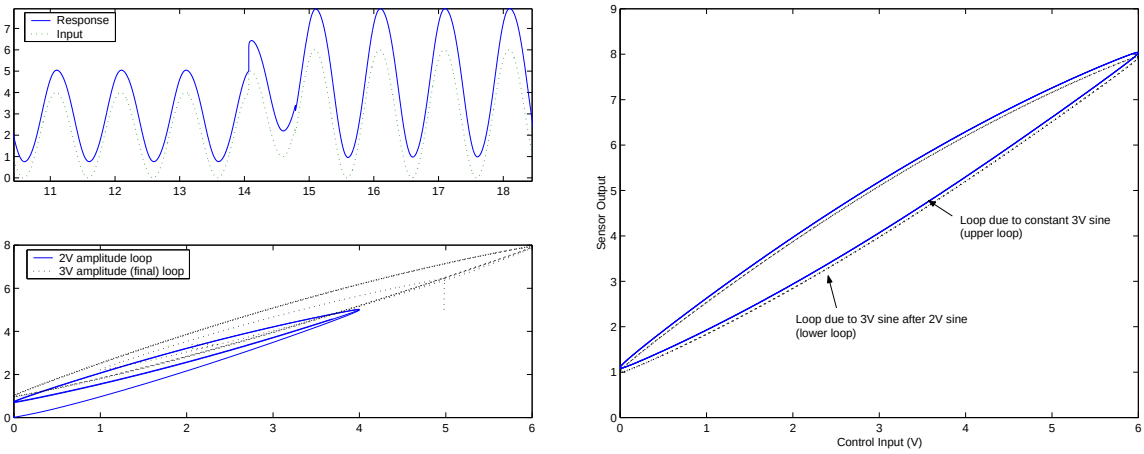

Figure 5.13. Verifying the 'wiping-out' property of hysteretic loops.

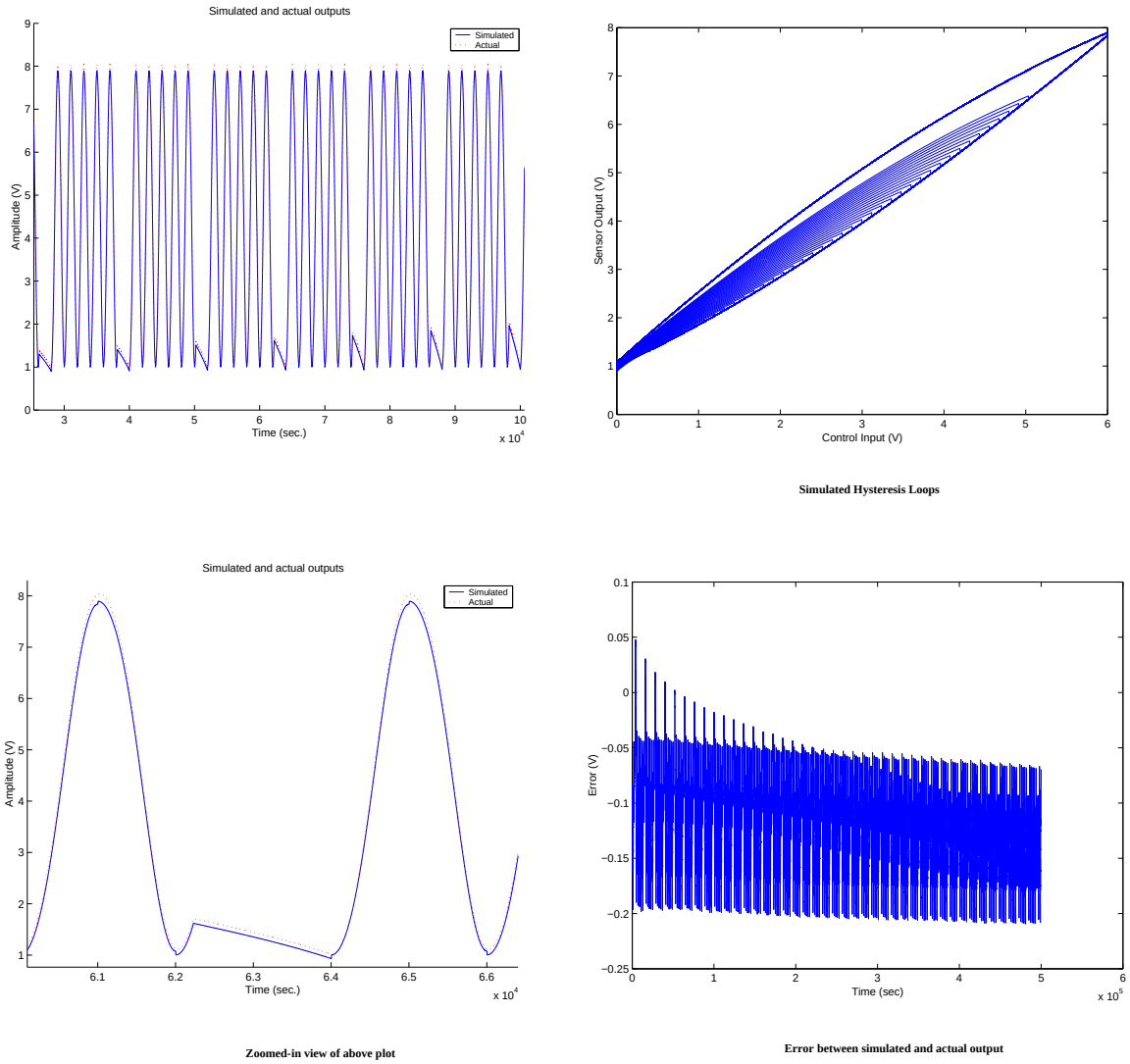

Figure 5.14. Simulation results using the generalized polynomial model. (i): Time history of simulated and actual outputs;(ii): Zoomed view of (i); (iii) Simulated hysteresis loops; (iv) Error between simulated and actual outputs.

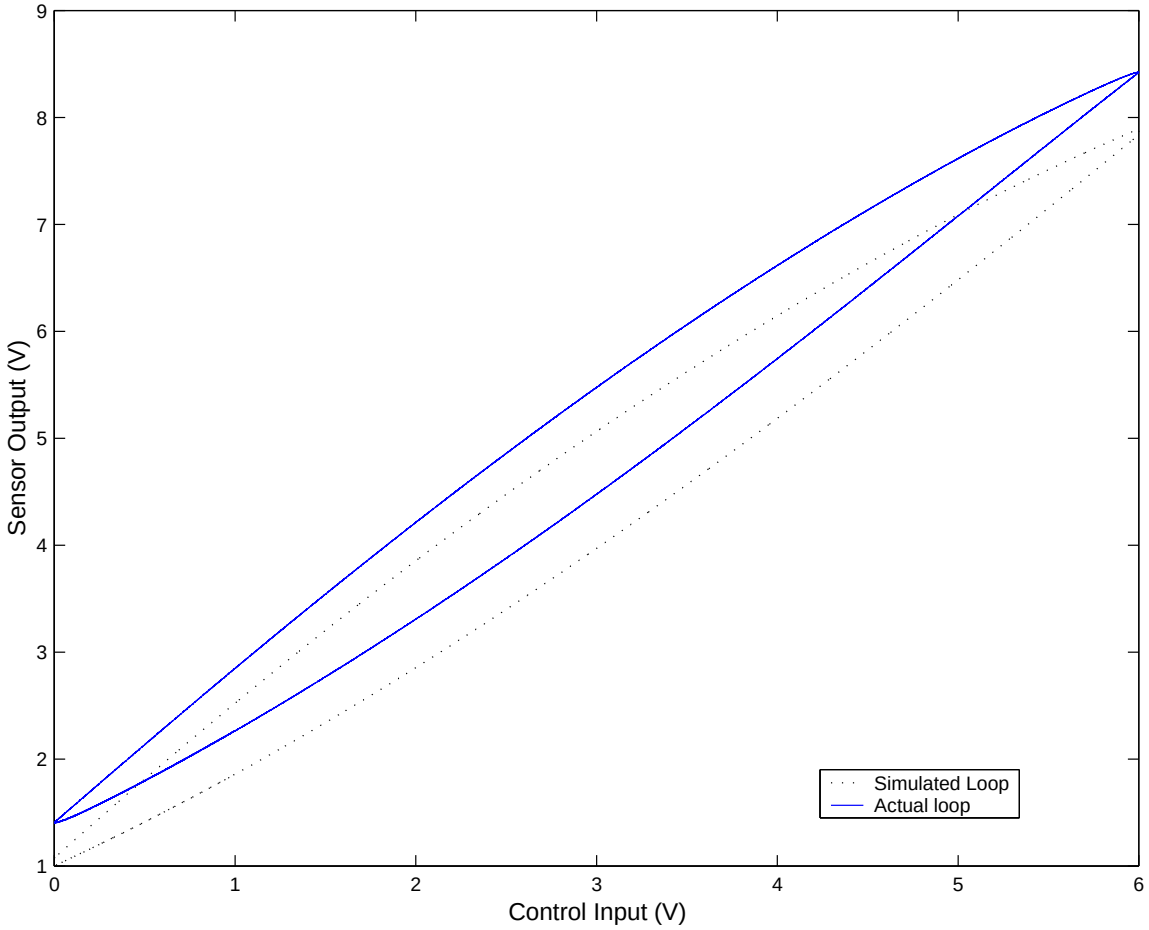

Figure 5.15. Simulation results for triangular inputs using polynomial interpolation model (polynomials are from sinusoidal test I-O data).

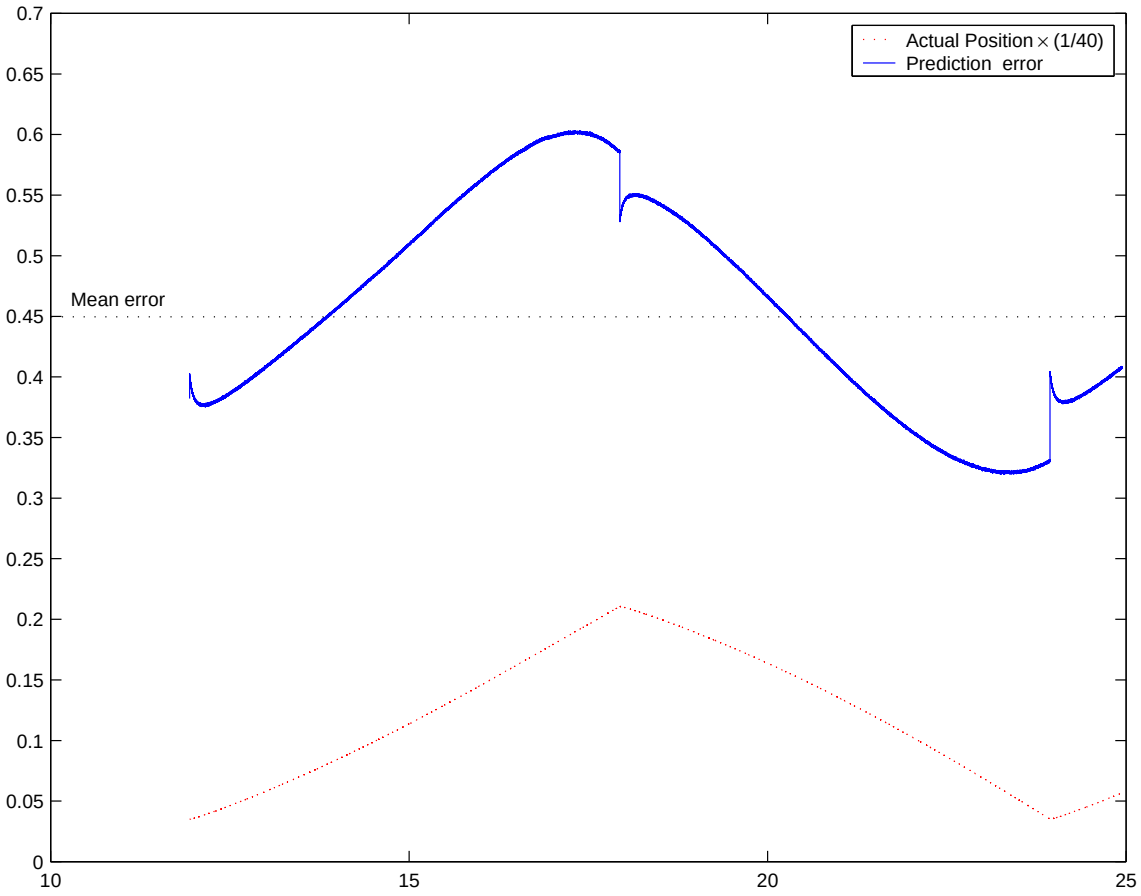

Figure 5.16. Prediction error for triangular inputs (shown above); (Actual output data given for time basis reference).

6. OVERALL MODEL OF PIEZOELECTRIC ACTUATORS

The models that have been proposed so far in Chapter 4 and Chapter 5 have approximated the fast dynamics (electrical and inertial) and the nonlinear phenomena (hysteresis and non-linear gain) independently. The experiments used to obtain the data to parameterize the proposed models were also performed in a manner to ensure that effects other than the one being modelled were insignificant. But to be used as a basis for either controller design or building a simulation model for the system, these independent models would be of little use as, a given reference input signal would be influenced by all the phenomena.

This chapter integrates the models that have been proposed earlier into what is referred to as the "*Overall Model*". The simulation results from this overall model is also compared with the experimental data to verify the validity of the proposed model.

6.1. Signal Flow of The Physical System

For piezoelectric actuators, the potential difference between two electrodes is transduced into a mechanical strain of the actuator stack. When the material is prevented from attaining the strained state, a stress develops in the stack which appears as a force on the restraining structure. This force causes the motion when a load is placed on the actuator (the load restrains the actuator from expanding). Based on this physical signal flow, an intuitive model for the system would be as in figure Figure 6.1 on page 118.

In the signal flow diagram, the transduction of the electric field to the strain is the nature of the (inverse) piezoelectric effect. The proposed mechanism for this effect is that the applied electric field causes a charge separation in the piezoelectric material. This charge developed on the electrodes across the ceramic disks induces a strain in the material. When the material is not allowed to deform freely, it exerts a force on the restraining structure. This force is what causes the motion of the moving platform on the P753.11C nano-positioning system.

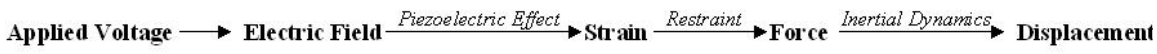

Figure 6.1. Signal flow in a Piezoelectric actuator.

It has been proposed by Celanovic and Goldfarb [15, 28] and Adriaens [16] that the hysteresis effect is seen in the transduction of the applied electric field/potential into the charge on the ceramic material. Celanovic and Goldfarb further support this proposition by presenting experimental data to show that the dynamics between the charge developed and the displacement of the actuator is linear. The signal flow diagram shown also agrees with this observation if one assumes that the relationship between the strain induced and the stress developed due to the restraint on the strain is linear. i. e. the material is still in the elastic deformation zone, which is a reasonable assumption. Therefore the overall model proposed should also reflect this sequence of signal flow in the system.

6.2. Overall Model of Piezoelectric Actuators

In proposing the overall model, one has to keep in mind the experimental conditions used. Considering all factors, the overall model proposed for the system is shown in the following figure Figure 6.2 on page 119 in which the meaning of various blocks are as follows:

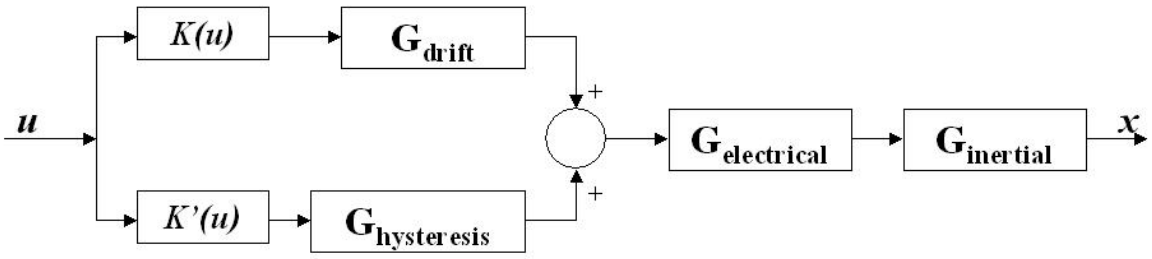

Figure 6.2. Overall model for the piezoelectric nano-positioning system.

$K(u)$:	Nonlinear gain of drift component (Figure 5.5)
$K'(u)$:	Nonlinear gain of the fast component (Figure 3.10)
G_{drift}:	Transfer functions approximating drift (Equation 5.1)
$G_{hysteresis}$:	Hysteresis model. (Polynomial model, Chapter 5)
$G_{electrical}$:	The electrical dynamics (Equation 4.4, Chapter 4)
$G_{inertial}$	The inertial dynamics (Equation 4.4, Chapter 4)

The discrepancy between the proposed model and the signal flow is in the location of the dynamics of the electrical subsystem. In the proposed signal flow diagram, the electrical dynamics affect the input to the piezoelectric block whereas in the proposed overall model, the electrical dynamics appear after the block representing the piezoelectric dynamics. This is because, in the experiments performed to isolate the dynamics of the electrical and the inertial subsystems, the conditions were such that the nonlinear piezoelectric effects were minimal (as explained in Chapters 3 & 4). Hence the transfer function obtained represented the combined dynamics of both subsystems. Also since the bandwidth of the electrical subsystem is quite high (in comparison to the dynamics of the slow component and the hysteresis model), it can be assumed that the applied input is not affected by the electrical dynamics at all.

7. CONCLUSIONS

In this work to study and model a piezoelectric actuator, the following has been completed to date:

- A commercial piezoelectric positioning system was installed and was used as the experimental test bed.
- Experiments were performed to study the behavior of the positioning system to typical inputs and the presence of nonlinearities was deduced from the responses.
- Models were proposed to fit the observed nonlinear effects and a linear model was proposed for the inertial and electrical dynamics of the positioning system.
- An overall model was proposed in accordance to the models developed for the nonlinear and linear behavior.

7.1. Possible directions for future work

Even though experiments were performed to characterize the behavior of the piezoelectric actuator, these by no means were comprehensive. For example, to determine the nonlinear behavior of the static gain to different step heights, rising step inputs were applied starting from 0 V. More experiments should be performed to completely characterize the behavior of the system with different starting values of the step inputs and also falling inputs.

With the results from the above mentioned tests, one could propose a model for the nonlinear gain with better confidence. The simple polynomial model proposed here may not be accurate enough. The experimental input-output data should also be used to verify the accuracy of the proposed overall model for the system.

The proposed model for hysteresis is difficult to be used in analysis of the behavior of the system. As mentioned in the introduction there are many more hysteresis models which lend themselves to analysis (Dahl's model, Coleman-Hodgdon's equations). They could be used to approximate the hysteretic behavior exhibited by the system.

Different controllers have been proposed in the literature to compensate for the nonlinear behavior of the system. Some of the control structures that show promise are Iterative Learning Control, Adaptive-Robust Repetitive Control and the Neural-Network Adaptive-Robust control structures. These controllers do not attempt to model hysteresis but rather they compensate for it using online learning schemes. These controllers could be used in place of the proposed simple lag compensator to achieve better performance of the closed loop system.

LIST OF REFERENCES

LIST OF REFERENCES

[1] Physik Instrumente (PI) GmbH & Co., *Nanopositioning catalog and tutorials*. www.physikinstrumente.com/tutorial/index.html, 1999.

[2] Standards Committee of the IEEE Ultrasonics, Ferroelectrics and Frequency Control Society, "An American National Standard: IEEE Standard on Piezoelectricity," Technical report, ANSI/IEEE, 1987.

[3] D. Croft, S. Stilson, and S. Devasia, "Optimal tracking of piezo-based nanopositioners," *Nanotechnology*, vol. 10, pp. 201–208, June 2001.

[4] K. Duong, E. Garcia, and H. Waites, "Smart piezo stacks as actuators for precision control of adaptive reflectors," in *Proceedings of the SPIE*, vol. 2190, pp. 454–462, SPIE: The International Society for Optical Engineering, 1994.

[5] K. Duong and E. Garcia, "Open loop compensation of stack-mass positioning system," *Journal of Intelligent Materials, Systems and Structures*, vol. 6, pp. 292–296, March 1995.

[6] P. Buckner, B. Gotz, and T. Martin, "Piezoelectrical actuators for dynamical applications," in *Proceedings of the SPIE conference on Smart Sturctures and Integrated Systems*, vol. 3329, pp. 550–561, March 1998.

[7] J. Rubio, J. Duduch, and A. Porto, "A micropositioning device using solid-state actuators for diamond turning machines: a preliminary experiment," in *Proceedings of the SPIE*, vol. 3044, pp. 317–326, 1997.

[8] T. Ohara and K. Youcef-Toumi, "Dynamics and control of piezotube actuators for subnanometer precision applications," in *Proceedings of the American Control Conference*, pp. 3808–3812, June 1995.

[9] Z. Li, K. Liu, B. Chen, and T. Lee, "Robust and perfect tracking control desigh of a hard disk drive with a dual-stage actuator," in *Proceedings of the American Control Conference*, pp. 3849–3854, June 2001.

[10] H. Numasato and M. Tomizuka, "Settling control and performance of dual-actuator system for hard disk drives," in *Proceedings of the American Control Conference*, pp. 2779–2885, June 2001.

[11] J.-D. Kim and S.-R. Nam, "Development of a micro-positioning grinding table using piezoelectric voltage feedback," *Proceedings of the Institution of Mechanical Engineers Part B-Journal of Engineering Manufacture*, vol. 211, no. B6, pp. 487–493, 1997.

[12] J.-D. Kim and S.-R. Nam, "Development of a micro depth control system for an ultra-precision lathe using a piezoelectric actuator," *International Journal of Machine Tools and Manufacturing*, vol. 37, no. 4, pp. 495–509, 1997.

[13] M. Pozzi and T. King, "Dynamic characteristics of piezoelectric multilayer stack actuators," in *Proceedings of the Second International Recent Advances in Mechatronics Conference*, pp. 461–466, Institute of Electrical Engineers, 1999.

[14] D. Croft and S. Devasia, "Hysteresis and vibration vompensation for piezoactuators," *Journal of Guidance, Control and Dynamics*, vol. 21, pp. 710–717, 1998.

[15] M. Goldfarb and N. Celanovic, "A lumped parameter electromechanical model for describing the nonlinear behavior of piezoelectric actuators," *Journal of Dynamic Systems Measurement & Control - Transactions of the ASME*, vol. 119, pp. 478–485, 1997.

[16] J. Adriaens, *Modeling and control of a piezo-actuated positioning mechanism*. PhD thesis, Department of Applied Physics, Delft University of Techonology, 2000.

[17] P. Chen and S. Montgomery, "A macroscopic theory for the existence of the hysteresis and butterfly loops in ferroelectricity," *Ferroelectrics*, vol. 23, pp. 199–208, 1980.

[18] R. Smith, Z. Ounaies, and R.Wieman, "A model for rate-dependent hystereis in piezoceramic materials operating at low frequencies," in *Proceedings of the SPIE*, vol. 3992, pp. 128–136, 2000.

[19] X. Zhou and A. Chattopadhyay, "Hysteresis behavior and modelling of piezoceramic actuators," *Journal of Applied Mechanics- Transactions of the ASME*, vol. 68, pp. 270–277, March 2001.

[20] C. de Wit, H. Olsson, K. Astrom, and P. Lischinsky, "A new model for control of systems with friction," *IEEE Transactions on Automatic Control*, vol. 40, pp. 419–425, March 1995.

[21] X. Sun and T. Chang, "control of hysteresis in a monolithic nanoactuator," in *Proceedings of the American Control Conference*, pp. 2261–2266, June 2001.

[22] J. Adriaens, R. Banning, and W. de Koning, "Modelling piezoelectric actuators," *IEEE/ASME Transactions on Mechatronics*, vol. 5, pp. 331–341, December 2000.

[23] D. Croft and S. Devasia, "High precision positioning stage for micro/nanolithography," in *Proceedings of the SPIE*, vol. 3225, pp. 68–75, 1997.

[24] S.-B. Jung and S.-W. Kim, "Improvement of scanning accuracy of PZT piezoelectric actuators by feed-forward model-reference control," *Precision Engineering*, vol. 16, pp. 49–55, 1994.

[25] J. Bakashwain, J. Refaee, M. Sunar, and M. Mohandes, "Artificial neural network for piezoelectric control systems," in *Proceedings of the SPIE Conference on Mathematics and Control*, vol. 3667, pp. 691–699, March 1999.

[26] C. Kwan, R. Xu, J. Lang, C. Lin, M. Stevenson, Y. Lin, Z. Ren, and L. Haynes, "Intelligent control of piezoelectric actuators for precision manufacturing," in *Proceedings of SPIE*, vol. 3833, pp. 2–11, 1999.

[27] D. Song and C. Li, "Modeling of piezo actuator's nonlienar and frequency dependent dynamcis," *Mechatronics*, vol. 9, pp. 391–410, June 1999.

[28] M. Goldfarb and N. Celanovic, "Modeling piezoelectric stack actuators for control of micromanipulation," *IEEE Control Systems Magazine*, vol. 17, pp. 69–79, 1997.

[29] W. Galinaitis and R. Rogers, "Control of a hysteretic actuator using inverse hysteresis compensation," in *SPIE Conference on Mathematics and Control in Smart Structures*, vol. 3323, pp. 267–277, 1998.

[30] F. Preisach, "Scalar models for hysteresis," *Magazine for Physics*, vol. 94, pp. 478–485, 1935.

[31] I. Mayergoyz, "Mathematical models of hysteresis," in *The IEEE Transactions on Magnetics*, vol. MAG-22; No. 5, pp. 603–608, 1986.

[32] P. Ge and M. Jouaneh, "Modeling hysteresis in piezoelectric actuators," *Precision Engineering*, vol. 17, pp. 211–221, 1995.

[33] P. Ge and M. Jouaneh, "Tracking control of a piezoceramic actuator," *IEEE Transactions on Control Systems Technology*, vol. 4, pp. 209–216, 1996.

[34] P. Ge and M. Jouaneh, "Generalized preisach model for hysteresis nonlinearity of piezoceramic actuators," *Precision Engineering*, vol. 20, pp. 99–111, 1997.

[35] D. Hughes and J. Wen, "Preisach modeling and compensation for smart material hystersis," in *Proceedings of the SPIE conference on Active Materials and Smart Structures*, vol. 2427, pp. 50–64, 1995.

[36] P. Sreeram and N. Naganathan, "Hysteresis prediction for piezoceramic actuator systems using preisach models," in *Proceedings of the SPIE*, vol. 2189, pp. 14–25, 1994.

[37] K. Kuhnen and H. Janocha, "Real-time compensation of hysteresis and creep in piezoelectric actuators," *Sensors & Actuators A-Physical*, vol. A79,No.2, pp. 83–89, 2000.

[38] K. Kuhnen and H. Janocha, "Compensation of the creep and hysteresis effects of piezoelectric actuators with inverse systems," in *Proceedings of the 6th International Conference on New Actuators*, pp. 309–312, ACTUATOR 98, 1998.

[39] K. Koops, P. Scholte, and W. de Koning, "Observation of zero creep in piezoelectric actuators," *Applied Physics A: Materials Science & Processing*, vol. A68, pp. 691–697, 1999.

[40] D. Croft, G. Shedd, and S. Devasia, "Creep, hysteresis and vibration compesnation for piezoactuators: Atomic force microscopy appliction," *Journal of Dynamic Systems Measurement & Control-Transactions of the ASME*, vol. 123, pp. 35–43, March 2001.

[41] G. Choi, J. Oh, and G. Choi, "Repetitive tracking control of a coarse-fine actuator," in *Proceedings of the 1999 IEEE/ASME Internation Conference on Advanced Intelligent Mechatronics*, pp. 335–340, IEEE/ASME, 1999.

[42] J. Main, E. Garcia, and D. Newton, "Precision position control of piezoelectric actuators using charge feedback," *Journal fo Guidance, Control and Dynamics*, vol. 18, pp. 1068–1073, September-October 1995.

[43] N. M. K. Furutani, M. Urushibata, "Displacement control of piezoelectric clement by feedback of induced charge," in *Nanotechnology*, vol. 9, pp. 93–98, June 1998.

[44] N. M. K. Furutani, M. Urushibata, "Improvement of control method for piezoelectric actuator by combining induced charge feedback with inverse transfer function compensation," in *Proceedings of the 1998 IEEE International Conference on Robotics and Automation*, vol. 2, pp. 1504–1509, June 1998.

[45] C. Li, H. Beigi, S. Li, and J. Liang, "Nonlinear piezo-actuator control by learning self-tuning regulator," *Journal of Dynamic Systems Measurement & Control - Transactions of the ASME*, vol. 115, pp. 720–723, December 1993.

[46] Q. Hao, G. Guo, S. Chen, and T.-S. Low, "A self-tuning robust track-following control of sampled-data hard disk drive servo system," in *Proceedings of the American Control Conference*, pp. 3843–3848, 2001.

[47] C.-Y. Su, "Robust control of piezoelectric actuated systems with unknown hysteresis," in *Smart Structures and Materials 2000: Mathematics and Control in Smart Structures*, vol. 3984, pp. 186–194, 2000.

[48] K. Kuhnen and H. Janocha, *Adaptive Inverse Control of Piezoelectric Actuators with Hysteresis Operators*. Laboratory for Process Automation, University of Saarland, Im Stadtwald, Geb. 13, Saarbrucken Germany; klaus@lpa.uni-sb.de.

[49] K. Kuhnen and H. Janocha, *Inverse Feedforward Controller for Complex Hysteretic Nonlinearitis in Smart-material Systems*. Laboratory for Process Automation, University of Saarland, Im Stadtwald, Geb. 13, Saarbrucken Germany; klauslpa.uni-sb.de.

[50] Y. Xu, P. Atherton, T. Hicks, and M. McConnell, *Design and Characterization of Nanometer Precision Mechanisms II*. Queensgate Instruments Ltd., Waterside Pard, Bracknell, TRG1RB, UK.

[51] J. Main and E. Garcia, "Piezoelectric stack actuators and control system design: Strategies and pitfalls," *Journal of Guidance, Control and Dynamics*, vol. 20, pp. 479–485, May-June 1997.

[52] J. Main and E. Garcia, "Precision position control of piezoelectric actuators using charge feedback," *Journal of Guidance, Control and Dynamics*, vol. 18, pp. 1068–1073, September-October 1995.

[53] J. Cruz-Hernandez and V. Hayward, "Phase control approach to hysteresis reduction," *IEEE Transaction on Control Systems Technology*, vol. 9, pp. 19–26, January 2000.

[54] J. Cruz-Hernandez and V.Hayward, "Reduction of Major aand Minor Hysteresis Loops in Piezoelectirc Actuator," in *Proceedings of the IEEE Conference on Decision and Control*, pp. 4320–4325, The IEEE, 1998.

[55] L. Chua and K. Stromsmoe, "Lumped circuit models for nonlinear inductors exhibiting hysteresis loops," *IEEE Transactions on Circuit Theory*, vol. CT-17, pp. 564–574, November 1970.

[56] L. Chua and K. Stromsmoe, "Mathematical models for dynamic hysteresis loops," *International Journal of Engineering Science*, vol. 19, pp. 435–450, 1971.

[57] L. Chua and S. Bass, "A generalized hysteresis model," *IEEE Transactions on Circuit Theory*, vol. CT-19, pp. 36–48, January 1972.

[58] G. Choi, H.-S. Kim, and C. Choi, "A study on position control of piezoelectric actuators," in *ISIE '97; Proceedings of the IEEE International Symposium on Industrial Electronics*, vol. 3, pp. 851–855, 1997.